3D RADIAL INFLOW TURBINE DESIGN AND ANALYSIS FOR A SMALL SCALE ORC APPLICATION

by

Emre Sezerkan

B.S., Mechanical Engineering, METU, 2014

Submitted to the Institute for Graduate Studies in
Science and Engineering in partial fulfillment of
the requirements for the degree of
Master of Science

Graduate Program in Mechanical Engineering

Boğaziçi University

2017

3D RADIAL INFLOW TURBINE DESIGN AND ANALYSIS FOR A SMALL SCALE ORC APPLICATION

APPROVED BY:

Assoc. Prof. Hasan Bedir (Thesis Supervisor)	.....
Prof. Günay Anlaş (Thesis Co-supervisor)	.....
Prof. Halim Gürgenci	.....
Prof. Hilmi Lus	.....
Prof. Kunt Atalik	.....

DATE OF APPROVAL: 09.01.2017

ACKNOWLEDGEMENTS

I would first like to express my sincere gratitude to my advisor Assoc. Prof. Hasan Bedir and Prof. Gunay Anlas for the continuous support of my master study and related research, for their patience, motivation, and immense knowledge. Their guidance helped me in all the time of research and writing of this thesis. I am also grateful to our lab coordinator Mr. Bora Isik for his support in overcoming numerous obstacles I have been facing through my research.

I would like to thank Onur Kardas and Umut Soysal in for the stimulating discussions, for the sleepless nights we were working together during the establishment of our laboratory, and for all the fun we have had in the last two years. I also thank my fellow labmates Mehdi Nabati, Hamed Shafiei and Alpay Asma for their feedback, cooperation and of course friendship.

Finally, I must express my very profound gratitude to my parents Serife Sezerkan and Erdogan Sezerkan for providing me with unfailing support and continuous encouragement throughout my years of study and through the process of researching and writing this thesis. This accomplishment would not have been possible without them. Thank you.

Emre Sezerkan

ABSTRACT

3D RADIAL INFLOW TURBINE DESIGN AND ANALYSIS FOR A SMALL SCALE ORC APPLICATION

In this study, the aim is to design and analyze a single stage subsonic radial inflow turbine for the Organic Rankine Cycle system established in Bogazici University Renewable Energy Technologies Laboratory, by using R245fa and R134a as the working fluids. Complete design process of the ORC turbine, from preliminary design to 3D blade design stage, is presented. Design point of the turbine is determined according to the cycle limitations and by comparing the maximum mach number, rotational speed and mass flow rate parameters found as a result of detailed preliminary turbine design and basic cycle analysis. Results of the streamline and CFD analysis of the designed turbine are compared and discussed from the point of Mach number distribution, turbine efficiency and power output. The comparison shows that the two analyses give similar efficiencies, power outputs and Mach number distributions. Streamline analyses results show that the maximum total to static turbine efficiency and power output are 87.5 % and 3.97 kW respectively.

ÖZET

KÜÇÜK ÖLÇEKLİ ORÇ UYGULAMASI İÇİN ÜÇ BOYUTLU RADYAL TÜRBİN TASARIMI VE ANALİZİ

Bu çalışmada, Boğaziçi Üniversitesi Yenilenebilir Enerji Teknolojileri Laboratuvarı'nda kurulu olan Organik Rankine Çevrim sistemi için R245fa ve R134a akışkanları kullanılarak, tek kademeli, ses hızı altında çalışacak, radyal girişli bir türbin tasarımı ve incelemesi yapılması amaçlanmıştır. Ön tasarım aşamasından üç boyutlu kanat tasarımına kadar, ORÇ türbininin tüm tasarım aşamaları gösterilmiştir. Türbin çalışma noktası, detaylı çevrim analizi ve türbin ön tasarımı sonucunda bulunan Mach sayısı, rotor dönüş hızı ve kütlesel akış hızı değişkenleri karşılaştırılarak, çevrim sisteminin sınırlamalarına uygun olarak belirlenmiştir. Tasarlanan türbinin CFD ve akış çizgi incelemelerinin sonuçları, Mach sayısı, türbin verimliliği ve güç çıkışı özelinde karşılaştırılmış ve tartışılmıştır. Karşılaştırmalar sonucunda, iki analiz yönteminin benzer verimlilik, güç çıkışı ve Mach sayısı değerleri verdikleri görülmüştür. Akış çizgi incelemelerinin sonuçlarına göre, en yüksek türbin verimliliği ve güç çıkışı değerleri sırasıyla 87.5 % ve 3.97 kW olarak bulunmuştur.

TABLE OF CONTENTS

LIST OF FIGURES

LIST OF TABLES

LIST OF SYMBOLS

a_{ij}	Description of a_{ij}
$\mathbf{A}$	State transition matrix of a hidden Markov model
c	Speed of sound
c_p	Specific heat constant for constant pressure
C_0	Stator inlet absolute flow velocity
C_1	Stator outlet absolute flow velocity
C_2	Rotor inlet absolute flow velocity
C_3	Rotor outlet absolute flow velocity
C_{u2}	Tangential component of rotor inlet absolute flow velocity
C_{u3}	Tangential component of rotor outlet absolute flow velocity
H_2	Enthalpy at rotor inlet *or* turbine exit
H_3	Enthalpy at rotor outlet *or* condenser exit
H_4	Enthalpy at pump exit
H_0^*	Total enthalpy at stator inlet
H_1^*	Total enthalpy at stator outlet
H_2^*	Total enthalpy at rotor inlet
H_3^*	Total enthalpy at rotor outlet
H_0	Total enthalpy at stator inlet
H_1	Total enthalpy at stator outlet
H_2	Total enthalpy at rotor inlet
H_3	Total enthalpy at rotor outlet
I	Rothalpy
K_a	Axial clearance coefficient
K_{df}	Disk Friction coefficient
K_r	Radial clearance coefficient
L_0	Stator leading edge height
L_1	Stator trailing edge height
L_2	Rotor leading edge height

L_3	Rotor trailing edge height
L_{ax}	Axial length of rotor
$\dot{m}$	Mass flow rate
$\dot{m}_{eq}$	Equivalent mass flow rate
M_{abs}	Absolute Mach number
M_{rel}	Relative Mach number
N	Turbine power output
Q_3	Rotor outlet volumetric flow rate
$\dot{Q}_{chiller}$	Chiller power capacity
$\dot{Q}_{heater}$	Heater power capacity
r_0	Stator inlet radius
r_1	Stator outlet radius
r_2	Rotor inlet radius
r_{3h}	Rotor outlet hub radius
r_{3m}	Rotor outlet mid radius
r_{3t}	Rotor outlet tip radius
T	Torque *or* temperature
T_2	Temperature at rotor inlet
T_3	Temperature at rotor outlet
T_2^*	Total temperature at rotor inlet
T_3^*	Total temperature at rotor outlet
U_2	Rotor inlet blade velocity
U_3	Rotor outlet blade velocity
W_2	Rotor inlet relative flow velocity
W_3	Rotor outlet relative flow velocity
α_0	Stator inlet absolute flow angle
α_1	Stator outlet absolute flow angle
α_2	Rotor inlet absolute flow angle
α_3	Rotor outlet absolute flow angle
$\alpha_0 m$	Stator inlet blade angle

$\alpha_1 m$	Stator outlet blade angle
$\alpha_2 m$	Rotor inlet blade angle
$\alpha_3 m$	Rotor outlet blade angle
α_i	Rotor incidence angle
β_2	Rotor inlet relative flow angle
β_3	Rotor outlet relative flow angle
$\Delta\eta_{tt}$	Efficiency loss factor for tip leakage
ΔH^*_{id}	Isentropic total enthalpy drop
η_{carnot}	Cycle efficiency
η_{cycle}	Cycle efficiency
η_{ts}	Turbine total to static efficiency
η_s	Turbine isentropic efficiency
ϵ_a	Axial clearance between rotor and shroud
ϵ_r	Radial clearance between rotor and shroud
τ_{fric}	Disk friction torque
ω	Turbine angular speed
θ_0	Stator inlet offset angle
θ_1	Stator outlet offset angle
θ_2	Rotor inlet offset angle
θ_3	Rotor outlet offset angle
ξ_{in}	Incidence loss coefficient

LIST OF ACRONYMS/ABBREVIATIONS

1D	One Dimensional
2D	Two Dimensional
3D	Three Dimensional
BURET Lab	Boğaziçi University Renewable Energy Technologies Laboratory
CFD	Computational Fluid Dynamics
LE	Leading Edge
TE	Trailing Edge
PR	Pressure Ratio
ORC	Organic Rankine Cycle
R134a	1,1,1,2-tetrafluoroethane
R245fa	1,1,1,3,3-pentafluoropropane

1. INTRODUCTION

Rankine Cycle is a conventional thermodynamic cycle for converting heat into mechanical energy by using steam as a working fluid. A simple Rankine cycle consists of 4 components which are evaporator, turbine, condenser and pump. Working fluid which is heated and pressurized by evaporator and pump respectively transfers its gained energy to turbine blades and finally returns to liquid phase at a condenser to complete the cycle.

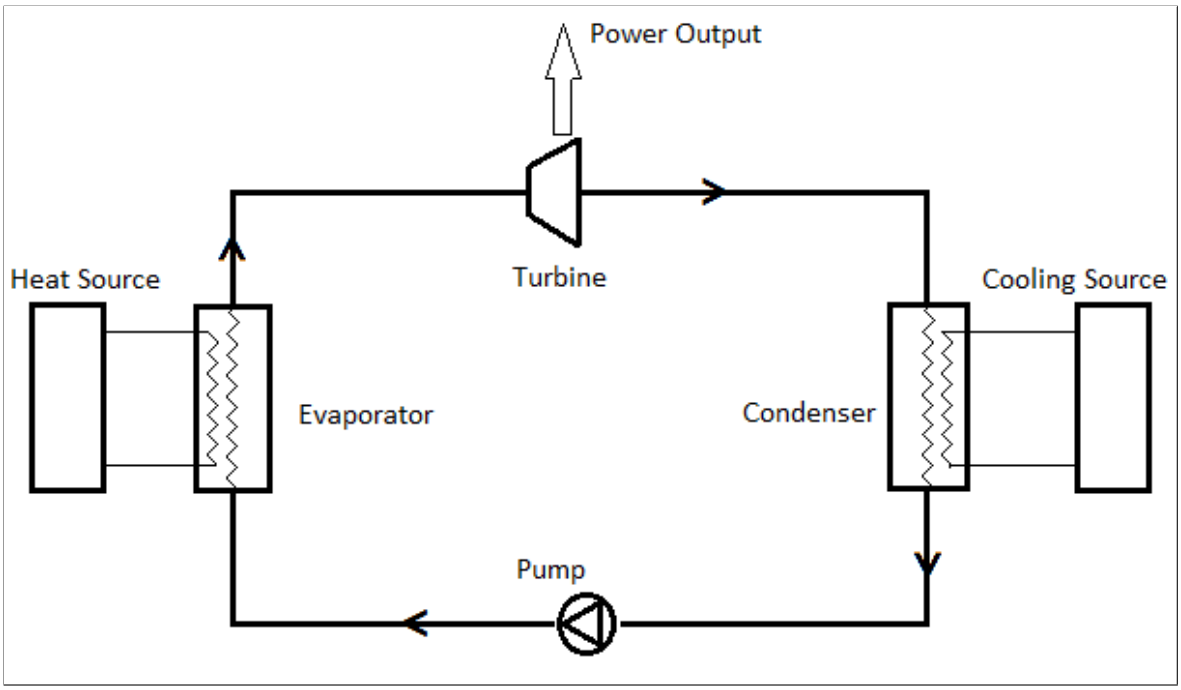

Figure 1.1. Schematic Diagram of a Simple Rankine Cycle.

In Figure 1.1, schematic diagram of cycle and the components are presented. Main purpose of the cycle is generating mechanical energy and the amount of this generation depends on the heat source of the system. Large capacity power plants use steam as the working fluid because the heat sources of these stations have high temperatures. However, for a low temperature sources such as geothermal, solar, biomass or waste heat, steam is not the most efficient way to transfer heat because steam can

not reach high pressure values at low temperatures. Therefore, while converting thermal energy into mechanical energy at low or middle level temperatures (from 40 ^0C to 600 ^0C) organic fluids which have a low boiling points are used. These systems, run with organic working fluid, is called Organic Rankine Cycle (ORC).

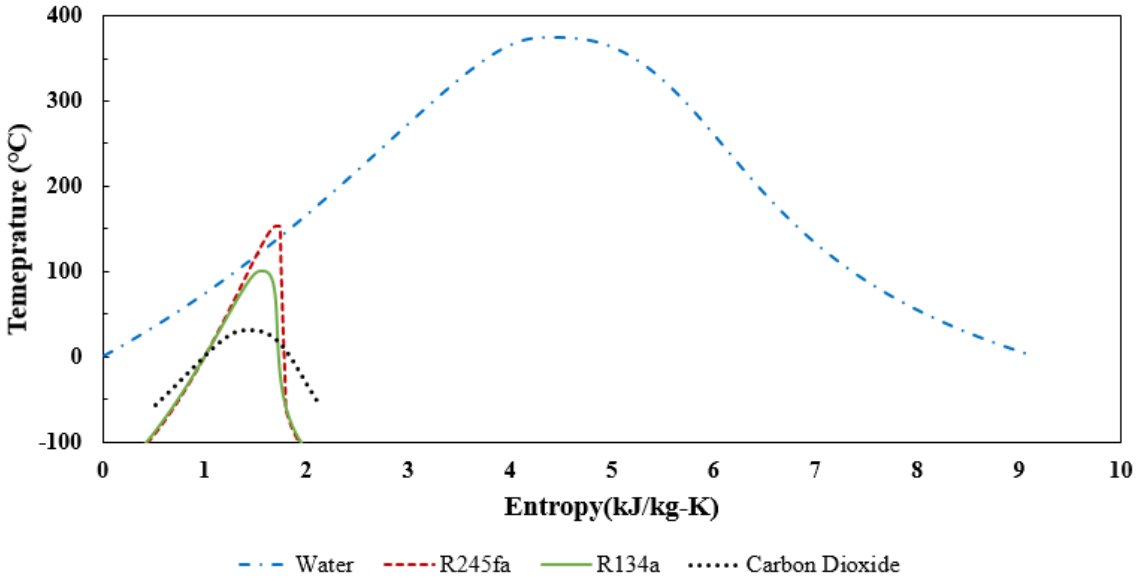

Figure 1.2. Saturation lines of several fluids in T-s diagram.

Thermodynamics differences between organic fluids and water can be observed in the T-s diagram presented in Figure 1.2. Saturation lines for water, R245fa, R134a and CO_2 are drawn in same scale to understand the regions of fluids that can be efficient in Rankine cycle. It can be seen that, organic fluids presented in Figure 1.2 give the opportunity to reach higher pressures at low temperatures when compared to water steam. For example, while the saturation pressure of steam is 1.01 bar at 100 ^0C, this value equals to 12.65 bar for R245fa at the same temperature.

These organic fluids, however, change the system characteristics because fluid properties affect the performance of components in cycle. For instance, a steam turbine cannot work at high efficiency with an organic fluid due to the different kinematic viscosity or speed of sound values of organic fluids. Therefore, fluid properties are one of the most important parameters during the cycle and turbine design process. As a

Table 1.1. Fluid Information from NIST Refprop.

	Unit	Water	Dry Air	R245fa	R134a
Molar Mass	kg/kmol	18.015	28.965	134.05	102.03
Specific Gas Constant	J/kg-K	461.50	287.04	62.02	81.49
Critical Temperature	^{0}C	373.95	-140.62	154.01	101.06
Critical Pressure	bar	220.64	37.86	36.51	40.59
Critical Density	kg/m^3	322.00	342.68	516.08	511.90
Kinematic Viscosity(@ 150 ^{0}C , 1 bar)	cm^2/s	0.2749	0.1343	0.0381	0.0569
Speed of Sound (@ 25 ^{0}C , 1 bar)	m/s	1496.70	346.25	136.62	161.55

result, every fluid require different blade design and different turbine dimensions. Therefore, blade design and optimization of turbine geometry for various organic fluids are important processes to enhance the system efficiency.

In Table 1.1, several main properties of air, water, R245fa and R134a are shown. It can be seen that R245fa and R134a have much higher molar mass and lower speed of sound values when compared with air and water. Also the critical density of organic fluids are higher than water while the critical pressures and temperatures are lower. These differences are the main reasons of requirement to a specific turbine design for organic fluids.

Water vapor has important differences from organic fluids as mentioned above but there are also critical distinctions exist between organic fluids. One of the main classification is made between the saturation curve slopes of fluids. In Figure 1.3, examples of three curve types are presented. Fluids with positive saturation curve slope is called as dry fluid. Cycles which works with dry fluid have the opportunity to work without superheat because there is no risk to be in liquid phase at the exit of the turbine. If the saturation line is vertical then fluid is called as isentropic and when the slope becomes negative, fluid is called as wet. Studies shows that, for an ORC application, dry or isentropic fluids are the most suitable options [1, 2]. In this study performance of R245fa and R134a are investigated which are isentropic and wet fluids respectively.

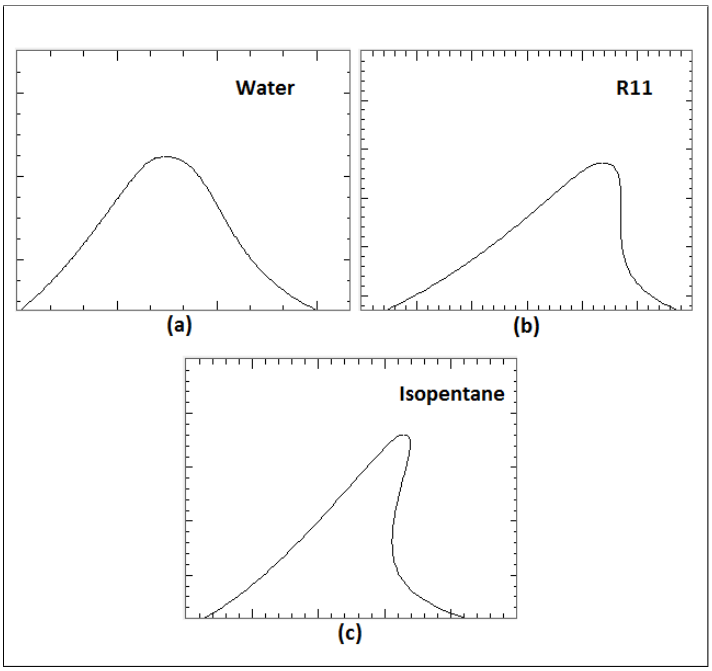

Figure 1.3. (a)Wet, (b)Isentropic and (c)Dry Fluids Saturation Curve Slopes in T-s Diagram.

As it was mentioned previously, ORC can be suitable for various type of energy sources [3] such as solar [4], geothermal [5] or waste heat [6]. There are many study in the literature related with the fluid selection process, effects of organic fluids on cycle efficiency, application areas of ORC, turbine selection for ORC application and ORC turbine design [7]. In this study, radial inflow ORC turbine design process is investigated, therefore the detailed literature survey mostly includes ORC turbines and their performances.

One of the first experimental study about ORC was introduced in 2001 by Yamamato *et al.*. They presented a new system to generate mechanical energy from low heat source by using organic working fluids instead of water in Rankine Cycle. In the experiment setup, an existing micro turbine with 30 mm rotor diameter was selected. According to the numerical simulations, it was found that the cycle gives more power output when organic fluid HCFC-123 is used instead of water. Also, experimental results show that the cycle with 19.9 kW evaporator input gives a 150 W turbine output

at 45000 rpm by using water as a working fluid while the cycle works with HCFC-123 generates 150 W turbine output at 35000 rpm with 13.0 kW evaporator input [8].

Rawlands *et al.* focused on the binary cycle geothermal applications of ORC systems and the preliminary design of radial inflow turbine for several ORC systems which use R134a, R143a, R236fa, R245fa and n-Pentane as the working fluids. Radial turbine design was performed based on a preliminary meanline analysis and it was found that the efficiencies of the turbines were about 77.0 % for 5 different design based on 5 different working fluids. Values of the power output were between 254 kW for n-Pentane and 338 kW for R134a. Also the minimum and maximum rotor radii were calculated as 69.6 mm for R143a and 144.3 mm for n-Pentane. As a result, it was found that the cycle/turbine couples which work with R134a and R143a were the promising ones because of their small rotor sizes and high power outputs [9].

In 2012, Fiaschi *et al.* presented a study about expansion model for real fluids instead of perfect gas model. Because when fluids are close to their critical conditions, perfect gas model may not give satisfactory results. Main objective of the study is to complete the preliminary design of a 50 kWe radial inflow turbine for six different organic fluids (R134a, R1234yf, R236fa, R245fa, Cyclohexane, N-Pentane). As a result, rotor diamaters were calculated between 50 mm and 80 mm where the rotational speeds were found betweeen 32000 and 55000 rpm for five organic fluids. It was observed that Cyclohexane requires 138 mm rotor diameter as an exception. Also the total to total turbine efficiencies were found between 78 % and 85 %. For Cyclohexane this value is 69 % [10].

In their next study, Fiaschi *et al.* proposed a zero dimensional model for the radial ORC turbine design by applying real equations of state and calculating the losses. Study aimed to present the effects of organic fluids (R134a, R1234yf, R236fa, R245fa, Cyclohexane, N-Pentane) on turbine design and performance. Target power output was 50 kW and the results showed that the maximum and minimum total to total efficiencies of the designed turbine were 80 % for R1234yf and 72 % for Cyclohexane [11].

Last study of Fiaschi *et al.* includes a design of 5 kW radial inflow turbine from preliminary design stage to 3D CFD analysis by using R134a as the working fluid. Designed turbine geometry requires 0.2 kg/s mass flow rate and 87645 rpm speed at its design point. Rotor inlet diameter was calculated as 35 mm. CFD analysis results of improved turbine geometry show that the total to static efficiency was 71.76 %. [12].

Ventura *et al.* also contributed to the literature with their one dimensional meanline code for preliminary design and performance estimation of radial inflow turbine [13].

Another experimental study of small scale ORC was conducted by Pei *et al.* in 2011. In this study, R123 was used as the working fluid. As a result of the experiments, 65 % isentropic turbine efficiency and 6.8 % cycle efficiency was obtained for the 70 ^{0}C temperature difference between hot and cold points of the cycle [14].

In 2012, Kang presented a study about design and test of an ORC. Also a radial turbine was designed based on a geometric similarity of an existing turbine. The aim was to produce 30 kW power output and R245fa was chosen as the working fluid. Experiments were conducted for three different evaporation temperatures which are 77.1,79.5 and 82.3 ^{0}C. As a result of the experiments, the average turbine efficiencies, electric power and cycle efficiencies were found as 76.0, 77.5, 82.2 % ; 24.5, 26.9, 31.2 kW and 5.05, 5.24, 5.66 % respectively for these evaporation temperatures [15].

Kang's next study was focused on designing an ORC and a two stage radial turbine expander to improve the cycle efficiency by using R245fa. The rotors of the designed turbine were connected in the same shaft and during the design process, the rotational speeds of the shaft was selected as 21,200 rpm by considering the performance of the low pressure stage of the turbine. As in the first study of Kang, 3D blade was designed based on the geometric similarity of an existing turbine. Experiment results showed that the average maximum power and cycle efficiency were 39.0 kW and 9.8 % respectively. For these cycle conditions, isentropic turbine efficiency for the

first stage, second stage and for the complete turbine were 52.1 %, 76.5 % and 68.5 % respectively while the turbine efficiency based on power output was 58.4 % [16].

Sauret *et al.* presented three dimensional viscous simulations of radial inflow turbine at nominal and off design conditions. Study, includes the design process of the 400 kW radial turbine where R143a was selected as the working fluid. During the design process of the turbine one dimensional design and three dimensional analysis were investigated. In the comparison of the meanline analysis and CFD results, the maximum total to static efficiencies and power outputs of the designed turbine were 76.8, 83.5 % and 393.6, 421.5 kW according to meanline and CFD analysis results respectively [17].

Another complete design process of radial inflow turbine was conducted by Lee *et al.* in 2015. Their study focused on designing a radial inflow turbine which works with R-22 to generate 2kWe at a closed cycle ocean thermal energy conversion plant. As a result of the turbine optimisation and design process, at the optimum efficiency point, power output, pressure ratio, mass flow rate, mach number and the efficiency values are 2.5 kW, 1.34, 0.41kg/s, 0.47 and 74 % respectively [18].

As a different turbine geometry design, Pini *et al.* presented a study on preliminary design and evaluation of multistage transonic radial outward turbine for an ORC application where the working fluid was Siloxane MDM. In this process, a mean-line code was created and results obtained from meanline code were verified with a CFD solver [19].

As a result, important studies exist related with ORC turbine design for various types (i.e. scroll, radial outflow, axial, radial inflow) and power output requirements. Some of these studies include only preliminary or meanline design steps. Also some of the studies take an existing turbine geometry as a reference and design a turbine by using the similarity rules. Only some of these studies investigate whole design processes for radial inflow turbine [17,18] and these studies were conducted for a geothermal and

ocean thermal application where the working fluids are R143a and R22 respectively. In addition, recently, a 5 kW radial ORC turbine design was presented by Fiaschi *et al.* [12] in 2016. Although this study includes preliminary design and CFD analysis of the designed turbine, turbine was designed for R134a. Up to now, to the best of author's knowledge, there is no study on complete radial inflow turbine design process which uses R245fa as the working fluid for 100 kW heat capacity ORC test system. Therefore, this study aims to contribute the literature by investigating the complete subsonic turbine design process starting form preliminary design to 3D blade design stage by using CFD and streamline analysis calculation methods according to specific ORC requirements and real R245fa and R134a gas properties.

In Chapter 2, basic knowledge about radial turbines and important formulations are explained. Then in Chapter 3 and 4, preliminary turbine design process in general and for specific case are investigated respectively. In Chapter 5, 3D blade optimization process is performed by using streamline and CFD analysis. Final turbine geometry is presented in Chapter 6. Lastly, CFD analysis results and are discussed in Chapter 7.Also, turbine performance results, generated with streamline calculations, are compared with CFD analysis results at several points to obtain whether there is a incompatibility between two methods. All these analysis are discussed for R245fa and R134a fluids.

2. FUNDAMENTALS OF RADIAL TURBINE

Turbine design process starts with preliminary design which provides general information about turbine geometry and thermodynamics boundary conditions. After deciding the boundary conditions, first 3D turbine geometry is generated in software by using the preliminary design results. Then, the streamline analysis of the raw turbine geometry is performed to observe the important turbine parameters such as mass flow rate, power output, efficiency, mach number and rotational speed. According to the results obtained from the streamline analysis, an iterative approach is carried out between 3D blade optimization and streamline analysis outputs. Main purposes of this design process are to create a 3D stator and rotor blade shapes that generate a subsonic flow path with the highest turbine isentropic efficiency at its design point. 3D blades are optimized manually. Velocity triangles and other design parameters are analyzed for each change of the blade geometry with streamline analysis method to reach the stated purposes. When the demanded turbine parameters are obtained according to streamline analysis result, 3D model of the designed turbine is analyzed in CFD solver at its design point to observe the problems that can not be seen in streamline calculations such as separation. Thus, the efficiency of designed turbine can be improved. During this process, result of CFD and streamline analyses are compared to see whether they match up with each other. Finally, turbine design is accomplished by considering the streamline and CFD analysis result.

2.1. Turbine Geometry

Radial turbine consists of four parts which are volute, nozzle(stator), rotor and diffuser.Flow enters the turbine from an inlet volute. In the volute, velocity of the flow increases, pressure drops and flow gains an important angular momentum.Then flow passes through the nozzle which has a stationary blade set. In the nozzle, velocity of the flow increases, pressure drops and flow is guided by this stationary blade set. After the nozzle, flow enters the rotor to develop work with rotating blade set by decreasing

the pressure and temperature of fluid. Finally, at the exit of the rotor, flow passes from the diffuser and velocity of the flow decreases and static pressure of the fluid increases. In Figure 2.1, these four parts are presented where stator and rotor parts are shown with blue and red blade sets respectively.

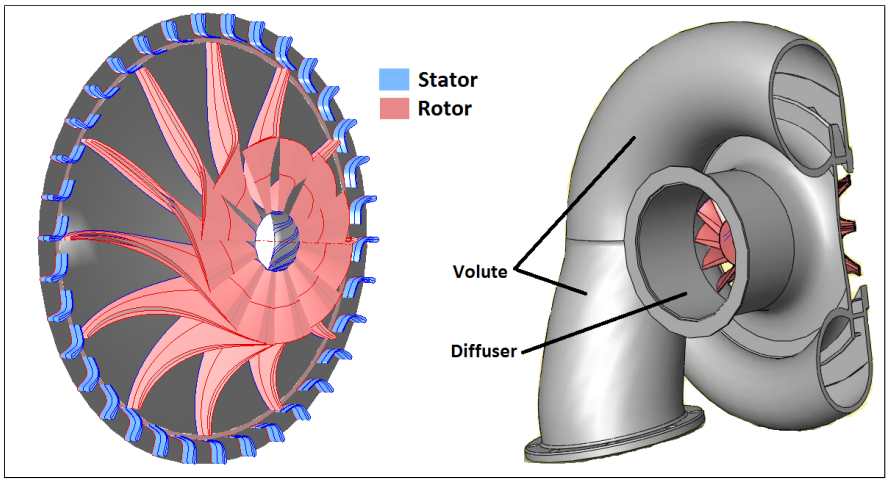

Figure 2.1. Sample turbine rotor and stator.

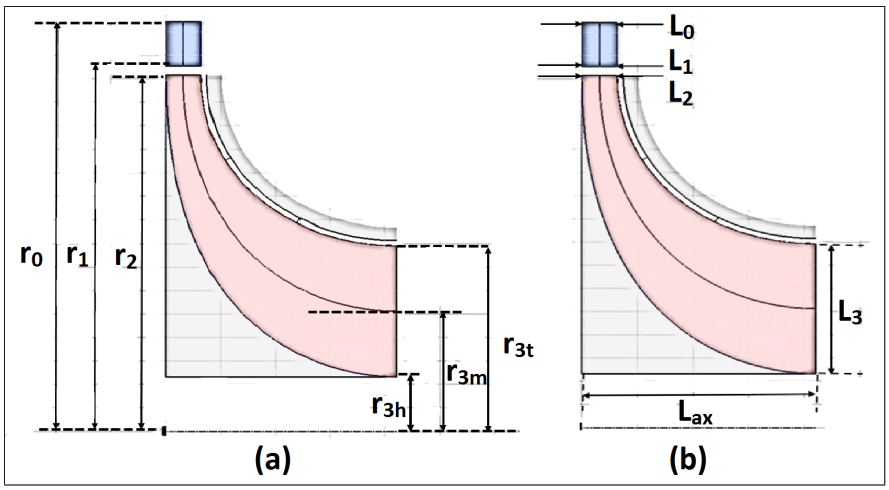

Figure 2.2. Geometry of Turbine Blades - (a)Radius, (b)Edge Heights.

Nomenclature used in the design process is presented in Figure 2.2. In part (a) of the Figure 2.2 several important radii of the turbine are shown. At the inlet and exit of the stator, radii are r_0 and r_1 respectively. At the inlet of the rotor, radius is r_2 and in this section there is no difference in radii between hub, middle and tip region of

the rotor. However, at the exit of the rotor, hub, mid and tip radii are represented with r_{3h}, r_{3m}, r_{3t} respectively.Edge widths also have an important place in the design process. Part (b) of the Figure 2.2 shows the edge heights of stator and rotor where L_0 and L_1 are stator leading and trailing edge widths; L_2 and L_3 are rotor leading and trailing edge widths respectively. Finally, L_{ax} represents the axial length of the turbine.

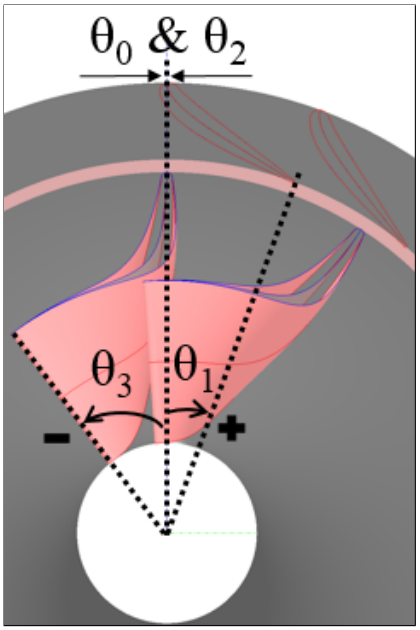

Figure 2.3. Offset Angles of Rotor and Stator.

In addition to the lengths of blades, several important angles are also used during the design process. In Figure 2.3, turbine blade offset, θ, angles with sign convention are presented. θ_0 and θ_1 represent the stator inlet and outlet offset angles respectively. Similarly, in rotor, these angles are θ_2 and θ_3 respectively. In this figure, θ_0 and θ_2 are both 0 degree therefore they are presented with vertical axis.

Finally, blade (metal) angles of stator and rotor are presented in Figure 2.4. Also in Figure 2.5, both offset and blade angles are presented in polar view to show the hub mid and tip section of the rotor clearly.

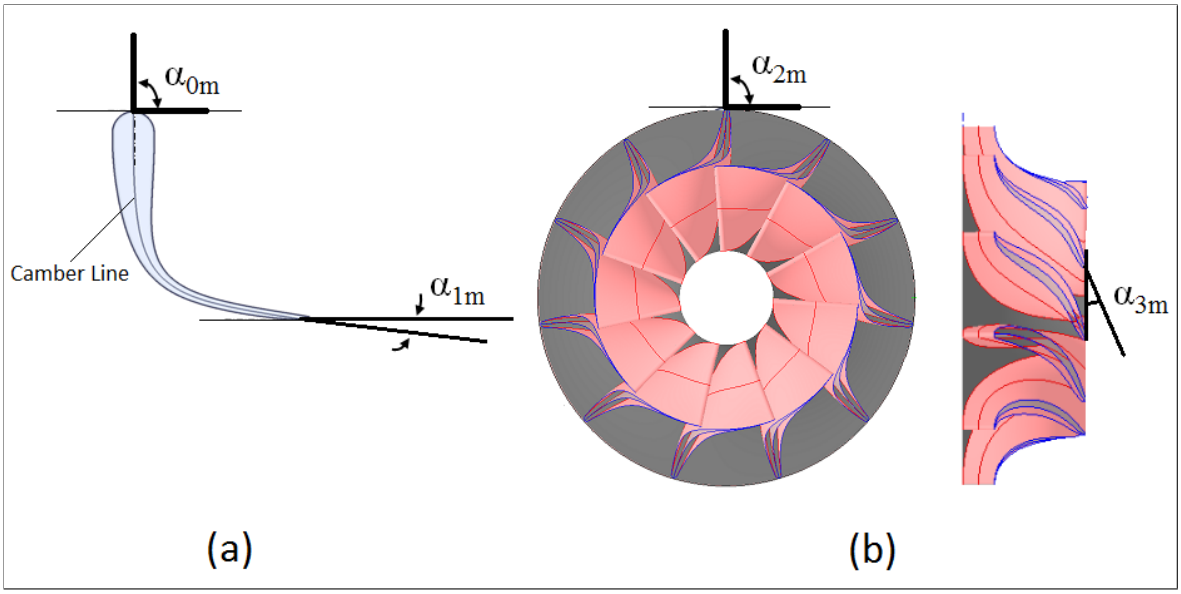

Figure 2.4. Blade(Metal) Angles of (a)Stator and (b)Rotor.

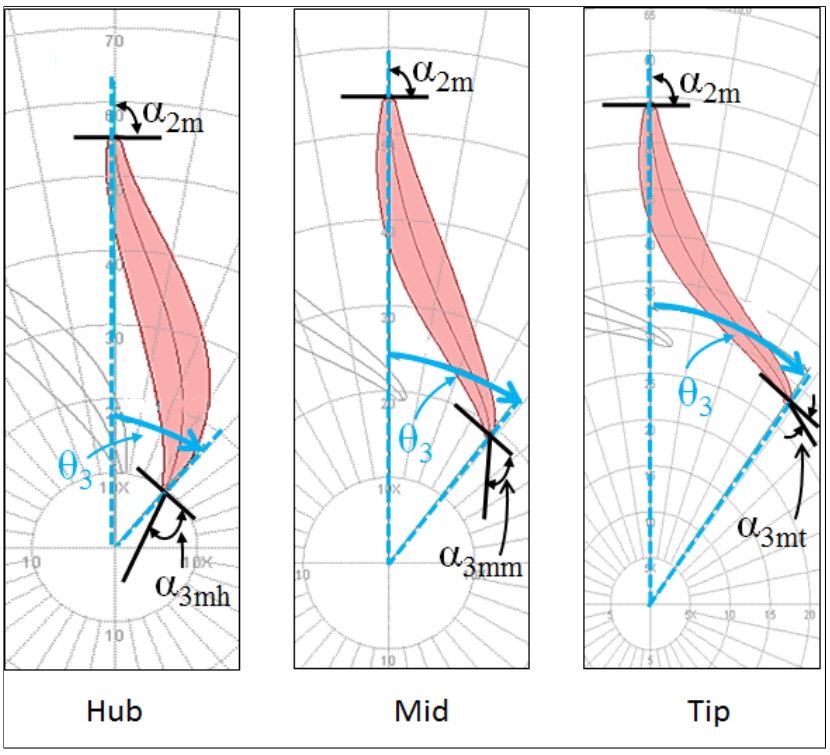

Figure 2.5. Offset and Blade(Metal) Angles of Rotor in polar view.

2.2. Turbine Power and Velocity Relation

Turbine is the Rankine Cycle component where the fluid transports its energy to the blades. Therefore, one should clarify the relationship between fluid velocity, blade velocity and turbine power output. For this purpose, firstly important angle conventions and velocities are defined. Then, the relation between velocity and power is explained by using thermodynamic and kinematic equations. As a result Euler Turbine Equation is derived.

2.2.1. Velocity Triangles and Angle Convention

In cascade notation, 3 velocity vectors are defined. Absolute velocity, $\vec{C}$, is the velocity of the fluid according to a stationary observer. $\vec{U}$ is the circumferential velocity of rotor. Finally, relative velocity, $\vec{W}$, is the velocity of fluid relative to turbine blades. Because there is no motion in the stator (i.e. blades are stationary) relative velocity and absolute velocity refers to same vector. Subscriptions used with velocities and angles indicate the location as it was shown in Figure 2.2.

In this study, tangential angle convention is used. Figure 2.6 presents the relative, absolute flow velocities and corresponding angles at the inlet and outlet sections. At the inlet of the rotor, α_2 and β_2 are the absolute and relative velocity angles respectively. Similarly, at the outlet of the rotor, α_3 and β_3 show the angles of absolute and relative velocities respectively.

2.2.2. Euler Turbine Equation

Euler Turbine Equation is one of the most important equation for the turbine design as it establishes relation between tangential component of absolute velocities and enthalpy difference at the rotor inlet-exit section by using the energy conservation law and angular momentum conservation law [20].

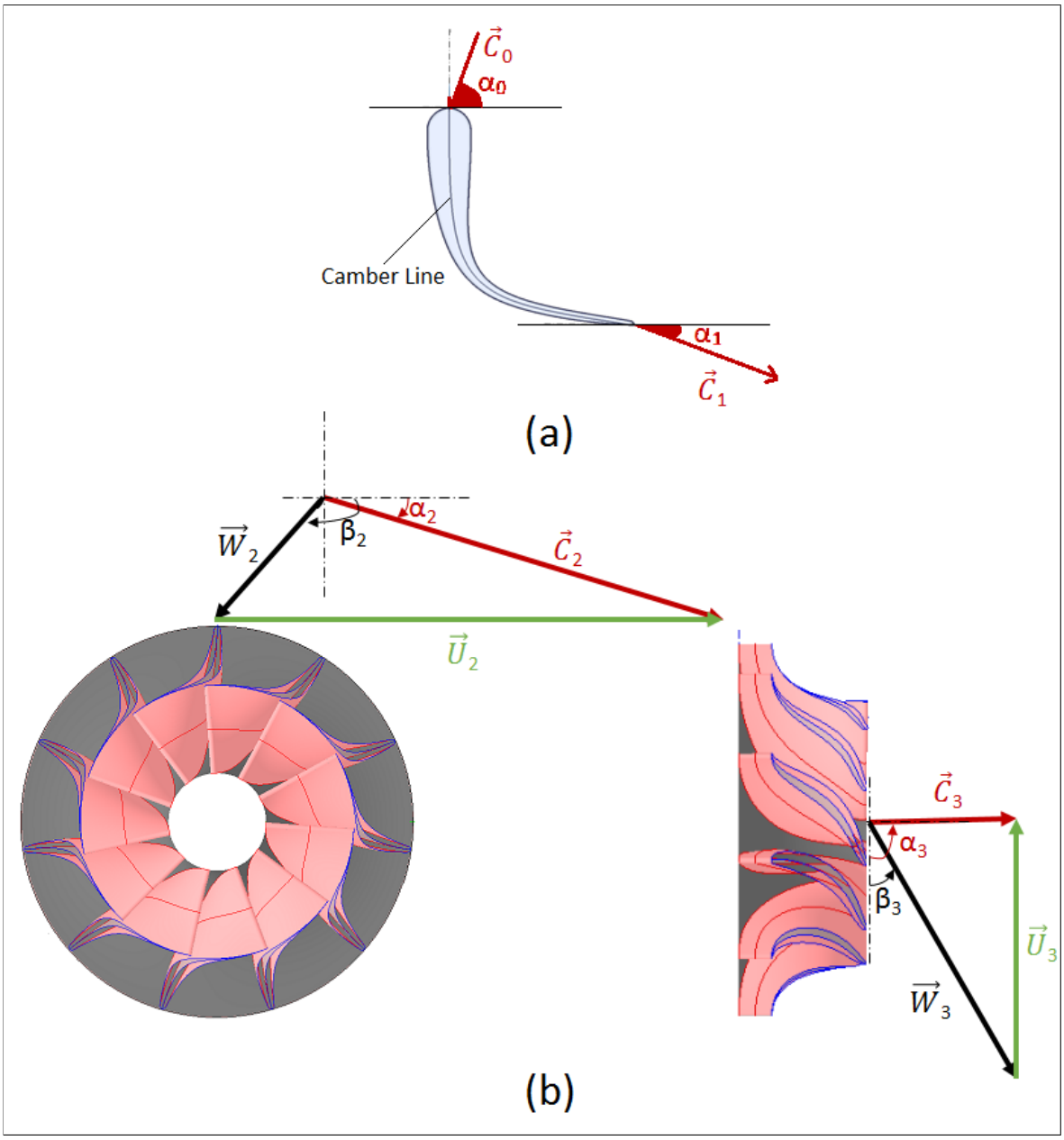

Figure 2.6. Velocity Vectors at (a) Stator and (b) Rotor.

According to the change in angular momentum equation;

$$T = \dot{m}(C_{u2}r_2 - C_{u3}r_3) \tag{2.1}$$

If one multiplies the torque with angular velocity of the rotor, power can be calculated as follows:

$$N = T\omega = \dot{m}\omega(C_{u2}r_2 - C_{u3}r_3) \tag{2.2}$$

The power can also be calculated from the total enthalpy change between rotor inlet and outlet by assuming there is no heat loss.

$$N = \dot{m}(H_2^* - H_3^*) \tag{2.3}$$

Combining equation 2.2 and 2.3, Euler Turbine Equation is given as;

$$H_2^* - H_3^* = (C_{u2}U_2 - C_{u3}U_3) \tag{2.4}$$

where the circumferential speed, U, is

$$U = \omega r \tag{2.5}$$

For an ideal gas with constant c_p value, equation 2.4 becomes

$$c_p(T_2^* - T_3^*) = (C_{u2}U_2 - C_{u3}U_3) \tag{2.6}$$

This is the basic version of the Euler Turbine Equation. After the definition of Rothalpy, another version of the Euler Turbine Equation will be derived. Rothalpy, I, is the result of rearrangement of Euler Turbine Equation and it is conserved in an

adiabatic, irreversible and steady system.

$$I = (H^* - C_u U) \tag{2.7}$$

Using the equation 2.7, rothalpy values at the inlet and exit of the rotor can be equalized according to conservation assumption.

$$(H_2^* - C_{u2} U_2) = (H_3^* - C_{u3} U_3) \tag{2.8}$$

where the total enthalpy can be described as follows:

$$H^* = H + \frac{1}{2} C^2 \tag{2.9}$$

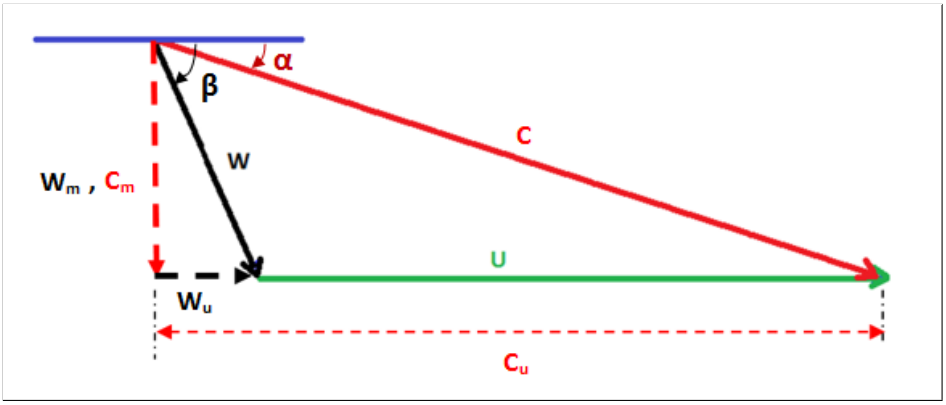

Figure 2.7. Sample Velocity Triangle of Rotor.

According to the velocity triangle shown in Figure 2.7, which can occurs at the inlet and exit of the rotor, rothalpy becomes:

$$I = H + \frac{1}{2} C^2 - C_u U \tag{2.10}$$

The tangential component of absolute velocity, $\vec{C}_u$, is described as follows:

$$\vec{C}_u = \vec{W}_u + \vec{U} \tag{2.11}$$

Also, absolute speed, C, can be written as follows:

$$C^2 = C_u^2 + C_m^2 \tag{2.12}$$

where C_m is the meridional component of absolute velocity. Therefore,

$$C^2 = (W_u + U)^2 + C_m^2 = W_u^2 + 2W_uU + U^2 + C_m^2 \tag{2.13}$$

Using equation 2.13 in equation 2.10, rothalpy becomes

$$I = H + \frac{1}{2}(W_u^2 + 2W_uU + U^2 + C_m^2) - (W_u + U)U \tag{2.14}$$

Note that

$$W_u^2 + C_m^2 = W^2 \tag{2.15}$$

Thus, rothalpy can be expressed as

$$I = H + \frac{W^2}{2} - \frac{U^2}{2} \tag{2.16}$$

Rothalpy is conserved as it was mentioned in equation 2.8. Therefore, equation 2.16 can be written as

$$I = H_2 + \frac{W_2^2}{2} - \frac{U_2^2}{2} = H_3 + \frac{W_3^2}{2} - \frac{U_3^2}{2} \tag{2.17}$$

where the subscriptions 2 and 3 define the inlet and outlet section of rotor respectively.

Enthalpy difference between the rotor inlet and outlet can be explained by using equation 2.17 as follows:

$$H_2 - H_3 = \frac{W_3^2}{2} - \frac{W_2^2}{2} + \frac{U_2^2}{2} - \frac{U_3^2}{2} \tag{2.18}$$

Then the total enthalpy difference becomes

$$H_2^* - H_3^* = \left(\frac{W_3^2}{2} - \frac{W_2^2}{2} + \frac{U_2^2}{2} - \frac{U_3^2}{2}\right) + \frac{C_2^2}{2} - \frac{C_3^2}{2} \tag{2.19}$$

Finally, Euler Turbine Equation can be described in a different aspect by using equation 2.4 and 2.19 as following.

$$\frac{N}{\dot{m}} = (C_{u2}U_2 - C_{u3}U_3) = \left(\frac{W_3^2}{2} - \frac{W_2^2}{2} + \frac{U_2^2}{2} - \frac{U_3^2}{2}\right) + \frac{C_2^2}{2} - \frac{C_3^2}{2} \tag{2.20}$$

Equation 2.20 is the Euler Turbine Equation where the turbine power output is related with rotor inlet and outlet velocity components.

2.2.3. Mollier Diagram

As it can be understood from the Euler Turbine Equation, power output is directly related with enthalpy difference between turbine inlet and outlet. Turbine enthalpy change observation is a critical part of the turbine design and analysis process to understand the reasons of losses and improve the turbine efficiency. Therefore enthalpy-entropy graph is explained in this section. In the next section, enthalpy data taken from this graph are used to generate non dimensional parameters such as turbine efficiency, isentropic velocity ratio.

Figure 2.8 is a simple H-S diagram of a single stage radial turbine. Blue and red lines indicates stator and rotor of the turbine. States from 0 to 3 specify the turbine sections which were presented in Figure 2.2. Constant pressure lines are shown with dashed lines. ΔH_{id}^* shows the isentropic enthalpy drop in the turbine. Star character,*,

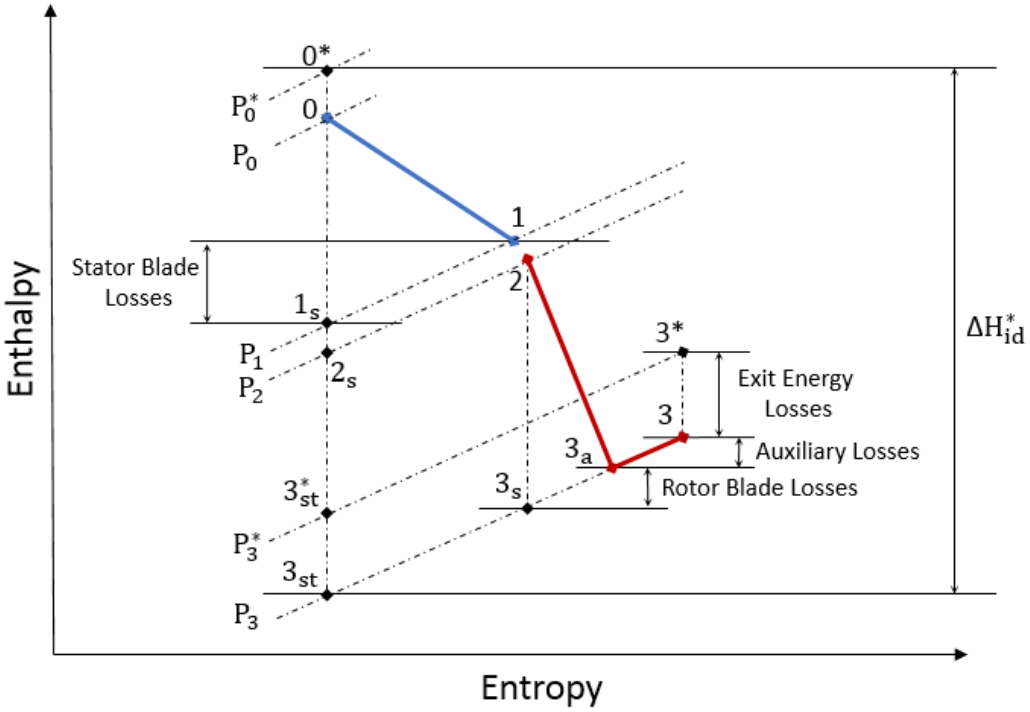

Figure 2.8. Turbine Enthalpy vs Entropy Diagram.

indicates the total properties at that point and subscript "s" presents the final point of a process in an isentropic case. For example, 1_s shows the outlet condition of stator for an isentropic process. Numbers with no subscripts present the static and actual states of that turbine section. Therefore, enthalpy difference between isentropic case and actual case of the same state gives the amount of enthalpy loss at that section. Finally, subscript "st", is presented to calculate the isentropic enthalpy difference for the complete turbine stage.

2.3. Non Dimensional Turbine Design Parameters

In this section, general non dimensional parameters used in turbine design and analysis processes are defined.

2.3.1. Degree of Reaction

Ratio of theoretical enthalpy drop in rotor to theoretical enthalpy drop in rotor and stator [21].

$$R = \frac{H_2 - H_{3s}}{(H_0 - H_{1s}) + (H_2 - H_{3s})} \tag{2.21}$$

For a turbine, degree of reaction must have a positive value. Optimum value for R is around 0.5.

2.3.2. Load Coefficient

Load coefficient is the ratio of isentropic enthalpy drop in turbine to exit circumferential kinetic energy of rotor [21].

$$\psi = \frac{H_0^* - H_{3st}}{U_3^2} = \frac{\Delta H_{id}^*}{U_3^2} \tag{2.22}$$

2.3.3. Isentropic Velocity Ratio

Isentropic enthalpy drop is used to create another important non dimensional preliminary design parameter as following [20];

$$\nu = \frac{U_2}{C_{s0}} \tag{2.23}$$

where spouting velocity, C_{s0}, is a theoretical velocity which is proportional to turbine isentropic ethalpy drop as following [20];

$$C_{s0} = \sqrt{2(H_0^* - H_{3st})} \tag{2.24}$$

2.3.4. Flow Coefficient

Flow coefficient is the ratio of meridional component of absolute speed at the exit of the rotor, C_{m3}, to the blade velocity at the exit of the rotor,U_3 [20].

$$\Phi = \frac{C_{m3}}{U_3} \tag{2.25}$$

2.3.5. Turbine Efficiency

There are several efficiency terms exist for the design of a radial turbine. First one is total to total stage efficiency which is used if kinetic energy of the fluid is consumed by the propelling nozzle or the next stage of the turbine at the rotor outlet. Second type is called total to static stage efficiency. This efficiency term is used if the kinetic energy of the fluid at the exit of the rotor is not spend by another purpose.

$$\eta_{ts} = \frac{H_0^* - H_3^*}{H_0^* - H_{3st}} \tag{2.26}$$

In this study, the designed radial turbine has one stage therefore total to static efficiency should be used. Total to static efficiency is presented in equation 2.26 [21].

2.4. Losses and Loss Models

Generating an efficient turbine geometry is the crucial part of this study therefore one should examine the sources of losses and observe the predicted performance of the turbine before staring the CFD calculations.

In the literature, sufficient testing data is not exist for radial turbine to evaluate the loss models due to its difficult shape when compared to axial turbines. Therefore loss models in the literature are based on overall stage data [22].

In this study, following loss models are used during the performance analysis;

- Profile (primary) losses model : AxS by Mitrohin-Stepanov
- Secondary Losses Model : AxS by Stepanov
- Deviation Angle Calculation Model : AxS Subsonic-Zero (real gas)

where profile losses contain friction losses inside the flow path, shock wave losses due to supersonic flow and trailing edge losses caused by wake flow after trailing edge. Secondary losses also have an important effect on turbine efficiency and they are caused by the vortices inside the boundary layer of blade passage.

Losses mostly occur at rotor section of the turbine. Stator loss coefficients are generally lower when they are compared to rotor losses [23]. Most significant rotor losses can be classified as following.

Incidence losses. In the turbine, fluid is guided by the stator to enter the rotor at the most suitable angle. However, small amount of energy is spent during this transition. Effect of this loss type increases at the off design condition of turbine because required energy increases at high or low rotational speed and mass flow rates. Incidence loss coefficient can be calculated as follows;

$$\xi_{in} = \frac{W_2^2 sin^2(\alpha_i)}{2} \tag{2.27}$$

In the literature, incidence angle lies between 20 and 40 degree to obtain the suitable flow path with minimum amount of vortices [24].

Passage losses. This losses occur between rotor blades and consist mostly loss of kinetic energy due to separation. Passage loss coefficient is firstly formulized by Futral

and Wasserbauer as following [23, 25];

$$\xi_p = \frac{0.3(W_2^2 cos^2(\alpha_i) + W_3^2)}{2} \tag{2.28}$$

Tip clearance losses. As the nature of turbine, there must be a gap between rotor blade tip and shroud. This gap causes some leakage and the distance between blade and shroud is decided according to aerodynamic and manufacturing necessities. As a result, this leakage results with energy loss in specific work [26, 27]. In the literature this loss is described with the following equation by Rodgers [22];

$$\Delta\eta_{tt} = K_a(\frac{\epsilon_a}{L_2}) + K_r(\frac{\epsilon_r}{L_3}) \tag{2.29}$$

Windage (Disk Friction) losses. In addition to the losses in the flow path and above the flow path, losses occurs also between the back side of the rotor and case of the turbine [22]. Disk frictional torque can be calculated with the equation created by Daily and Nece [28] as following;

$$\tau_{fric} = K_{df}(0.25)\rho U_2^2 r_2^3 \tag{2.30}$$

3. PRELIMINARY DESIGN

Turbines are the most critical component of cycles and even a small change in its isentropic efficiency directly affects the cycle efficiency and power output. Therefore, turbine designs should be cycle specific to be able to get the maximum power from cycle. Turbine preliminary design is the first and most important step of whole turbine design process and there are important studies in the literature for design process [20,29,30]. In this chapter, firstly, a general, simple ORC analysis is performed for R245fa and R134a organic fluids in order to observe the potential power output and cycle efficiency. Then, results found in cycle analysis are used to estimate the suitable turbine geometries and parameters. After generating the maps to understand the relationship between cycle boundary conditions and turbine parameters, finally the specific turbine preliminary design is performed in Chapter 4 by taking into consideration the limitations of BURET Laboratory ORC system facility.

3.1. Basic ORC Analysis for R245fa and R134a

Organic fluids consist of varied molecular structures therefore they can have different thermodynamics parameter values at same boundary conditions. (i.e. for same temperature and pressure values). Because the primary purpose is to design an efficient radial inflow turbine with a subsonic flow path at its design point, main variable of the cycle analysis will be the pressure ratio between turbine inlet and outlet. In Figure 3.1, temperature-entropy diagram of R245fa and cycle process states are presented. 1, 2, 3 and 4 are the turbine inlet, outlet, condenser outlet and pump outlet state respectively.

Cycle analyses are performed for three pressure ratio values. Maximum pressure ratio is selected according to the recommended limitation for an efficient, subsonic one stage radial inflow turbine design [31]. Six different turbine outlet pressure values are selected and cycle efficiencies are calculated for these six outlet pressure values at three different pressure ratio. Outlet pressure values for R245fa and R134a are selected

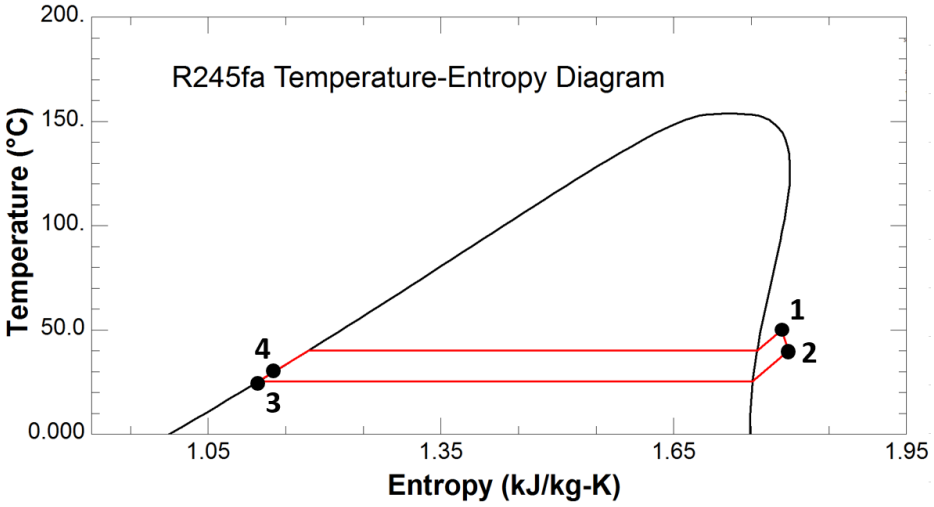

Figure 3.1. Temperature vs Entropy Diagram of R245fa.

according to their saturation temperatures. Details of the selected boundary conditions can be seen in Appendix A. Several important assumptions used during the analyses are listed below:

- Turbine efficiency is 85 %
- Cycle pressure losses are neglected.
- Temperature (Enthalpy) rise at the pump is neglected (ie. $H_3 = H_4$)

Given or known parameters are as following:

- Turbine outlet pressure
- Cycle pressure ratio
- For R245fa, turbine inlet temperature(max. 1^0C super heat)
- For R134a, turbine outlet temperature(max. 1^0C super heat)
- Saturated liquid enthalpy value at condenser pressure
- Cycle power input is 100 kW.

To start the analysis, turbine inlet pressure is calculated for a given outlet pressure and pressure ratio. Because R245fa is a dry fluid, there is no possibility of the expanding gas to end up in a liquid-gas mixture state. Therefore, temperature of the turbine inlet is fixed and the outlet temperature value is found in gas phase for an isentropic process. However, R134a is a wet fluid, therefore during the cycle analysis for this fluid, temperature of the turbine outlet is fixed so that the fluid is still in gas phase after expansion process. As a result, turbine inlet temperature is found for an isentropic process. Thus, turbine inlet and outlet conditions are fixed. Condenser pressure is the same as turbine outlet pressure. Then, the corresponding liquid enthalpy value for the given condenser pressure is found. With the known enthalpy values at the inlet of the turbine and exit of the condenser, mass flow rate can be calculated for a given heat rate input as follows:

$$\dot{m} = \frac{\dot{Q}_{heater}}{H_1 - H_4} \tag{3.1}$$

After finding mass flow rate, one can calculate the required chiller capacity by using the following equation:

$$\dot{Q}_{chiller} = \dot{m}(H_2 - H_3) \tag{3.2}$$

$$N = \dot{m}(H_1 - H_{2s})\eta_s \tag{3.3}$$

Thus, turbine power output is found according to ideal enthalpy drop and 85.0 % turbine efficiency with equation 3.3. Finally, efficiency of the cycle is calculated by using the following equation:

$$\eta_{cycle} = \frac{H_1 - H_2}{H_1 - H_4} \tag{3.4}$$

As a result, cycle efficiencies are found at 18 boundary conditions for three different pressure ratio by using R245fa and R134a. Results are presented in Figure 3.2 and 3.3 respectively for R245fa and R134a. Details of the results can be seen in Appendix A.

Figure 3.2 shows that the highest cycle efficiency, 10.4 %, is reached when the pressure ratio is maximum. Also it is observed that the efficiency is increasing with rising turbine outlet pressure for the same pressure ratio. Minimum cycle efficiency is found as 5 % for the PR=2.

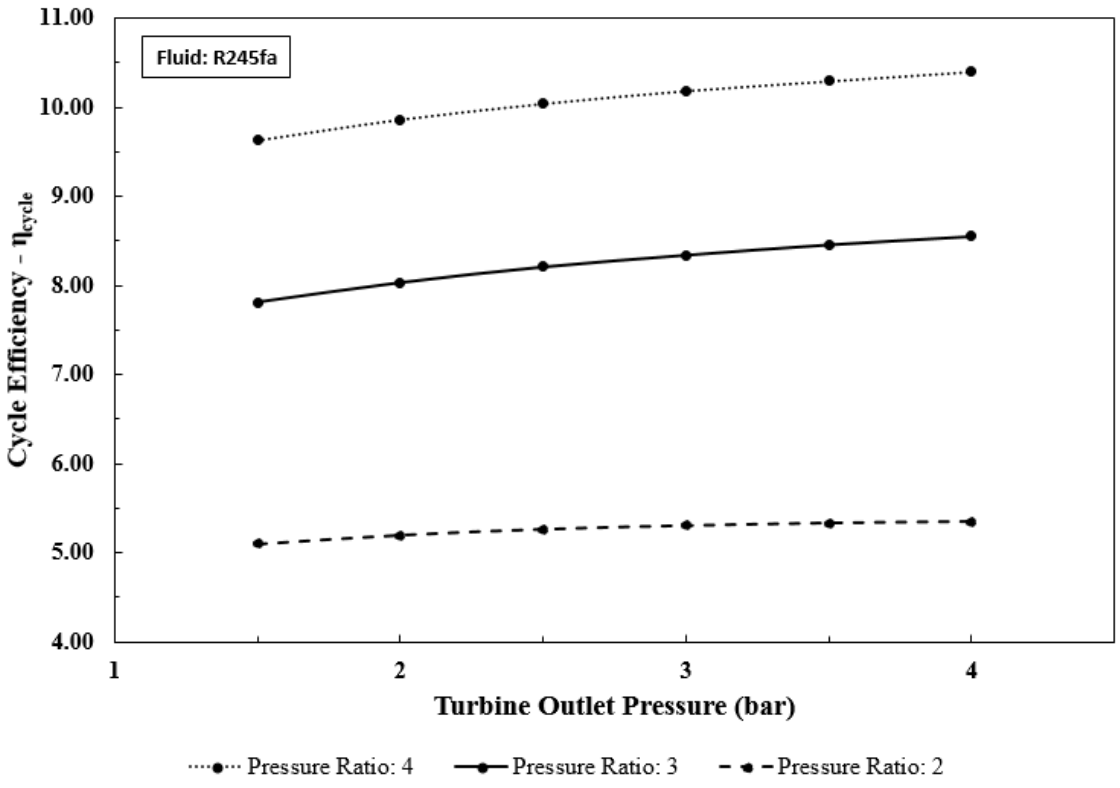

Figure 3.2. R-245fa Cycle Efficieny vs Turbine Outlet Pressure Lines for Different Pressure Ratio.

In Figure 3.3, cycle efficiencies for R134a are shown where the pressure ratio values are same as R245fa case. Maximum efficiency for R134a is found as 11.4 % at PR=4 which is 1 % higher than the cycle that works with R245fa.

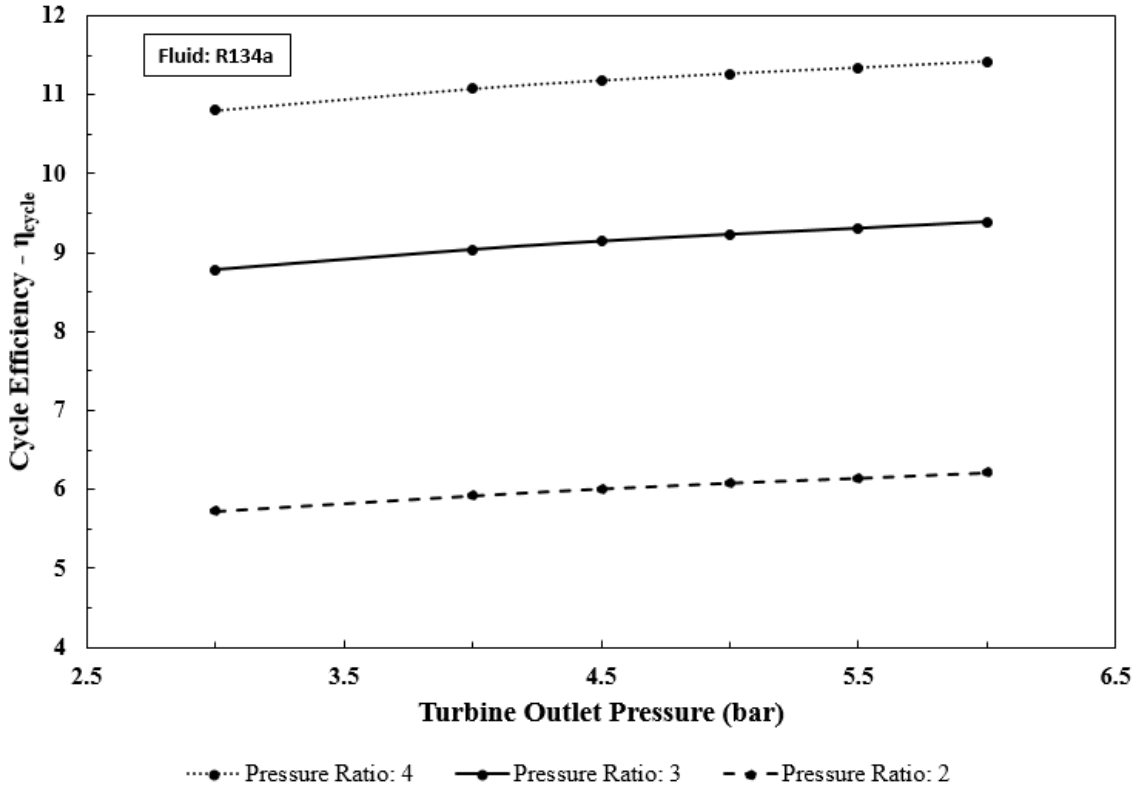

Figure 3.3. R-134a Cycle Efficieny vs Turbine Outlet Pressure Lines for Different Pressure Ratio.

Results show that, maximum cycle efficiency values of ORC for given pressure ratios are around 10 % which is significantly lower than average steam cycle (i.e. Rankine Cycle) efficiency. However this is not a surprising result because, working condition of steam cycles have much higher pressure ratio and temperature values than ORC. In Table 3.1, maximum theoretical (Carnot) cycle efficiency values are presented with the actual cycle efficiency values for given pressures. It can be seen that the maximum theoretical efficiency is 12.0 % for the case where the maximum actual cycle efficiency

was found. As a reminder, Carnot cycle efficiency is calculated as following;

$$\eta_{carnot} = 1 - \frac{T_C}{T_H} \tag{3.5}$$

Table 3.1. Actual vs Carnot Cycle Efficiency.

Highest Cycle Pressure (bar)	Lowest Cycle Pressure (bar)	Actual Cycle Efficiency (%)	Carnot Cycle Efficiency (%)
3.0	1.5	5.1	5.5
4.5	1.5	7.8	8.6
6.0	1.5	9.6	10.9
6.0	3.0	5.3	5.7
9.0	3.0	8.3	9.1
12.0	3.0	10.2	11.5
8.0	4.0	5.4	5.9
12.0	4.0	8.6	9.4
16.0	4.0	10.4	12.0

Increase in the pressure ratio results with higher enthalpy difference in the turbine. However, at high pressure ratio values, shock waves occur in the turbine flow path and it affects the turbine efficiency dramatically. Therefore, pressure ratio should be limited to avoid choked flow in the turbine flow path and low turbine efficiency.Detailed results of the calculations for several cycle conditions can be seen in Appendix A and B.

In Section 3.2, turbine geometries will be generated by taking into consideration the cycle boundary conditions. Also, maps that show the suitable turbine geometries for each boundary condition are presented.

3.2. Preliminary Turbine Geometry Generation

For the generated boundary conditions, one can start to evaluate the geometry of turbine. There are many correlations in the literature and in this study Aungier's Turbine Aerodynamics book is used [20] as a reference. In his book, design process

starts with Balje's specific speed definition which is shown in Equation 3.6.

$$n_s = \frac{\omega\sqrt{Q_3}}{(\Delta H_{id}^*)^{0.75}} \tag{3.6}$$

Specific speed, n_s, is chosen as 0.55 according to turbine total to static efficiency - specific speed graph in Aungier's Turbine Aerodynamics book where the recommended range is between 0.45 and 0.75 [20]. For the given range, total to static efficiency shows difference between 80 % and 85 %. Also the volume flow rate, Q_3, can be calculated for given mass flow rate using density of the fluid at the exit of the turbine. Thus, the rotational angular speed is found by putting the isentropic total enthalpy drop, ΔH_{id}^*, value into equation 3.7.

$$\omega = \frac{n_s(\Delta H_{id}^*)^{0.75}}{\sqrt{Q_3}} \tag{3.7}$$

To calculate the basic parameters of the turbine rotor, equations from 3.7 to 3.22 are used.

Firstly, rotor inlet blade speed is calculated as follows:

$$U_2 = \vartheta_s C_{s0} \tag{3.8}$$

where the result of spouting velocity, C_{s0}, and total to static velocity ratio, ϑ_s are found as follows:

$$C_{s0} = \sqrt{2\Delta H_{id}^*} \tag{3.9}$$

$$\vartheta_s = 0.737 n_s^{0.2} \tag{3.10}$$

Inlet and outlet hub radius of the rotor are calculated with the following two equations respectively.

$$r_2 = \frac{U_2}{\omega} \tag{3.11}$$

$$r_{3h} = 0.185 r_2 \tag{3.12}$$

Leading edge height of the turbine, L_2, can be calculated by using the definition of mass flow rate follows:

$$L_2 = \frac{\dot{m}}{2\pi r_2 \rho_2 C_{2m}} \tag{3.13}$$

Meridional component, $\vec{C}_{2m}$, and tangential component, $\vec{C}_{2u}$, of absolute velocity, $\vec{C}$, are determined from the following two equations respectively.

$$C_{2m} = C_{2u} \tan \alpha_2 \tag{3.14}$$

$$C_{2u} = \frac{U_2 \eta_s}{2\vartheta_s^2} \tag{3.15}$$

In equation 3.15, η_s is the isentropic turbine efficiency. Also, in equation 3.14, α_2 indicates the rotor inlet absolute flow angle and it is calculated as follows:

$$\alpha_2 = 10.8 + (14.2)n_s^2 \tag{3.16}$$

.

Relationship between inlet and outlet meridional flow speed is shown in the following equation:

$$C_{3m} = C_{2m}\left[1 + 5\left(\frac{L_2}{r_2}\right)^2\right] \tag{3.17}$$

Rotor outlet tip radius, r_{3t}, is proportional with inlet radius of rotor so that;

$$r_{3t} = 1.29 n_s r_2 \tag{3.18}$$

Finally, rotor trailing edge height, L_3, and axial rotor length , L_{ax}, can be calculated by

$$L_3 = r_{3t} - r_{3h} \tag{3.19}$$

$$L_{ax} = 1.5\,(r_{3t} - r_{3h}) \tag{3.20}$$

Preliminary turbine geometry can now be generated by using equations from 3.6 to 3.20. Detailed results of the calculations for several cycle conditions can be seen in Appendix B.

3.3. Turbine and Cycle Relation

In the final section of this chapter, relationships between cycle boundary conditions and turbine geometries, which are calculated according to the preliminary design considerations, are presented.

During the analysis, three pressure ratio values are investigated at three heat rate (power input) cases which are 100 kW, 500kW, 1MW. The main reason is to show the effects of energy source capacity on turbine dimensions. As a result, relation between rotor diameter, rotational speed, mass flow rate, rotor inlet absolute mach number and turbine power output are presented in the following figures for R245fa and R134a. These relations are presented at three different pressure ratio and three cycle power inputs.

In Figure 3.4 and 3.5, rotational speed change with respect to outlet pressure for R245fa and R134a are shown respectively. First important observation is the reduction of rotational speed with increase in power supply for all pressure ratio. Proportional increase of mass flow rate with power supply is the reason of this reduction for the same pressure ratio and outlet pressure value.In addition, rise in the outlet pressure value also causes an increase in rotational speed for a constant power input and pressure ratio due to the density augmentation at turbine outlet condition. Finally, for all heat input cases, it is observed that the pressure ratio and rotational speed are proportional to each other.

Similar behaviors can be observed for both R245fa and R134a. However, a slight difference exists between rotational speeds of two fluids for the same pressure ratio and heat supply. For example, rotational speeds are calculated as 50000 and 55000 rpm for R-245fa and R134a respectively while the pressure ratio is 3 and heat input value is 100 kW at 3 bar turbine outlet pressure. This rotational speed difference between two organic fluids changes inversely proportional with heat supply capacity of system.

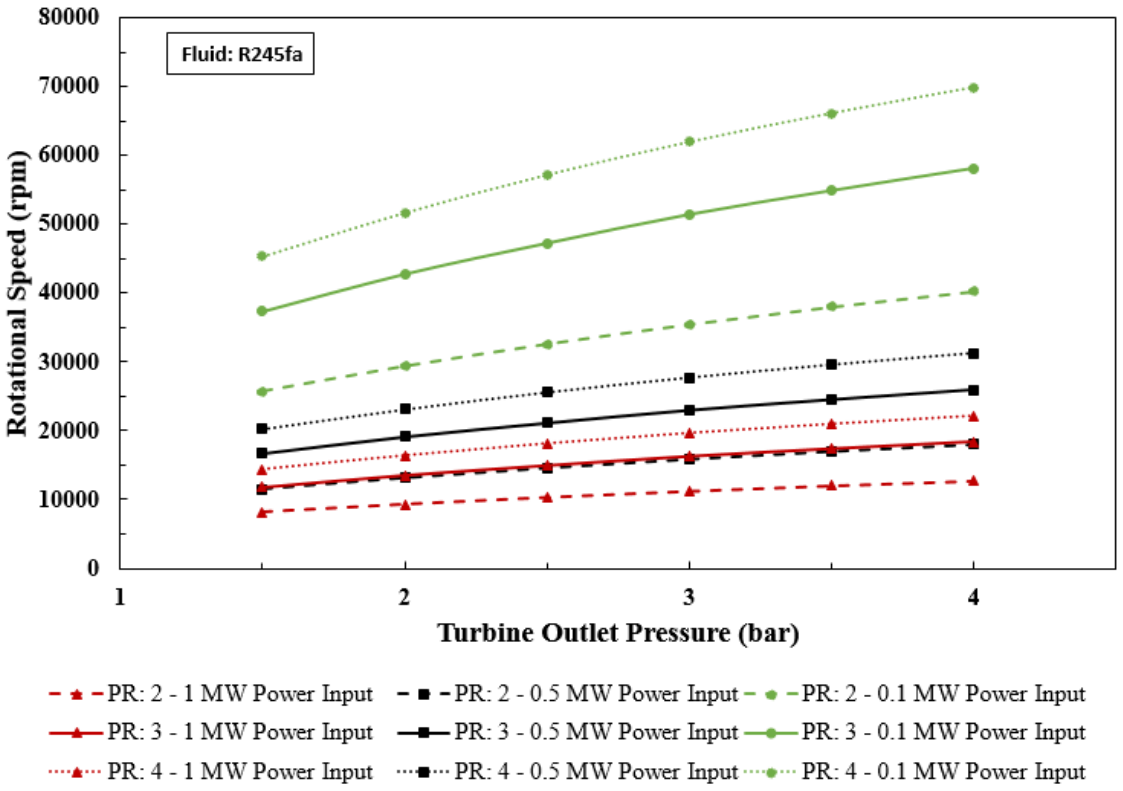

Figure 3.4. R-245fa Rotational Speed vs Turbine Outlet Pressure Lines for Different Pressure Ratio.

Figure 3.6 and 3.7 present the required rotor inlet diameters for given pressure ratio and heat input. General trends show that rotor inlet diameter increases with rising heat input. A cycle with 100 kW power input, requires a rotor diameter which changes between 40 mm. and 80 mm. according to pressure ratio and outlet pressure value while this range is between 125 mm. and 250 mm. for a cycle with 1 MW heat supply. As it can be seen, turbine outlet pressure decision gains more importance at high power sources.

Another important observation is the inverse proportionality between pressure ratio and rotor diameter independent from heat source capacity. Similar behaviors are observed for both fluids and it can be said that the diameter requirements of R134a and R245fa are close to each other.

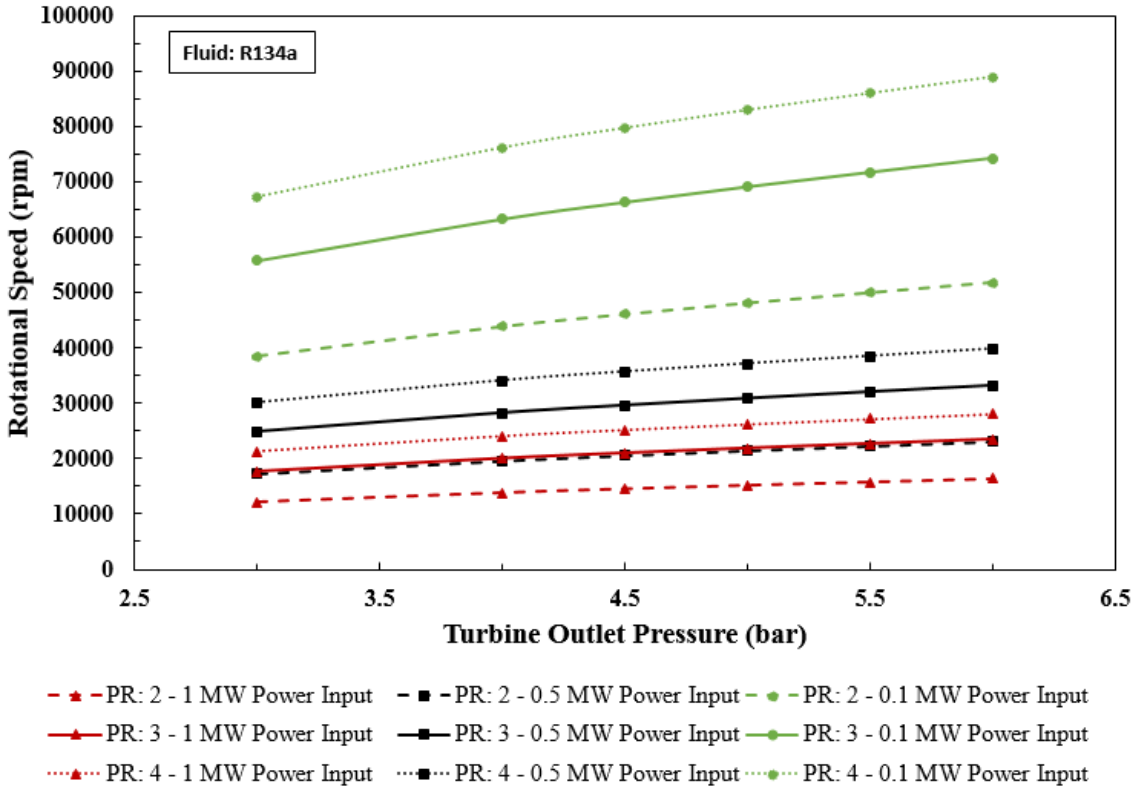

Figure 3.5. R-134a Rotational Speed vs Turbine Outlet Pressure Lines for Different Pressure Ratio.

During the boundary condition decision process for turbine, one of the most critical parameter that should be investigated is the Mach number. Shock waves are one of the main reasons for turbine losses. Therefore, before the detailed 3D turbine design, one should estimate the maximum Mach number that can be occurred in the turbine sections.

Absolute and Relative Mach number at the turbine is calculated by using the following equations respectively. Speed of sound, c, data are taken from NIST Refprop 9.1 fluid properties database.

$$M_{abs} = \frac{C}{c} \tag{3.21}$$

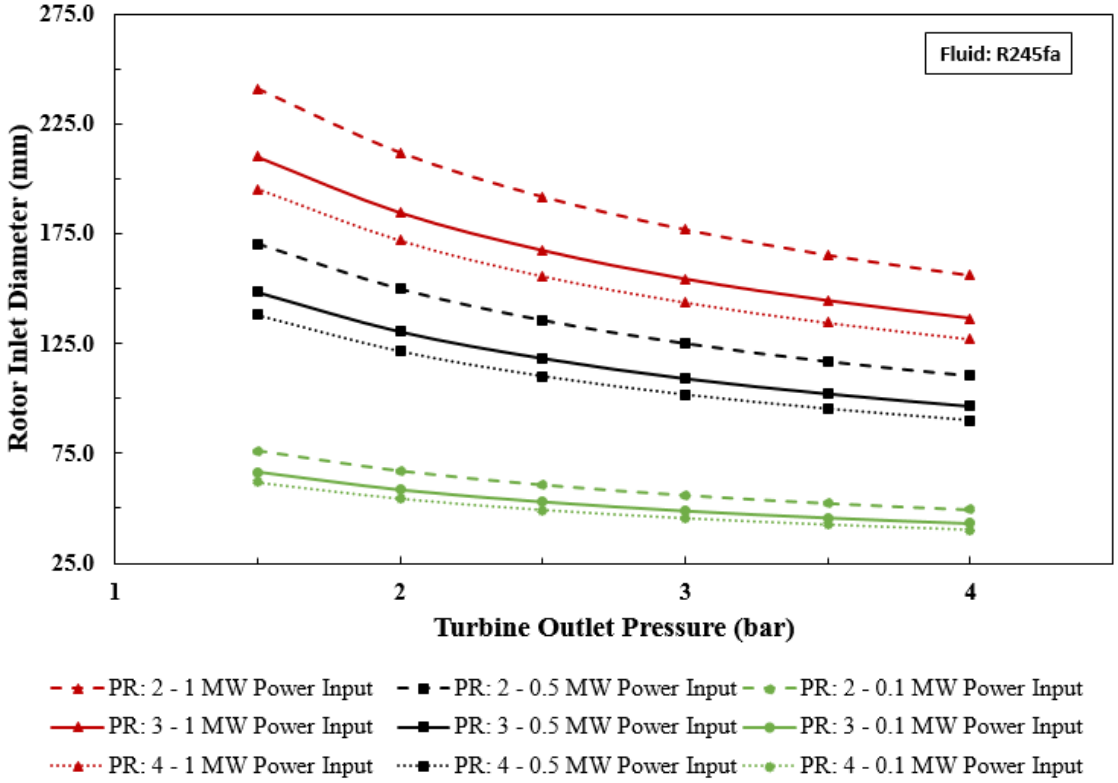

Figure 3.6. R-245fa Rotor Inlet Diameter vs Turbine Outlet Pressure Lines for Different Pressure Ratio and Power Input.

$$M_{rel} = \frac{W}{c} \tag{3.22}$$

In Figure 3.8 and 3.9, rotor inlet absolute Mach numbers are presented. At the inlet of the rotor relative velocity is smaller than the absolute velocity while the relative velocity at the outlet of the rotor is higher than absolute velocity. Therefore, one should check absolute velocity at the rotor inlet and relative velocity at the rotor exit.

Increase in the pressure ratio results a higher Mach number as expected. It is seen that to stay in the subsonic flow regime, pressure ratio should not exceed 3 if the outlet pressure value is smaller than 1.5. This ratio should be reduced for higher turbine outlet pressures. Results are similar for both fluids as expected.

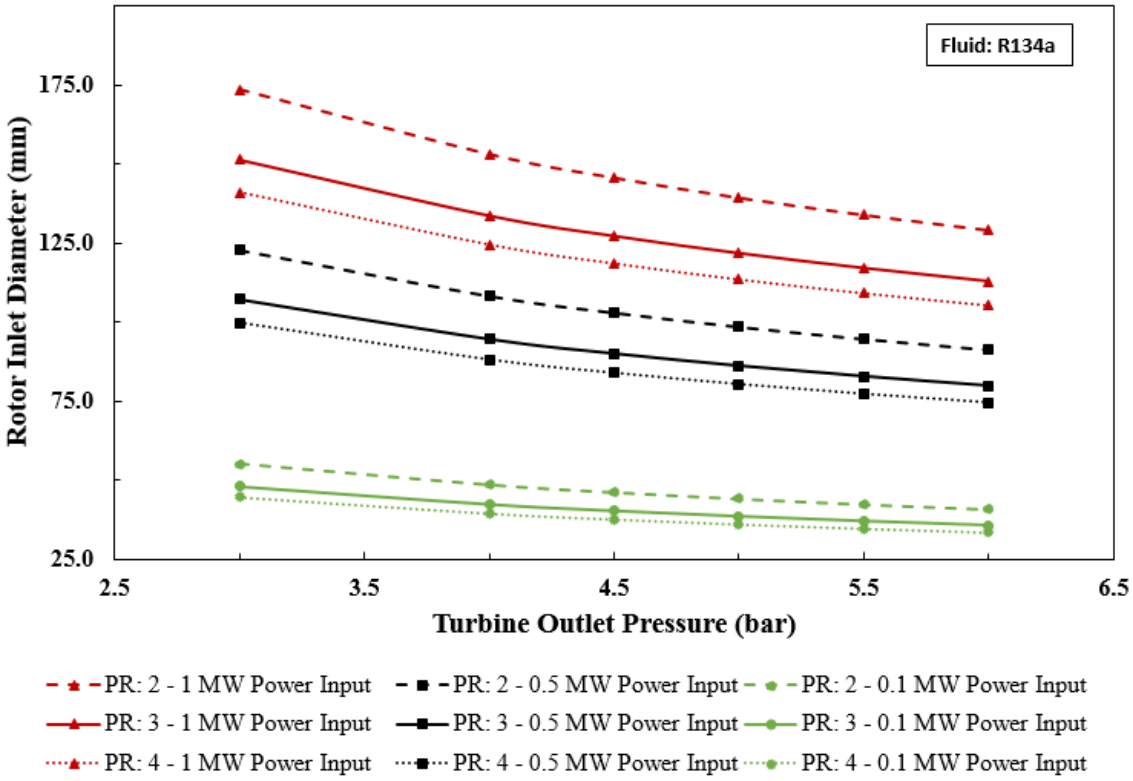

Figure 3.7. R-134a Rotor Inlet Diameter vs Turbine Outlet Pressure Lines for Different Pressure Ratio and Power Input.

As the last two comparisons, mass flow rates and turbine power outputs with respect to rotor inlet diameters are presented.

In Figure 3.10 and 3.11, mass flow rate and rotor inlet diameter relation for efficient turbine design are shown. There are three group of turbine dimension exist which are separated from each other according to cycle heat supply capacities.

For R245fa cycles with 100, 500 and 1000 kW power input capacity, it is calculated that the necessary mass flow rates should be close to 0.5, 2.5 and 5 kg/s while the rotor diameters changes between 40 to 80, 90 to 170 and 125 to 225 mm. respectively. Points on the pressure ratio lines are the outlet pressure values shown in the previous figures.

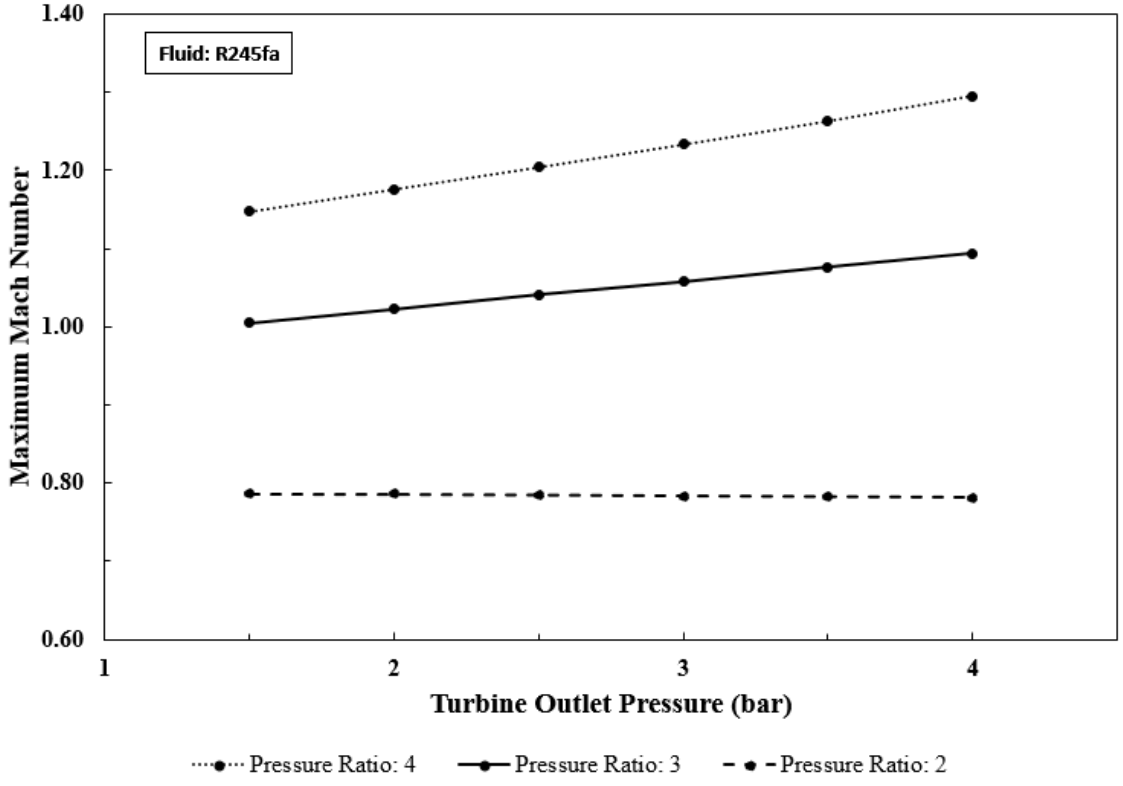

Figure 3.8. R-245fa Rotor Inlet Absolute Mach Number vs Turbine Outlet Pressure Lines for Different Pressure Ratio.

Similar mass flow rate and diameter distribution is also observed for R134 cycle at all levels of heat source capacity. Details can be seen in Figure 3.11.

Lastly, in Figure 3.12 and 3.13, generated power from corresponding turbine dimensions are presented for R245fa and R134a cycles respectively. Pressure ratio is the key factor to obtain desired power output for a specific power source. However, it is seen that the effect of pressure ratio increases with rising power input.

As a result of all these analyses, dimensions of turbines for several power output purposes were generated and their mass flow rate, rotational speed requirements were calculated for different pressure ratio values. With all these experiences about relationship between turbine kinematic and thermodynamics parameters, one can start a

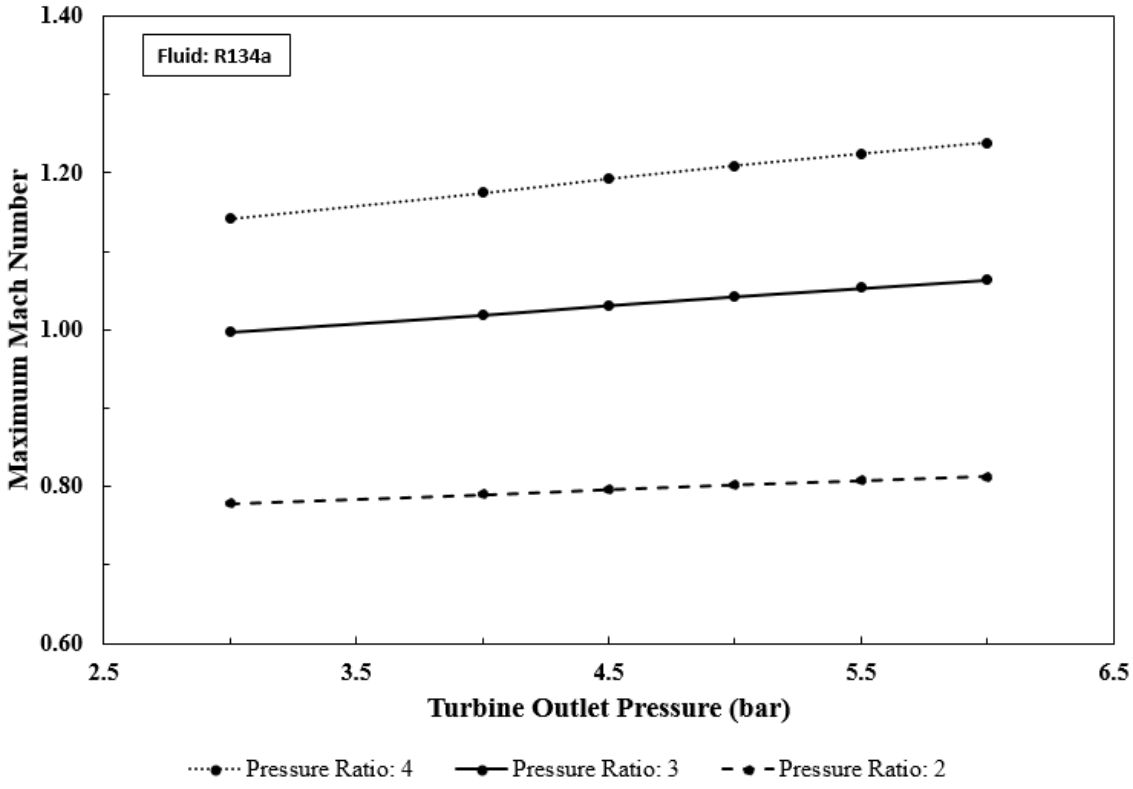

Figure 3.9. R-134a Rotor Inlet Absolute Mach Number vs Turbine Outlet Pressure Lines for Different Pressure Ratio.

preliminary design for a specific case. After this point, all studies are conducted to generate a unique turbine geometry for a specific ORC system which has a 100 kW power input.

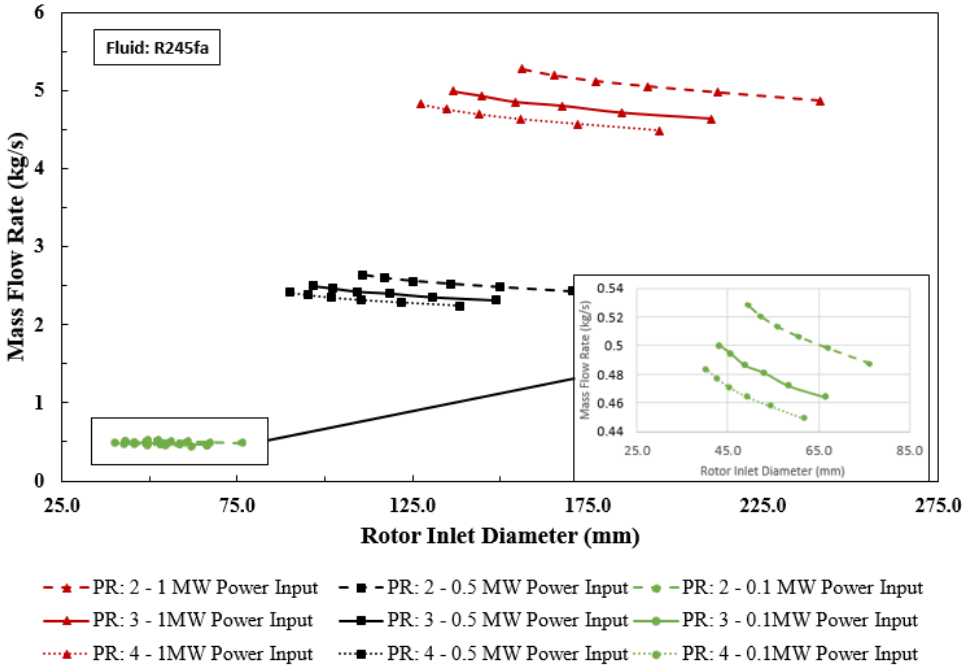

Figure 3.10. R-245fa Mass Flow Rate vs Rotor Inlet Diameter Lines for Different Pressure Ratio and Power Input.

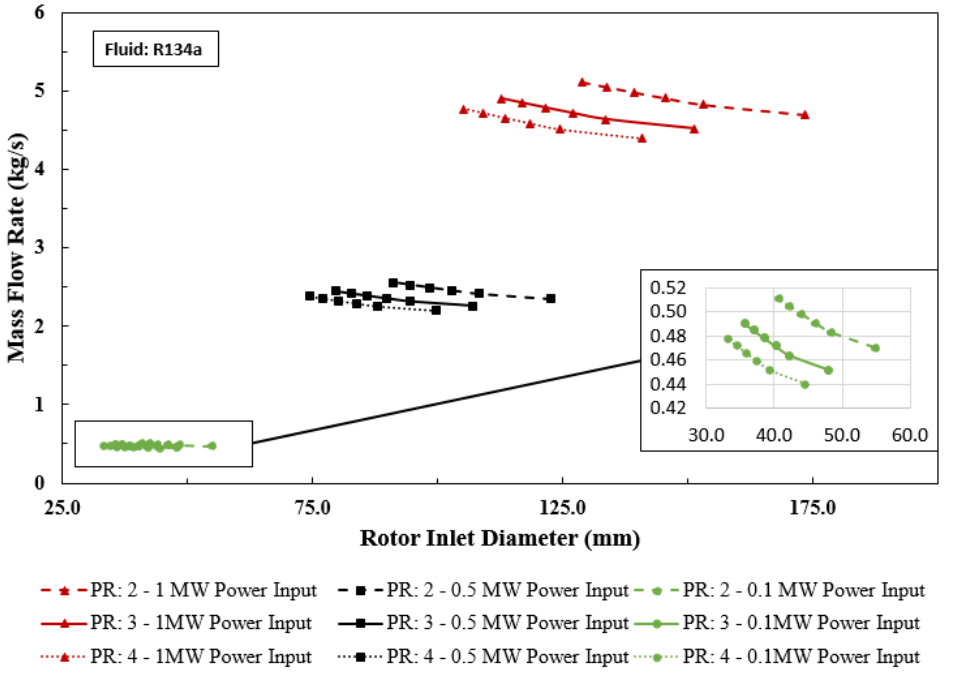

Figure 3.11. R-134a Mass Flow Rate vs Rotor Inlet Diameter Lines for Different Pressure Ratio and Power Input.

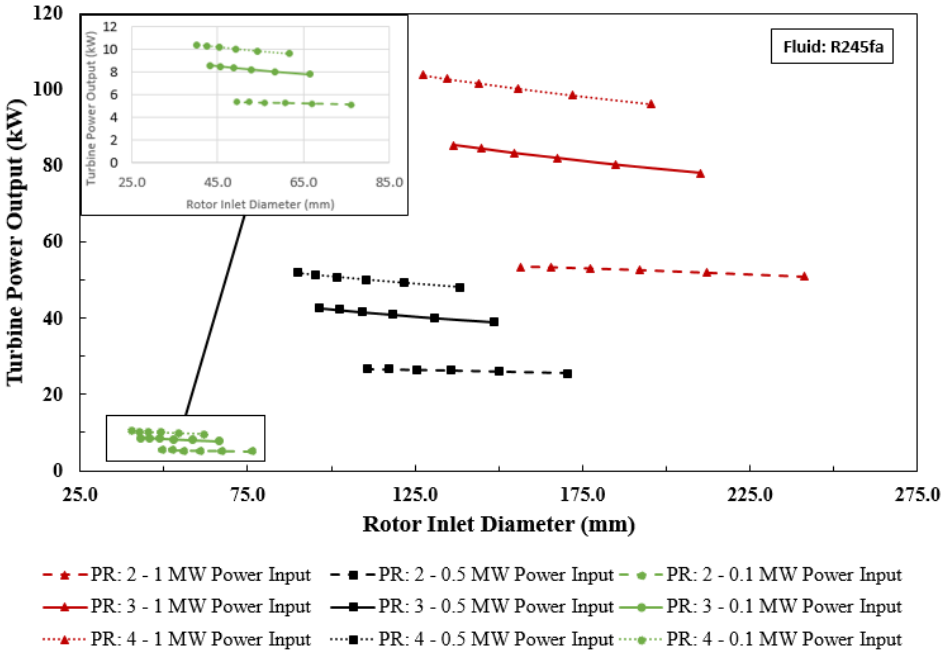

Figure 3.12. R-245fa Turbine Power Output vs Rotor Inlet Diameter Lines for Different Pressure Ratio and Power Input.

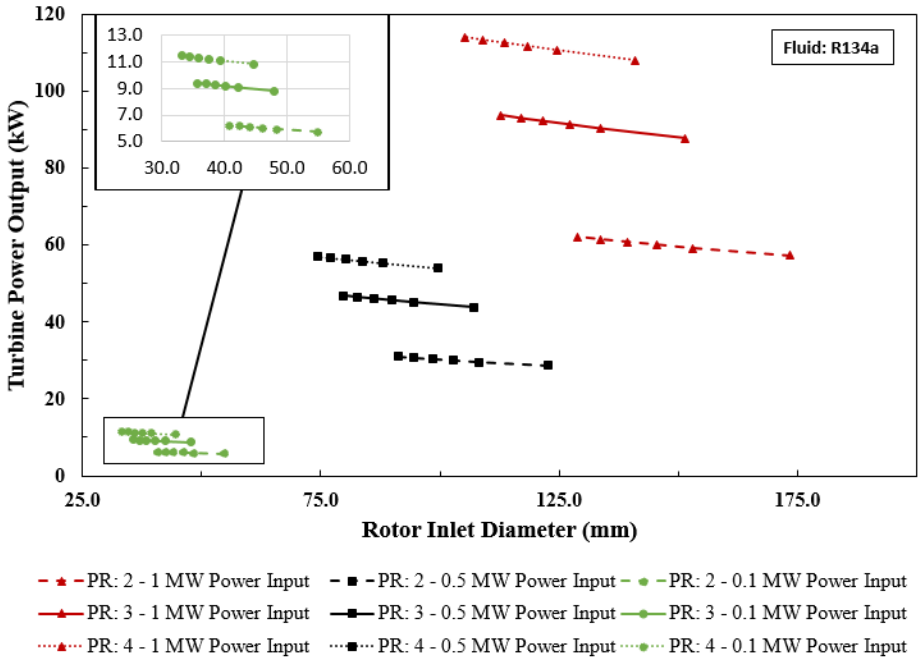

Figure 3.13. R-134a Turbine Power Output vs Rotor Inlet Diameter Lines for Different Pressure Ratio and Power Input.

4. PRELIMINARY DESIGN FOR SPECIFIED ORC SYSTEM

Preliminary design process for a specific case consist of two parts. In the first part, boundary conditions are decided and in the second part, these parameters are used to determine the basic turbine geometry.

4.1. Determination of Design Condition

In this section, design conditions of the turbine are determined by satisfying the Bogazici University Renewable Energy Technologies Laboratory (BURET Lab.) ORC test bed limitations. Photographs of the ORC test bed, heater and chiller of the established system can be seen in Figure 4.1 and Figure 4.2 respectively. Primary constraints of the ORC system in BURET Lab. are listed as follows:

- Capacity of Electric Heater:

$$N_{heater} = 100kW$$

- Capacity of Chiller:

$$N_{chiller} = 100kW$$

- Condenser inlet pressure:

$$p_3 = 1.5bar$$

During the preliminary design process, these limitations will be the guide to find the optimum design conditions of the turbine. In order to specify the inlet and outlet conditions, four parameters should be fixed. Firstly, outlet pressure and temperature

Figure 4.1. Organic Rankine Cycle.

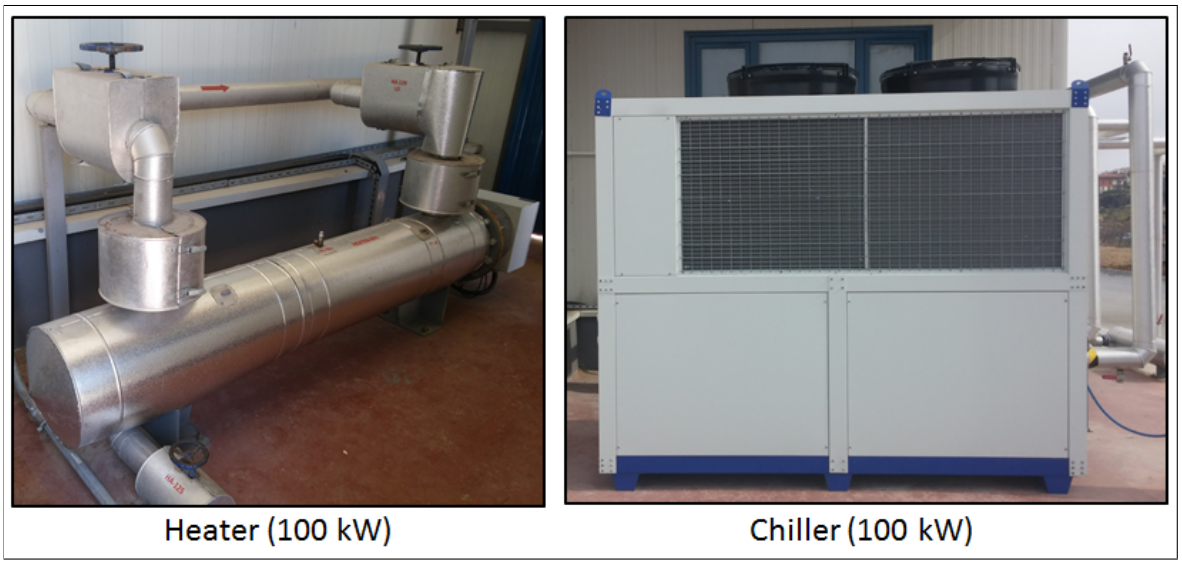

Figure 4.2. Heater and Chiller.

values of the turbine are fixed to 1.5 bar and 33 ^0C respectively. Liquid enthalpy of the fluid at desired outlet condition can be seen in Table 4.1.

Table 4.1. Saturation Point Data of R245fa at 1.5 bar

Pressure	bar	1.50
Temperature	^0C	25.32
Liquid Enthalpy	kJ/kg	232.88

Last two parameters to be fixed are the turbine inlet temperature and pressure values.To decide the proper pressure value to stay in the subsonic region at the turbine inlet, three different cases are generated and investigated for three different pressure ratio. By using the constant outlet pressure and temperature values, for an isentropic expansion process, inlet temperatures of the turbine at these three assigned inlet pressures can be found. In Table 4.2, inlet and outlet boundary conditions of these three cases are shown.

Table 4.2. Boundary Conditions for 3 Different Pressure Ratio

Fluid: R245fa	Unit	Case-1		Case-2		Case-3	
		Inlet	Outlet	Inlet	Outlet	Inlet	Outlet
Pressure Ratio	-	4.0		3.0		2.0	
Pressure	bar	6.0	1.5	4.5	1.5	3.0	1.5
Temperature	^0C	70.3	33.0	61.8	33.0	50.6	33.0
Density	kg/m^3	33.14	8.36	24.64	8.36	16.42	8.36
Enthalpy	kJ/kg	455.6	430.3	450.3	430.3	442.9	430.3
Speed of Sound	m/s	131.8	136.6	134.1	136.6	135.9	136.6

After fixing the temperature and pressure values of the three cases, maximum mass flow rates can be calculated with equation 3.1 by taking into consideration the heater and chiller capacity of the specified ORC system.

Finally, in Table 4.3 estimated net power output and mass flow rate values for three different pressure ratio are shown. Isentropic turbine efficiency are assumed to be 85.0 % for all cases. As a result, Case-1 which has the highest pressure ratio, generates more power than others as expected. However, final decision for the design point

Table 4.3. Results of 3 different boundary case according to limitations

	Unit	Case-1	Case-2	Case-3
Max. Heater Power Input	kW	100	100	100
ΔH_{id}	kJ/kg	25.2	20.0	12.6
Mass Flow Rate	kg/s	0.45	0.46	0.48
Estimated Turbine Efficiency	%	85	85	85
Net Power Output	kW	9.6	7.8	5.1

should not be given yet because there is an optimum pressure ratio for a given mass flow rate value to design an efficient turbine and to stay in the subsonic region. Therefore, velocity triangles should be generated for these 3 cases and mach numbers should be calculated. For this purpose, in the following section, preliminary turbine geometry parameters are going to be calculated for these 3 cases.

4.2. 2D Turbine Geometry Generation

As it was mentioned in Section 3.2, turbine rotor parameters are calculated by using equations from 3.7 to 3.22. Detailed results of these calculations for 3 cases can be seen in Table 4.4.

Table 4.4. Geometric and Thermodynamics Preliminary Design Results of 3 cases

Fluid: R245fa	Unit	Case-1		Case-2		Case-3	
		Inlet	Outlet	Inlet	Outlet	Inlet	Outlet
GEOMETRIC RESULTS							
Rotational Speed	rpm	45360		37655		26150	
Blade Tip Velocity	m/s	146.87	104.20	130.76	92.77	103.73	73.59
Rotor Hub Radius	mm	30.92	5.72	33.16	6.13	37.88	7.01
Rotor Tip Radius	mm	30.92	21.94	33.16	23.53	37.88	26.88
Blade Height (LE and TE)	mm	1.77	16.22	2.56	17.39	4.38	19.87
Rotor Axial Length	mm	24.33		26.09		29.80	
Rotor Blade thickness	mm	1.24	0.62	1.33	0.66	1.52	0.76
Rotor Absolute Flow Angle	deg	15.10	90.00	15.10	90.00	15.10	90.00
THERMODYNAMICS RESULTS							
Mass Flow Rate	kg/s	0.45		0.46		0.48	
Temperature	^0C	70.30	33.00	61.80	33.00	50.60	33.00
Pressure	bar	6.00	1.50	4.50	1.50	3.00	1.50
Mach Number	-	1.15	0.29	1.00	0.26	0.81	0.22
Density	kg/m^3	33.13	8.36	24.64	8.36	16.42	8.36

According to the results obtained from preliminary turbine geometry calculations, thermodynamics boundary conditions and geometric estimations, Case-3 is chosen as the design point due to its low (subsonic) mach number value at the inlet of the rotor. From this point on, turbine design is going to be performed by using the results of Case-3.

In Chapter 5, these results are used to create the first 3-D model of the turbine. Then, streamline analysis is performed for this 3-D turbine geometry and the results are compared with the results of preliminary design stage to see whether the raw 3-D turbine geometry satisfies the boundary conditions and performance expectations.

5. 3D BLADE DESIGN

3-D turbine geometry is generated in software after completing preliminary design stage by using the preliminary design results of Case-3. Generated turbine has 24 stator blade and 16 rotor blade. This composed turbine geometry should be analyzed to check whether the mass flow rate, power output and turbine efficiency values found in preliminary design step meet the requirements for the given boundary conditions.

5.1. Streamline Analysis

In the streamline analysis, inlet total pressure, temperature, outlet static pressure and rotational speed are defined as input parameters. As a result, important thermodynamics and kinematic parameters such as turbine efficiency,power output, velocity triangles, enthalpy drop and also temperature, pressure, mach number, density distribution are calculated by considering the losses. In Table 5.1, comparison of preliminary design and streamline analysis results of the generated turbine is shown.

Results of the streamline analysis show that, calculated mass flow rate value, 0.84 kg/s, for the generated turbine geometry exceeds the desired value according to ORC system limitations. Also the 75.4 % turbine efficiency is below the targeted point while the power output is relatively high due to the high mass flow rate. Lastly, both calculation methods give similar Mach numbers at the inlet and outlet.

During the blade design process, one of the most important guide will be the velocity triangles of the turbine. In Figure 5.1, velocity triangles of the rotor are presented. These vectors are found as a result of streamline analysis performed for preliminary turbine geometry.

Because of the differences between the requirements and the calculated results of the streamline analysis, shape of the stator and rotor are optimized by changing their

Table 5.1. Comparison of Streamline Analysis and Preliminary Design Results

Fluid: R245fa	Unit	Streamline Analysis Result		Preliminary Design Result	
		Inlet	Outlet	Inlet	Outlet
Temperature (T)	^0C	50.60	33.00	50.60	33.00
Pressure (P)	bar	3.00	1.50	3.00	1.50
Mach Number (M)	-	0.78	0.37	0.81	0.22
Blade Tip Velocity (U)	m/s	103.73	73.59	103.73	73.59
Absolute Flow Velocity (C)	m/s	102.29	51.40	106.77	29.67
Relative Flow Velocity (W)	m/s	71.15	104.86	27.81	79.35
Absolute Flow Angle (α)	deg	40.40	67.16	15.10	90.00
Relative Flow Angle (β)	deg	111.29	26.86	90.00	21.96
Total to Static Efficiency (η_{ts})	%	75.40		85.00	
Power Output ($\dot{W}$)	kW	7.95		5.09	
Rotational Speed (n)	rpm	26,150		26,150	
Mass Flow Rate ($\dot{m}$)	kg/s	0.84		0.48	

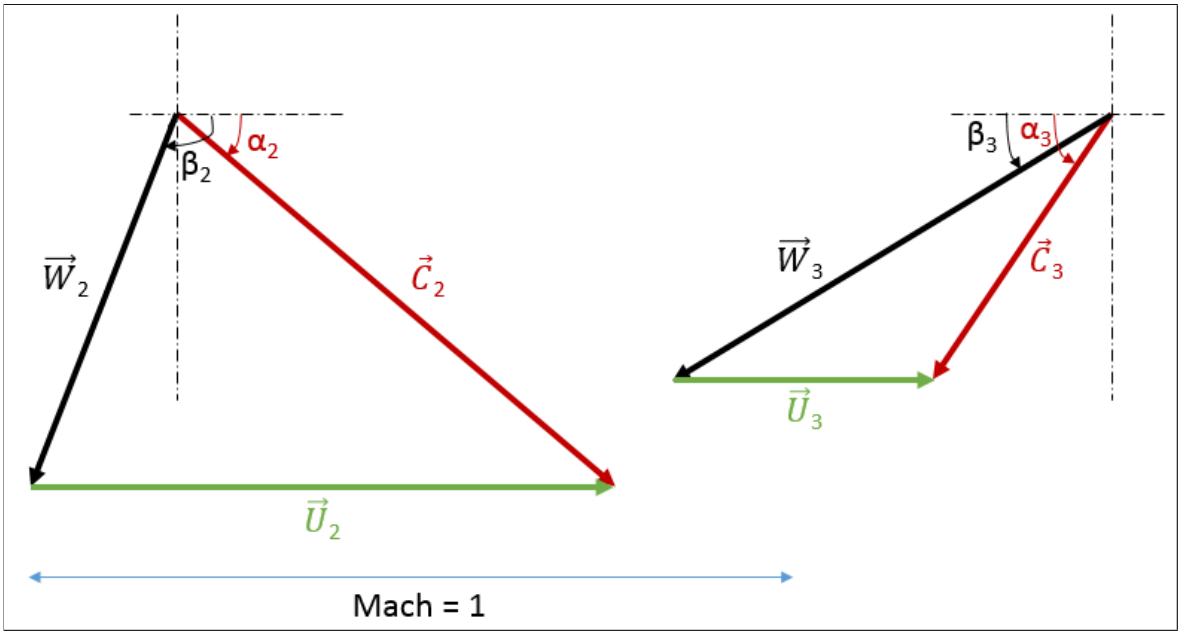

Figure 5.1. Preliminary Design Velocity Triangles at Rotor Inlet and Outlet.

geometric and kinematic parameters to reach the maximum efficiency at the design point by using AxStream 3-D Blade Design Tool. Flow chart used during the 3-D blade design process is presented in Figure 5.2.

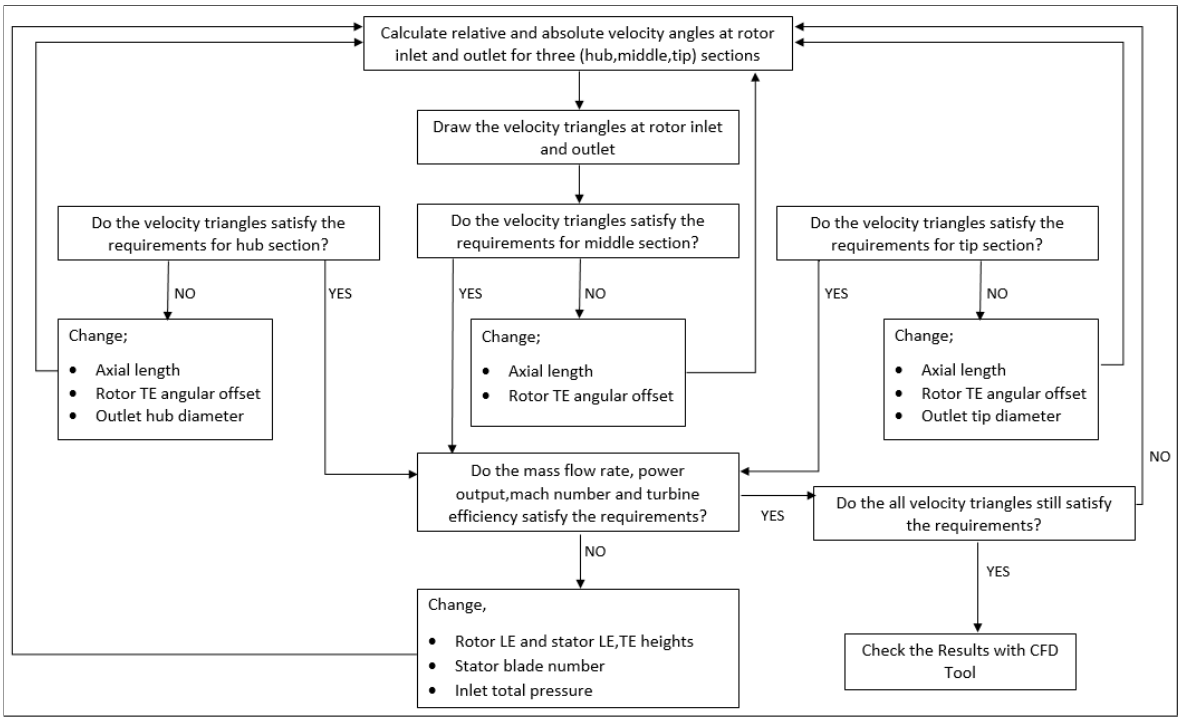

Figure 5.2. Streamline Analysis and 3D Blade Design Optimization Process Scheme.

As the final step of 3D blade design process, in Section 5.2, details of the CFD analysis performed during and after the design process are explained.

5.2. 3D CFD Analysis

CFD analysis of the designed turbine is performed to compare and support the results found in streamline analysis and find the reasons of losses such as separation by using AxCFD software which includes a mesh generator and 3D Navier-Stokes Solver. With the 3D CFD analysis, parameters such as surface roughness, turbulence model and heat transfer calculation are taken into consideration.

5.2.1. Turbulence and Heat Transfer Modelling

During the CFD analysis for all boundary conditions, SST k-ω turbulence model with middle level initial turbulence is chosen. While calculating the heat transfer, sand grain roughness is selected as 0.1 mm and blade temperature are selected as the average of the turbine inlet and outlet temperature values for each boundary conditions.

5.2.2. Thermodynamics Properties

In this study, turbine is designed for R245fa organic fluid however during the analysis process, performance of the turbine is also investigated by using R134a as the working fluid. Redlich-Kwong-Aungier Real Gas Model are used during the CFD analysis with R245fa and R134a. Gas constant values for R245fa and R134a were previously shown in Table 1.1.

5.2.3. Computational Mesh

Mesh generation process is performed according to two different mesh quality methods which are Jacobian Matrix Determinant and Angle of the cell's edge. The jacobian matrix value can be varied in the range of -1.0 and 1.0. Major part of the Jacobian matrix determinant should be close to 1.0 and cell's edge angles should not be smaller than 12 degree for a good mesh generation. Detailed distributions of meshes satisfying these criteria are presented in Table 5.2 and generated meshes are presented in Figure 5.3.

5.2.4. Convergence Criteria

During the CFD calculations, convergence criteria is mass flow rate. In the beginning, inlet and outlet mass flow rates start at different values. Iteration process is terminated when the inlet and outlet mass flow rate values converge to the same value. This result also should be close to the mass flow rate value which was assigned to the

Table 5.2. Detailed Quality of Meshes by Jacobian and Angle

Mesh Quality by Jacobian		Mesh Quality by Angle	
Total count mesh element	523908	Total count mesh element	523908
count with determinant <= 0.3	0	Count with angle <= 12	0
count with determinant <= 0.4	0	Count with angle <= 20	0
count with determinant <= 0.5	0	Count with angle <= 30	3286
count with determinant <= 0.6	0	Count with angle <= 40	19540
count with determinant <= 0.7	22	Count with angle <= 50	57780
count with determinant <= 0.8	573	Count with angle <= 60	41925
count with determinant <= 0.9	3152	Count with angle <= 70	73280
count with determinant <= 1	520161	Count with angle <= 90	328097

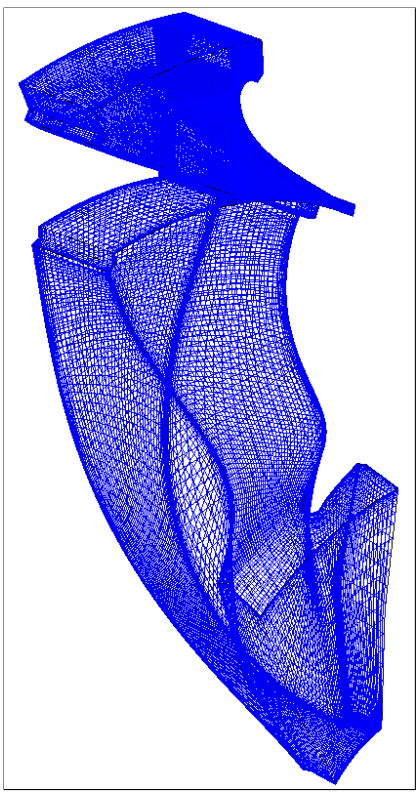

Figure 5.3. Geometry Mesh of the Turbine.

system in the beginning. As an example, convergence result for the design point of the turbine is show in Figure 5.4. For this specific example, it is observed that the inlet and outlet mass flow rate values are converged to 0.48 kg/s in 3000 iteration.

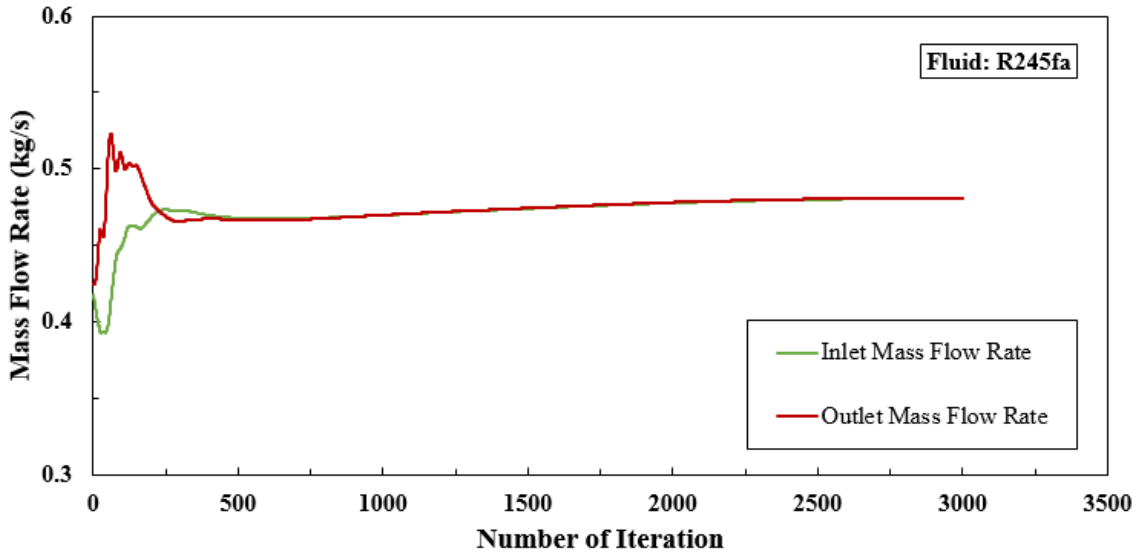

Figure 5.4. Convergence of Inlet and Outlet Mass Flow Rate Values.

6. RESULTS

Optimized turbine flow path is generated based on the requirements stated in preliminary design step. Thermodynamics and kinematics parameters are also obtained by CFD calculations for the generated geometry. Design process was terminated when the CFD results are compatible with streamline calculation results.In the following sections, results of streamline and CFD analyses are presented. In addition, effect of several turbine dimensions on velocity triangles are also presented in Section 6.4.

6.1. Streamline Analysis Results

At the end of this iterative design process,turbine inlet total pressure at the design point is selected as 2.5 bar. The underlying reason of this change is to satisfy the required mass flow rate value and stay at the subsonic region both at stator and rotor. There is a correlation between mass flow rate, rotational speed, inlet pressure and turbine geometry. To decrease the mass flow rate, firstly the leading edge and inlet rotor diameter value had been decreased however this alteration had required to increase the rotational speed and it was concluded with high Mach number value at the inlet of the rotor. Stator blade shape, number and other rotor geometry parameters were also changed to avoid the high Mach number at the inlet.

Table 6.1. Streamline Analysis Result after Blade Design Process

Parameters	Unit	Values
Inlet Total Pressure	bar	2.5
Inlet Total Temperature	^0C	50
Outlet Static Pressure	bar	1.5
Mass Flow Rate	kg/s	0.483
Shaft Rotational Speed	rpm	24700
Power	kW	3.974
Total To Static Efficiency	-	0.875
Total To Total Efficiency	-	0.916
Mach Number at Rotor Inlet	-	0.62

Table 6.2. Details of Velocity Triangles after Blade Design Process

Angles (degree)		Velocities (m/s)	
α_2	16.97	C_2	85.04
α_3	91.68	C_3	30.01
β_2	131.72	W_2	33.25
β_3	29.17	W_3	61.55
		U_2	103.46
		U_3	54.63

As a result, inlet pressure value has decreased to 2.5 bar at the end of optimization process shown in Figure 5.2 to design a turbine with reasonable rotor diameter and rotational speed range at its design point. Also the temperature was set to 50 ^0C which is 10 ^0C higher than the saturation point at 2.5 bar. Details of design point after blade design is presented in Table 6.1.

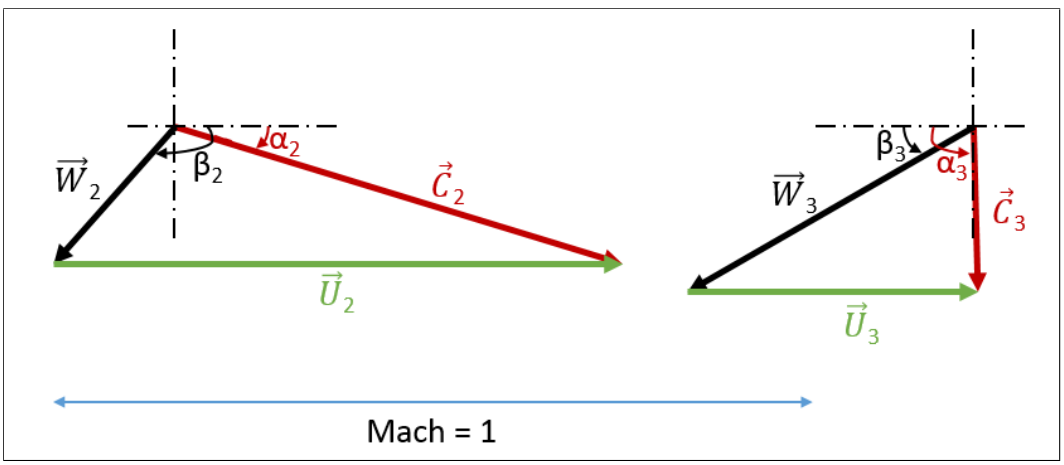

Figure 6.1. Final Design Velocity Triangles at Rotor Inlet and Outlet.

In Figure 6.1, velocity triangles of the turbine rotor at its design point are presented according to streamline analysis results. Magnitude of the speed of sound at the design condition is also drawn to compare the magnitude of velocity vectors at the inlet and outlet of rotor. Speed of sound values at the inlet and outlet of the rotor are both close to 138 m/s. Kinematic results of streamline analysis at design point can be observed in Table 6.2.

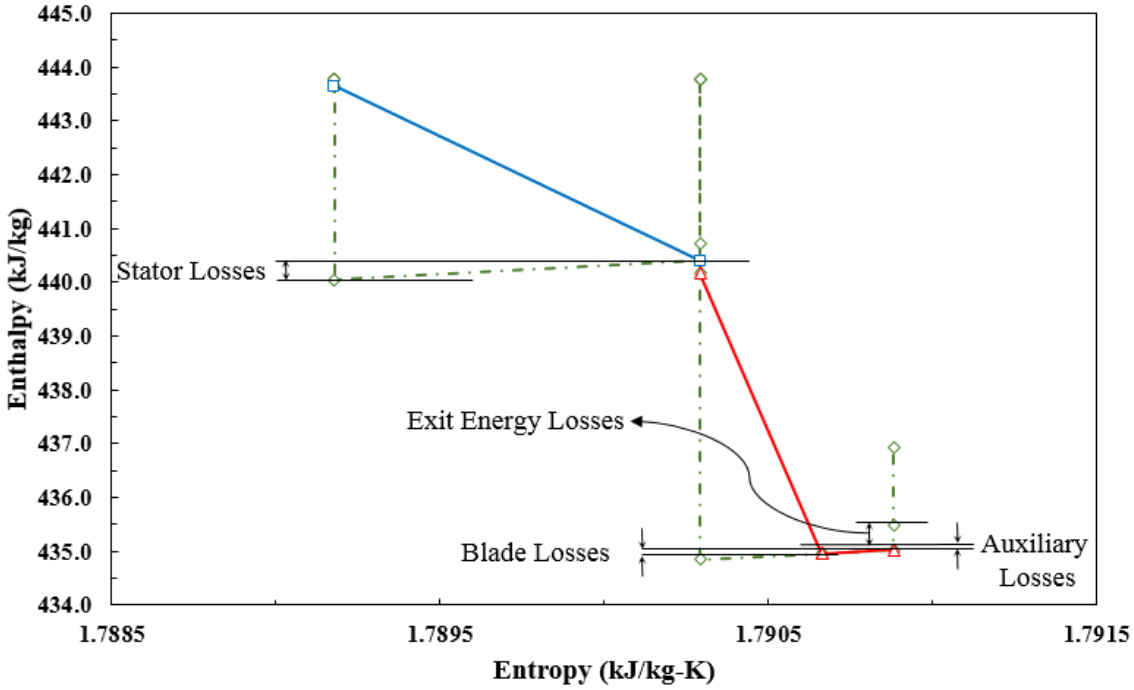

Figure 6.2. Final Design Enthalpy vs Entropy Diagram.

Mollier diagram of the turbine at its design point according to streamline analysis result is shown in Figure 6.2. Degree of Reaction value was found as 0.59. It is seen that the losses are minimized both at the stator and rotor. Also, results of the losses can be matched up with the previous studies in the literature [11, 24]. Results were calculated by the software according to the equations presented in Section 2.4. Efficiency loss due to stator is found as 1.3 % while the disk friction loss is 0.5 %. Results of radial inflow ORC turbine design of Fiaschi *et al.* show that, for R245fa, stator losses and disk friction losses are found as 1.7% and 2.3 % respectively [11]. Also in this study, incidence and passage losses are found as 0.4 % and 3.0 % respectively while these values equal to 0.27 % and 6.0 % in the study of Fiaschi *et al.*.

6.2. CFD Analysis Results

At the design point of final turbine geometry, thermodynamics and kinematic parameters are calculated in CFD. Results are presented in Table 6.3. Mass flow rate

and turbine efficiencies are found satisfactory according to design requirements of ORC and turbine.

Table 6.3. CFD Analysis Result after Blade Design Process

Parameters	Unit	Values
Inlet Total Pressure	bar	2.5
Inlet Total Temperature	^0C	50
Outlet Static Pressure	bar	1.51
Mass Flow Rate	kg/s	0.481
Shaft Rotational Speed	rpm	24700
Power	kW	3.828
Total To Static Efficiency	-	0.897
Total To Total Efficiency	-	0.957
Mach Number at Rotor Inlet	-	0.65

Temperature and relative meridional velocity distribution of the designed turbine at its design point appear in Figure 6.3. Further detailed analyses of CFD results are discussed in Chapter 7.

6.3. Detailed Geometry

The resulting 3D model of the designed turbine is shown in Figure 6.4. Details of the designed turbine geometry are presented in table 6.4. Rotor and stator blade numbers have been decreased to 11 and 18 respectively. Major parameters as leading edge, trailing edge heights, axial length, rotor and stator diameters are optimized according to streamline and CFD analysis results.

Stator and rotor blade curvatures are optimized to generate an efficient flow path by investigating the CFD results. In this process, blade metal angles, offset angles and thickness values along the blade meridional length for 3 sections were edited. At the end of design process, offset angle and thickness distribution of the rotor blades were found as in Figure 6.5. As in the literature [12], thickness distributions were edited symmetrically according to the meanline and also the maximum thickness values were reached at the middle of camberline for all sections.

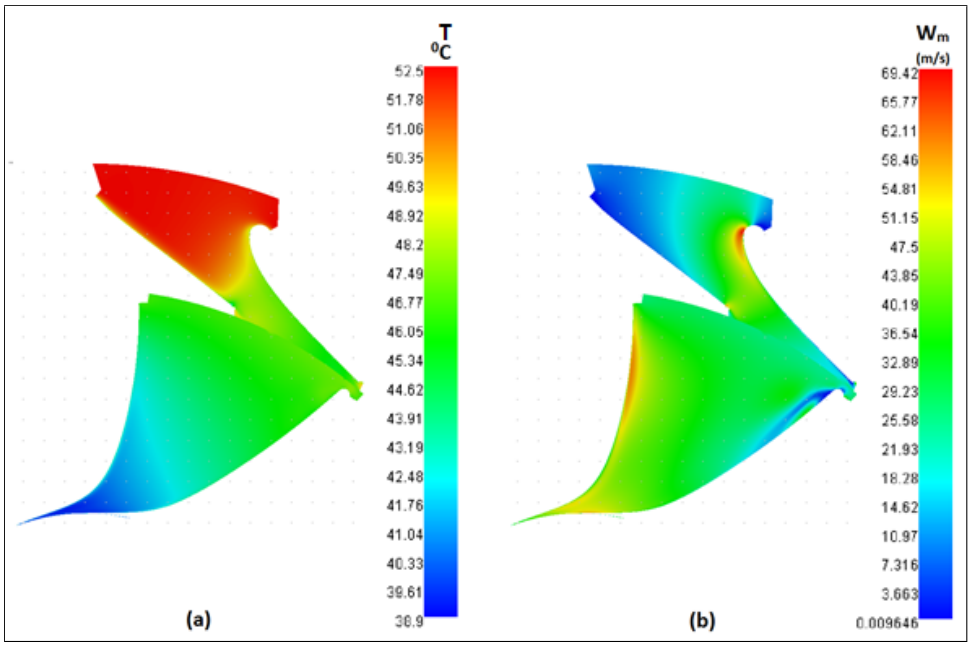

Figure 6.3. (a)Static Temperature Distribution and (b) Relative Meridional Velocity of Turbine at Its Design Point.

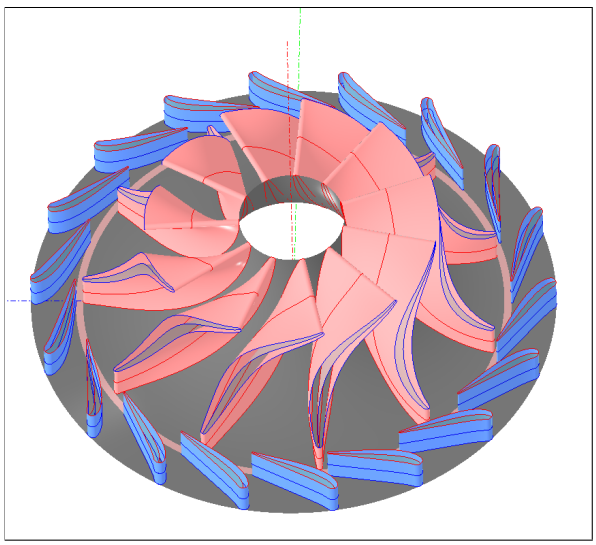

Figure 6.4. Final Turbine Rotor and Stator.

Table 6.4. Final Turbine Geometry Details

Rotor Geometry			Improved Design	Preliminary Design
Number of Blades	-	-	11	12
Inlet Metal Angle	α_{2m}	deg	90	90
Outlet Metal Angle Tip	α_{3mt}	deg	39	19.7
Outlet Metal Angle Mid	α_{3mm}	deg	55	25.5
Outlet Metal Angle Hub	α_{3mh}	deg	71	26.8
LE Angular Offset	θ_2	deg	0	0
TE Angular Offset	θ_3	deg	-38	-46.4
Tip Diameter at Inlet	d_2	mm	80	75.8
Hub Diameter at Outlet	d_{3h}	mm	20	14
Tip Diameter at Outlet	d_{3t}	mm	56	53.8
Leading Edge Height	L_2	mm	7	4.4
Trailing Edge Height	L_3	mm	18	19.9
Axial Length	L_{ax}	mm	27	29.8
Stator Geometry			Improved Design	Preliminary Design
Number of Blades	-	-	18	25
Inlet Metal Angle	α_{0m}	deg	90	90
Outlet Metal Angle	α_{1m}	deg	12.15	15.1
Leading Edge Angular Offset	θ_0	deg	0	0
Trailing Edge Angular Offset	θ_1	deg	20	6.4
Diameter at Inlet	d_0	mm	99.8	94.8
Diameter at Outlet	d_1	mm	82.8	81
Leading and Trailing Edge Heights	L_0 , L_1	mm	7	4.4

6.4. Effect of Turbine Dimensions on Velocity Triangles

Final design of the turbine has passed from many optimization processes and the operations performed during this period has been already presented in Figure 5.2. Now, the effects of these turbine parameters on velocity triangles are investigated by using streamline calculation method. During this analysis, parameters of the designed turbine are changed and streamline calculation is performed for every change.

In Figure 6.6, generated velocity triangles for five different leading edge heights are shown. Triangles at the top presents the rotor inlet velocities while the triangles at the bottom shows the rotor outlet velocities. Leading edge for the final design of the

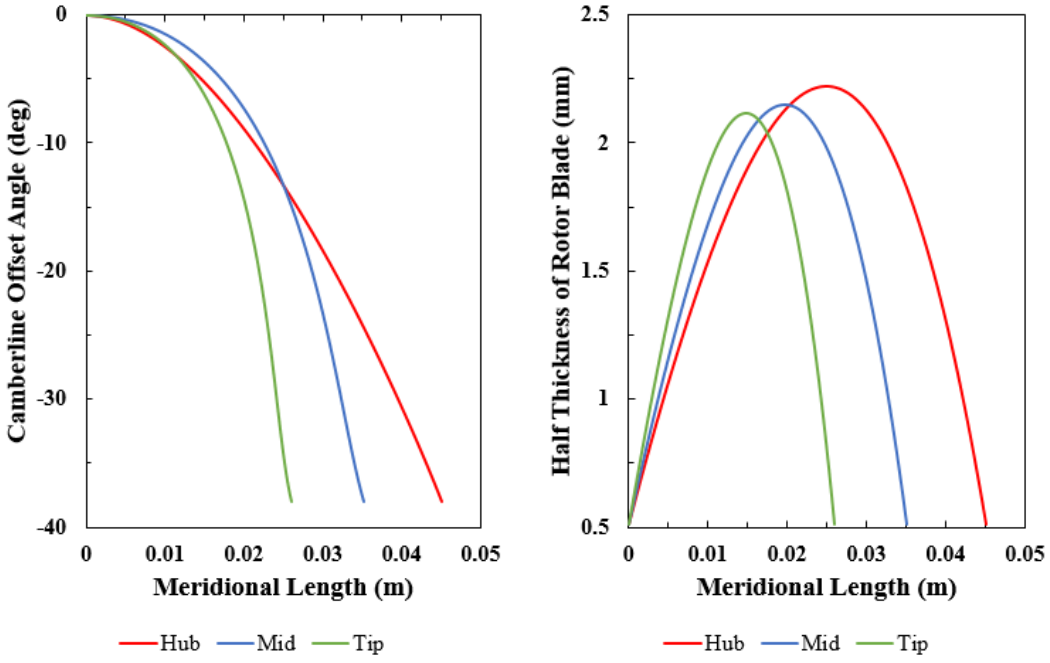

Figure 6.5. Offset Angle and Thickness Distribution of Rotor Blade for 3 section.

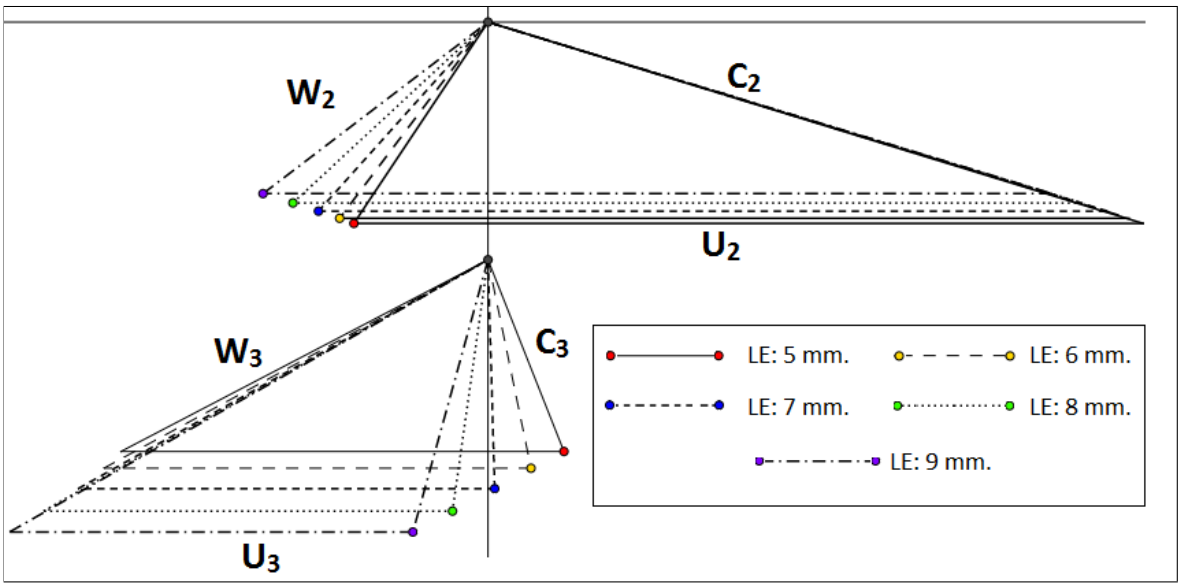

Figure 6.6. Effect of Leading Edge Height on Rotor Inlet and Outlet Velocity Triangles.

turbine is 7 mm. According to design procedure, desired absolute velocity at the rotor exit should be close to axial direction and this requirement is obtained when 7 mm. is selected as the leading edge length.

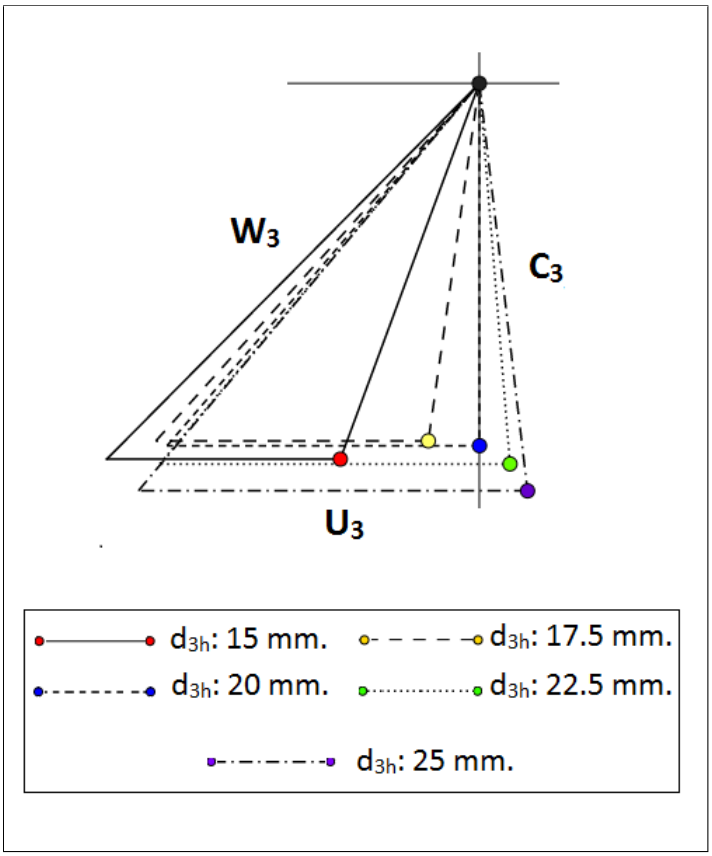

Figure 6.7. Effect of Rotor Outlet Hub Diameter on Rotor Outlet Hub Velocity Triangles.

In Figure 6.7, effect of the outlet hub diameter change on outlet hub velocity triangle is shown. Comments about the direction of exit absolute velocity has already done previously and this requirement is met when the hub diameter equals to 20 mm.

7. DISCUSSION AND CONCLUSIONS

7.1. CFD Analysis Results

CFD analysis is performed for different boundary conditions by using R245fa and R134a as the real gases. In this study, one of the main targets is to design a turbine with a subsonic flow region. Therefore, analyzing the Mach number distribution becomes crucial. Following figures presents the turbine absolute and relative mach number distribution at different boundary conditions. Analysis are performed for both stator and rotor part of the turbine. Figures present the middle section flow path of the turbine.

Stator is the stationary part of the turbine therefore in that region, only velocity that can be observed is the absolute velocity. However, at the exit of the stator, relative velocity is also calculated according to rotational speed of the turbine. As a result, one should investigate absolute and relative mach numbers at stator and rotor part of the turbine respectively.

7.1.1. Working Fluid: R245fa

In Figure 7.1, relative mach number distributions of turbine at four different boundary conditions are shown. Pressure ratio values from 1.67 to 3.00 is observed at different rotational speeds. It is seen that the separation region is minimized at pressure side of the rotor for the design point as a result of the design optimization. However, this region expands with increasing pressure ratio and it decreases the efficiency of the turbine from 89.7 % to 72.5 %.

At the suction side, there is no problem with the flow path until the pressure ratio reaches to 3.00 at 24700 rpm. At that pressure ratio, flow path in the rotor becomes supersonic and separation also occurs at the suction side. As a result, 72.5 % total to

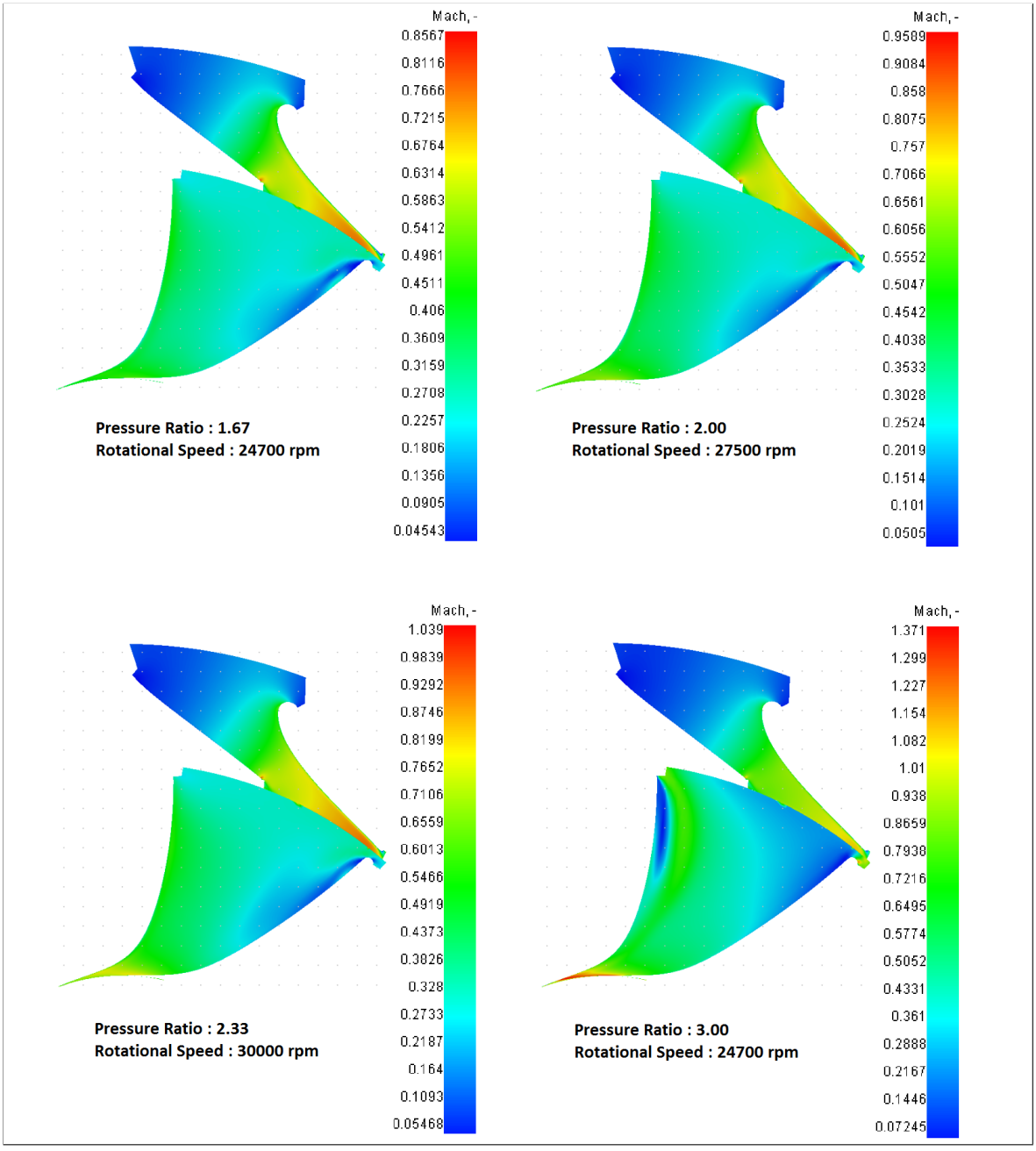

Figure 7.1. R245fa - CFD Result Comparison of Relative MACH Number Distribution at Different Pressure Ratios.

static turbine efficiency is found for this boundary condition.

In Figure 7.2, absolute Mach number distributions of the turbine flow paths for the same working conditions with previous figure are presented. As it was mentioned before, absolute mach number gains importance at the inlet part of rotor. Thus, flow regimes at the entrance region of rotor are investigated in this figure. It is seen that the absolute velocity vectors exceed the speed of sound when the pressure ratio is 2. However, there is no significant difference observed up to the flow path where pressure ratio is 3. In this case, rotational speed value of the turbine was assigned to 24700 rpm which is lower than its most efficient point. As a result, absolute Mach number reaches to 1.8 for this condition and the total to static turbine efficiency drops dramatically to 72.5 % due to the expanding turbulent region and shock wave loss. Detailed CFD results of these working conditions will be presented and discussed in Section 7.2.

7.1.2. Working Fluid: R134a

Although the turbine design was conducted by using R245fa as the working fluid, CFD analysis are also performed by using R134a on the same turbine geometry.

In Figure 7.3, relative Mach number distributions are presented for 3 different working conditions. It is observed that there is no significant difference between performance of two fluids at similar working conditions. For the first condition where pressure ratio is 1.67 and rotational speed is 24700, maximum relative mach number value is found as 0.87. This result shows similarity with the condition where R245fa is working fluid. However for the other two conditions, similar Mach number distributions with R245fa are reached at slightly high rotational speeds. Also it is found that the power outputs of these working conditions are higher when it is compared to R245fa cases.

In Figure 7.4, absolute Mach number distributions of the flow path are presented for R134a cases. In the first working condition where pressure ratio is 1.67, it is observed

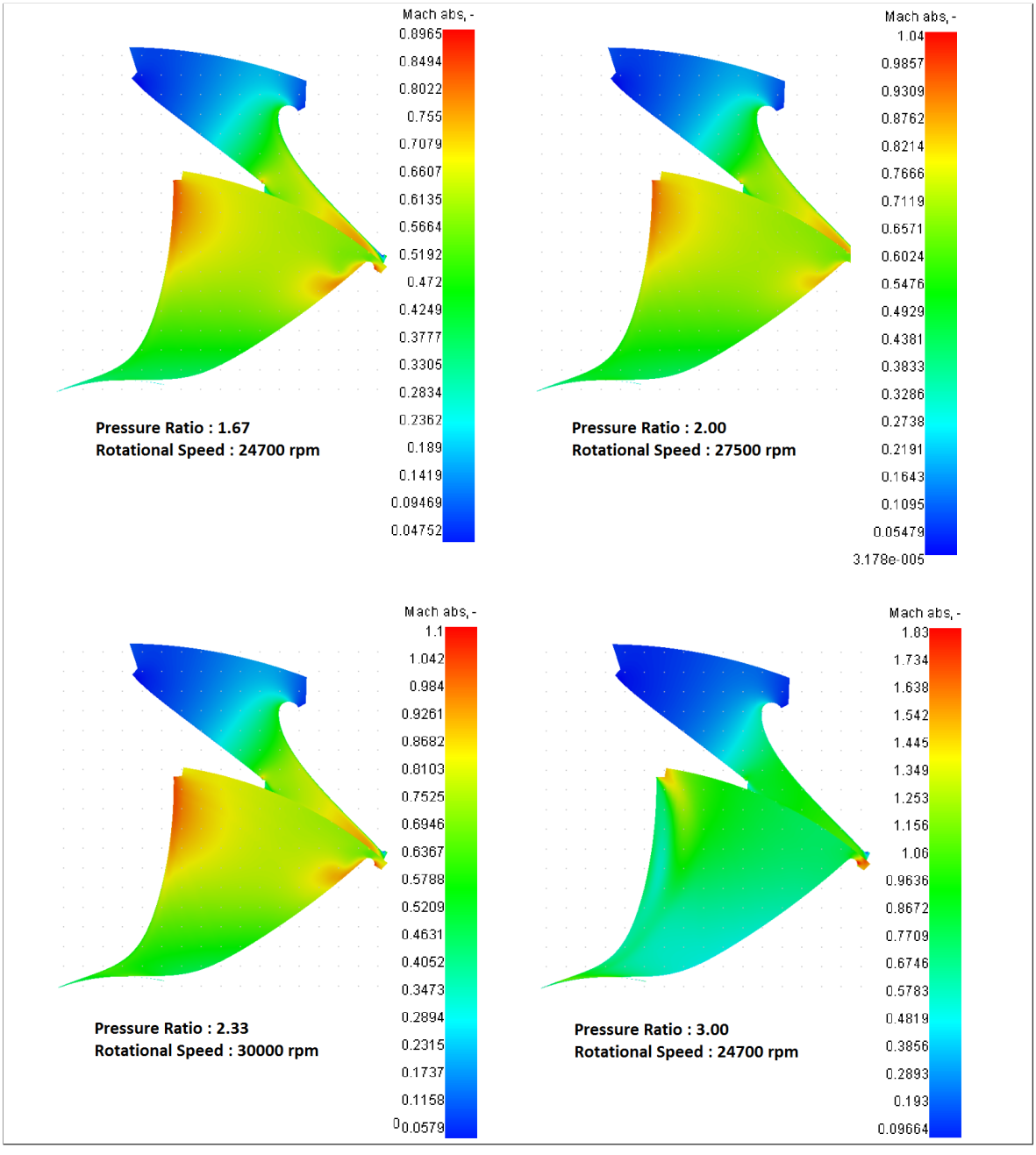

Figure 7.2. R245fa - CFD Result Comparison of Absolute MACH Number Distribution at Different Pressure Ratios.

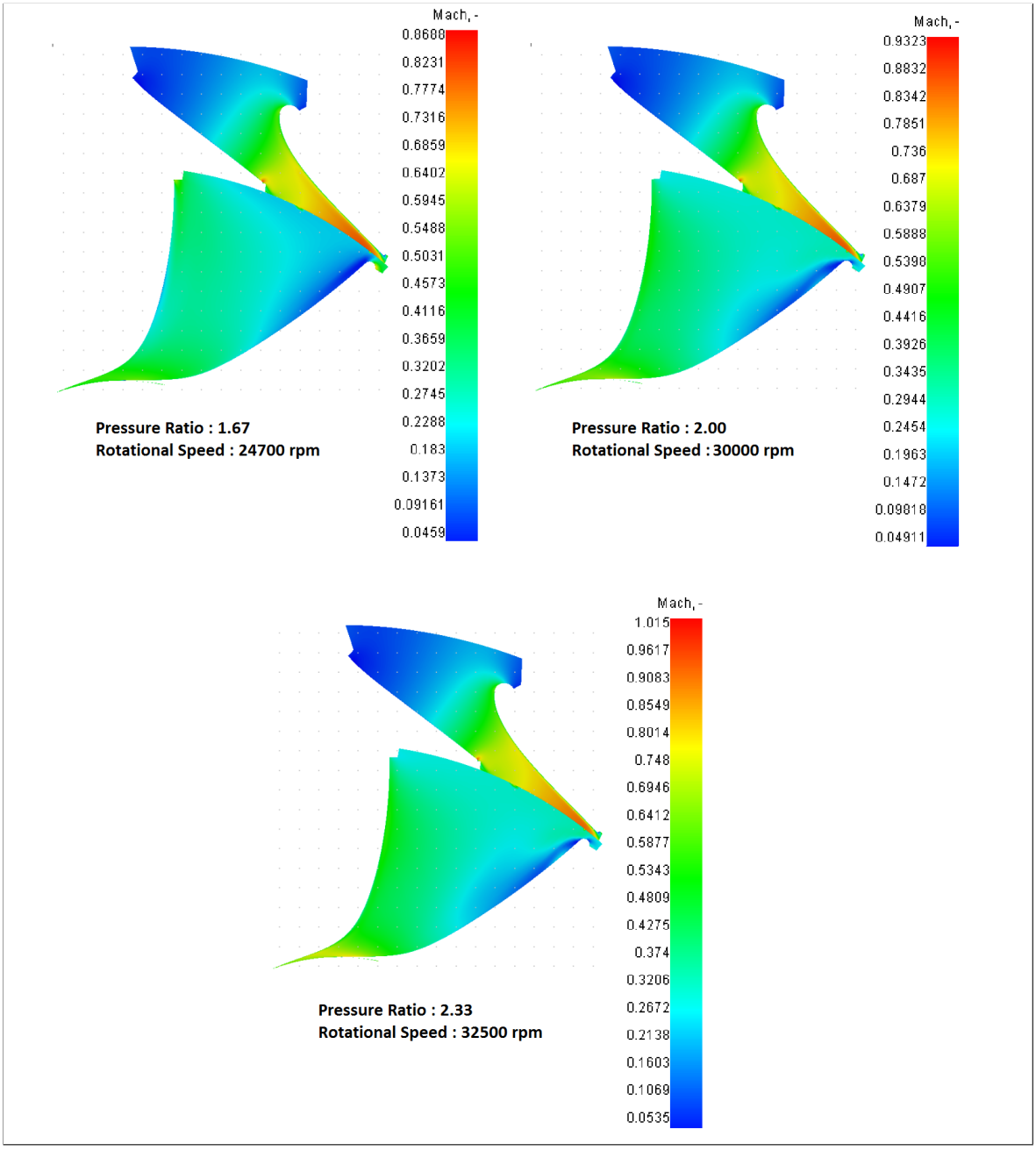

Figure 7.3. R134a - CFD Result Comparison of Relative MACH Number Distribution at Different Pressure Ratios.

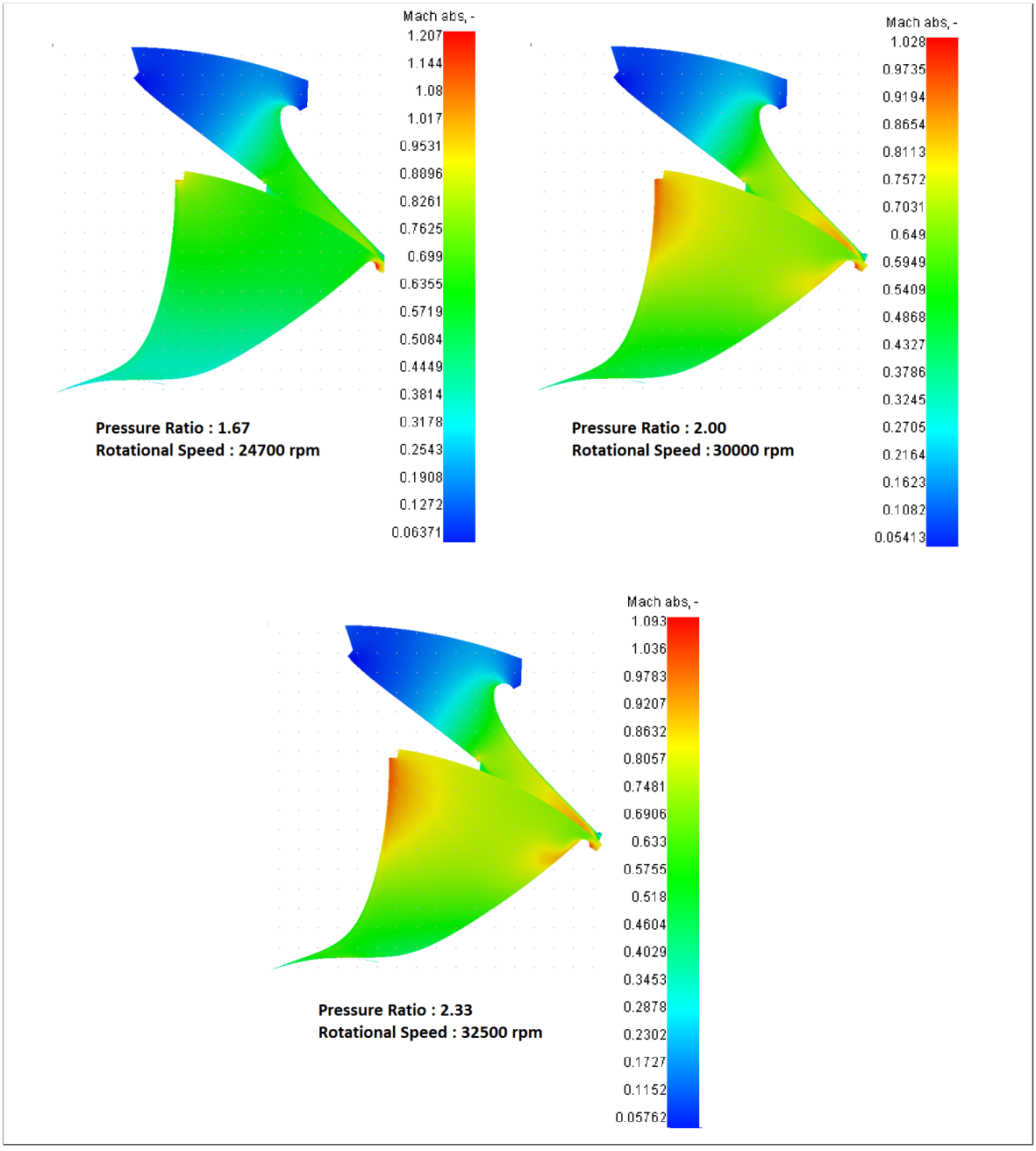

Figure 7.4. R134a - CFD Result Comparison of Absolute MACH Number Distribution at Different Pressure Ratios.

that the maximum absolute Mach number reaches to 1.2 while this value was 0.9 for R245fa case. As it was mentioned in the previous paragraph, rotational speed is the main reason for this result. It can be said that the most efficient rotational speed values for R134a is slightly higher than the R245fa cases at same pressure ratios.

7.2. Comparison of CFD and Streamline Results

In this section, streamline and CFD results are compared at several conditions to obtain the difference and decide whether streamline analysis results are suitable for generating turbine performance maps. For this purpose, turbine power output, mass flow rate, turbine efficiency and Mach number results are presented and compared for each calculation methods.

7.2.1. Working Fluid: R245fa

Streamline analysis and CFD results are observed and compared at four different conditions while the working fluid is R245fa.

Table 7.1. R245fa - Streamline and CFD Result Comparison at 2.5 Bar Inlet Pressure

Fluid: R245fa	Unit	CFD Result	Streamline Result
Turbine Inlet Total Pressure	bar	2.5	2.5
Turbine Outlet Static Pressure	bar	1.51	1.5
Inlet Total Temperature	C	50	50
Rotational Speed	rpm	24700	24700
Mass Flow Rate	kg/s	0.481	0.483
Power	kW	3.83	3.97
Total to Static Efficiency	-	89.7	87.5
Stator Inlet Mach Number (middle section)	-	0.1265	0.13
Mixing Surface Absolute Mach Number (middle section)	-	0.655	0.62
Rotor Outlet Relative Mach Number (middle section)	-	0.34	0.44

In table 7.1, result of important turbine parameters calculated by streamline and CFD analysis are presented at the design point where the pressure ratio is 1.67. For the same boundary conditions, it is observed that the mass flow rate, power output

and turbine isentropic efficiency values found in streamline calculation show similarity with CFD. Mach numbers at the critical parts of the turbine are also calculated with streamline analysis and results matches with the CFD analysis for inlet of the stator and rotor. At the exit of the rotor there is a slight difference between streamline and CFD result and the 2 % efficiency difference may occur due to this variation.

Figure 7.5 shows the relative mach number distribution at the mixing surface (i.e. surface between stator and rotor) and rotor exit surface according to CFD and streamline analysis at the design point of turbine. It can be seen that the streamline analysis gives similar result to CFD both at the inlet and outlet section of the rotor. In general, major deviation occurs at the rotor outlet and this difference is increasing towards to tip of the trailing edge where the average difference is 0.1 Mach.

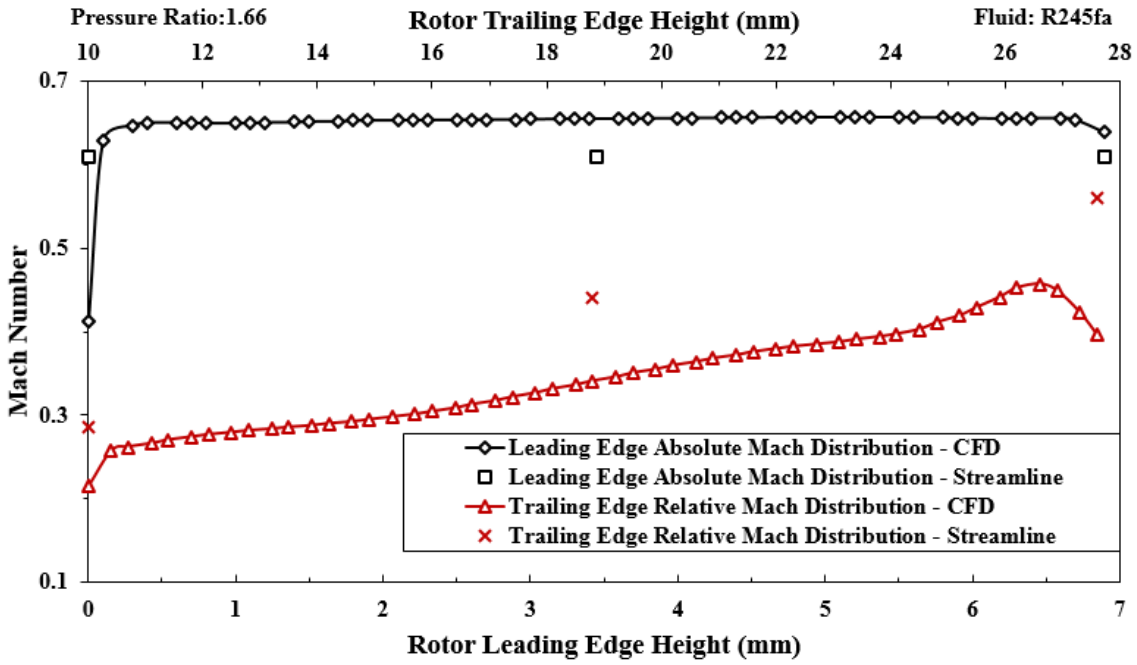

Figure 7.5. R245fa - MACH Number Distribution Results at 2.5 bar Inlet Pressure by Streamline and CFD calculation.

Table 7.2. R245fa - Streamline and CFD Result Comparison at 3 Bar Inlet Pressure

Fluid: R245fa	Unit	CFD Result	Streamline Result
Turbine Inlet Total Pressure	bar	3	3
Turbine Outlet Static Pressure	bar	1.51	1.5
Inlet Total Temperature	C	50	50
Rotational Speed	rpm	27500	27500
Mass Flow Rate	kg/s	0.621	0.63
Power	kW	6.53	6.85
Total to Static Efficiency	-	0.891	0.867
Stator Inlet Mach Number (middle section)	-	0.1356	0.14
Mixing Surface Absolute Mach Number (middle section)	-	0.7569	0.7116
Rotor Outlet Relative Mach Number (middle section)	-	0.4438	0.5544

Several off design points are also investigated to observe and clarify the deviation between CFD and streamline results. In table 7.2, this comparison is presented at 3 bar inlet pressure and 27500 rpm. Results shows that the amount of deviation is similar to boundary condition with 2.5 bar inlet pressure.

Similar to first boundary condition, mach number distribution for 3 bar inlet pressure is shown in Figure 7.6. Streamline analysis results gives 0.04 lower absolute mach number at the inlet of the rotor and approximately 0.1 higher relative mach number at the outlet of the rotor.

Table 7.3. R245fa - Streamline and CFD Result Comparison at 3.5 Bar Inlet Pressure

Fluid: R245fa	Unit	CFD Result	Streamline Result
Turbine Inlet Total Pressure	bar	3.5	3.5
Turbine Outlet Static Pressure	bar	1.51	1.5
Inlet Total Temperature	C	52	52
Rotational Speed	rpm	30000	30000
Mass Flow Rate	kg/s	0.743	0.758
Power	kW	9.35	9.91
Total to Static Efficiency	-	0.8705	0.8556
Stator Inlet Mach Number (middle section)	-	0.139	0.144
Mixing Surface Absolute Mach Number (middle section)	-	0.81	0.77
Rotor Outlet Relative Mach Number (middle section)	-	0.573	0.653

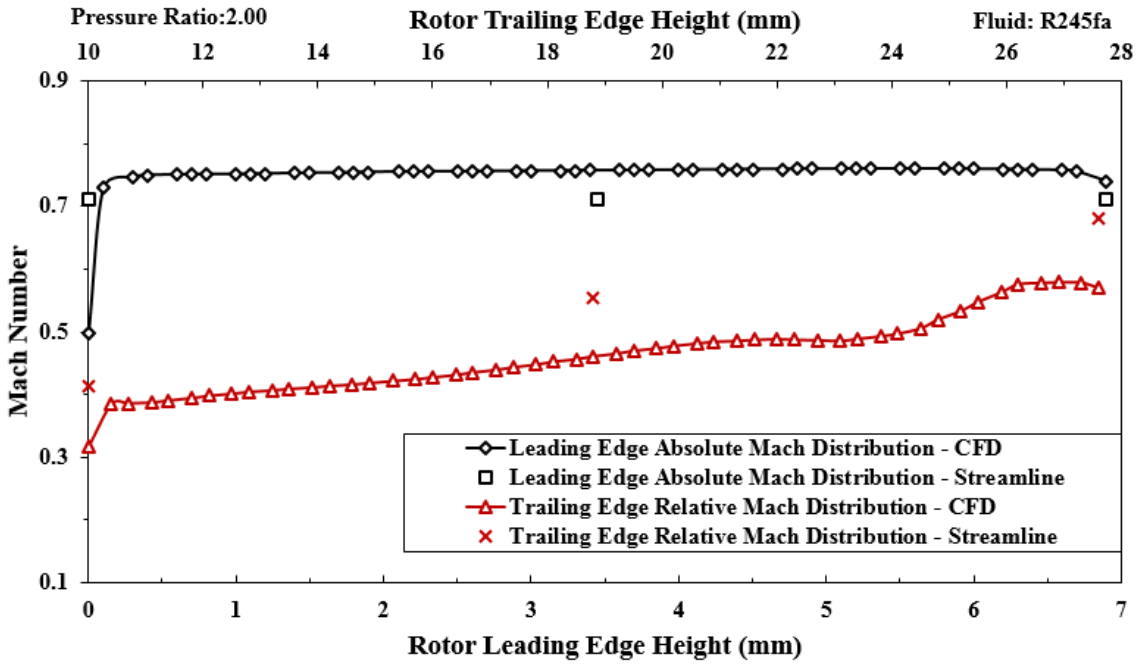

Figure 7.6. R245fa - MACH Number Distribution Results at 3 bar Inlet Pressure by Streamline and CFD calculation.

The third comparison for R245fa is performed at 3.5 inlet pressure where the outlet pressure is still 1.5 bar and results are presented in Table 7.3. In this boundary condition rotational speed is increased to 30000 rpm and it is observed that streamline results are still compatible with CFD results and the deviation does not increased by changing pressure or rotational speed for R245fa.

Mach number distribution for the third boundary condition is shown in Figure 7.7. Differences at the mach numbers are still same with previous boundary conditions therefore it can be said that the performance maps of the designed turbine can be generated by using streamline calculations for R245fa.

Finally, the last comparison is performed at a higher pressure ratio where the supersonic flow regime affects turbine efficiency and power output. Previously, in figure 7.2, it is observed that the absolute mach number reaches to 1.8 at the rotor inlet

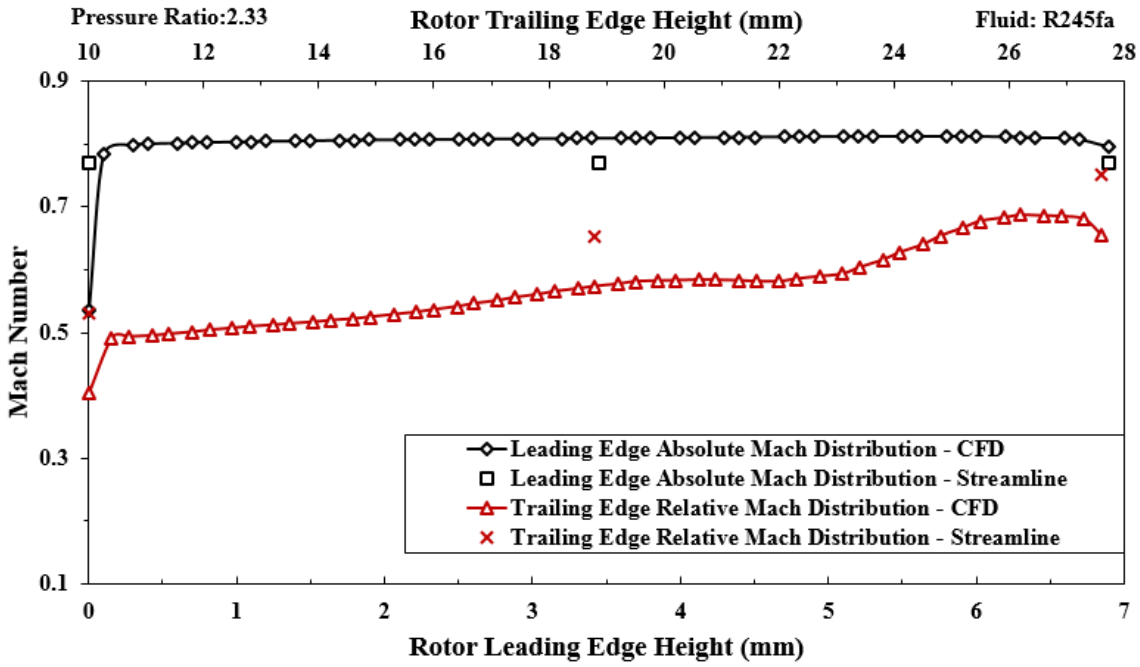

Figure 7.7. R245fa - MACH Number Distribution Results at 3.5 bar Inlet Pressure by Streamline and CFD calculation.

suction side region while the middle section is close to 0.9. This condition definitely affects the efficiency of the turbine. Detailed results of this condition is presented in Table 7.4. Results shows that, total to static efficiency is found as 72.5 % for both calculation methods. Also the power output, mass flow rate and Mach number values are similar to each other.

In Figure 7.8, mach number distributions at the inlet and outlet are presented for 4.5 bar inlet pressure working condition. This pressure ratio and rotational speed is selected as the final condition because it is one of the turbine off design condition and streamline resuls should be checked before generating design and off design performance maps of the turbine. As a result, it is seen that the deviation at the inlet part is still same with previous conditions.In addition, CFD and streamline calculations give different results at the exit tip section of the rotor while the exit meanline section results coincide with each other.However,it is seen that, differences at the tip and hub

Table 7.4. R245fa - Streamline and CFD Result Comparison at 4.5 Bar Inlet Pressure

Fluid: R245fa	Unit	CFD Result	Streamline Result
Turbine Inlet Total Pressure	bar	4.5	4.5
Turbine Outlet Static Pressure	bar	1.5	1.5
Inlet Total Temperature	C	64	64
Rotational Speed	rpm	24700	24700
Mass Flow Rate	kg/s	0.987	1.008
Power	kW	15	14.76
Total to Static Efficiency	-	72.5	72.5
Stator Inlet Mach Number (middle section)	-	0.147	0.15
Mixing Surface Absolute Mach Number (middle section)	-	0.96	0.9
Rotor Outlet Relative Mach Number (middle section)	-	0.79	0.85

sections does not affect the efficiency and other important streamline calculation results.

7.2.2. Working Fluid: R134a

CFD studies are also conducted for R134a organic fluid to observe whether streamline analysis results are applicable for a different fluid characteristics. As a result, designed turbine is analyzed at two different pressure ratio by using R134a and the detailed comparison of streamline and CFD analysis results are presented in Table 7.5 and 7.6.

Table 7.5. R134a - Streamline and CFD Result Comparison at 2.5 Bar Inlet Pressure

Fluid: R134a	Unit	CFD Result	Streamline Result
Turbine Inlet Total Pressure	bar	2.5	2.5
Turbine Outlet Static Pressure	bar	1.51	1.5
Inlet Total Temperature	C	50	50
Rotational Speed	rpm	24700	24700
Mass Flow Rate	kg/s	0.431	0.4345
Power	kW	4.63	4.69
Total to Static Efficiency	-	0.85	0.85
Stator Inlet Mach Number (middle section)	-	0.1287	0.13
Mixing Surface Absolute Mach Number (middle section)	-	0.696	0.65
Rotor Outlet Relative Mach Number (middle section)	-	0.34	0.43

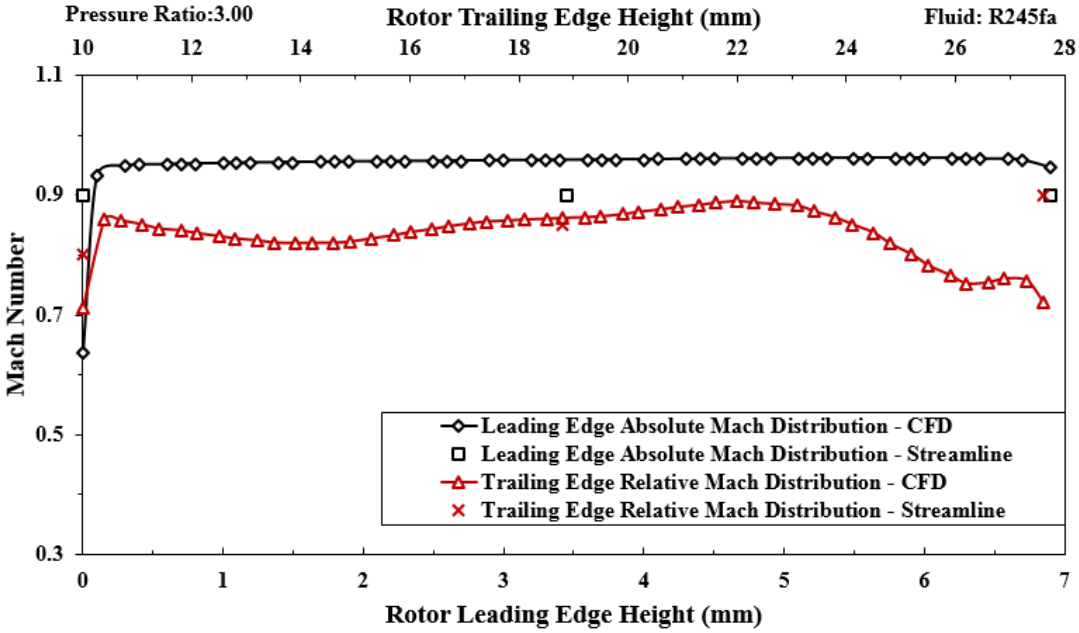

Figure 7.8. R245fa - MACH Number Distribution Results at 4.5 bar Inlet Pressure by Streamline and CFD calculation.

First boundary condition is selected as the design point for R245fa to see the turbine reaction on R134a. Results shows that the efficiencies, power outputs and mass flow rates are found close to each other two calculation method. Also it is observed that the power output value is higher although the mass flow rate is smaller when it is compared to the R245fa case with same boundary conditions.

Table 7.6. R134a - Streamline and CFD Result Comparison at 3.5 Bar Inlet Pressure

Fluid: R134a	Unit	CFD Result	Streamline Result
Turbine Inlet Total Pressure	bar	3.5	3.5
Turbine Outlet Static Pressure	bar	1.5	1.5
Inlet Total Temperature	C	21	21
Rotational Speed	rpm	32500	32500
Mass Flow Rate	kg/s	0.686	0.696
Power	kW	10.3	10.8
Total to Static Efficiency	-	0.8534	0.856
Stator Inlet Mach Number (middle section)	-	0.138	0.14
Mixing Surface Absolute Mach Number (middle section)	-	0.797	0.75
Rotor Outlet Relative Mach Number (middle section)	-	0.5275	0.51

Turbine is also observed at 3.5 inlet pressure and 32500 rpm. Results are presented in Table 7.6 and it is seen that there is no significant difference in the power output, mass flow rate and efficiency.

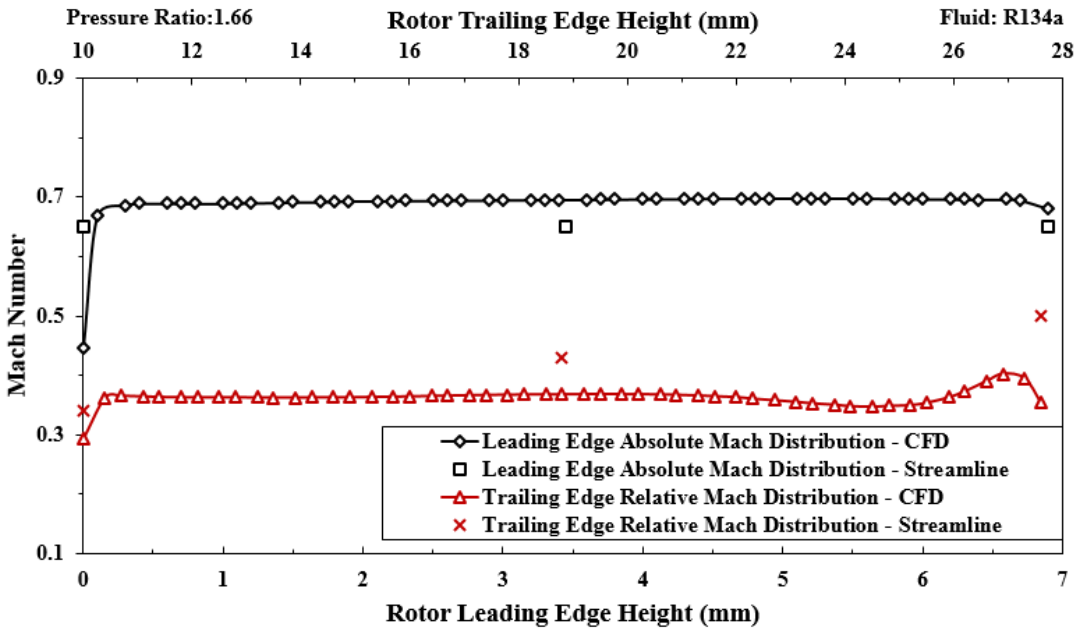

Figure 7.9. R134a - MACH Number Distribution Results at 2.5 bar Inlet Pressure by Streamline and CFD calculation.

Detailed mach number distributions of CFD and streamline analyses for R134a cases are shown in Figure 7.9 and 7.10. At both pressure ratio, results show that the streamline analysis are still valid and can be used to create performance chart by using R134a.

In conclusion, six working condition were investigated with two organic fluids. Results show that,although 0.1 Mach number deviation exists at some points, streamline and CFD calculations gives similar efficiency, power output, mass flow rate values at different working conditions. Therefore one may generate performance map of the turbine by using streamline calculation to prevent time consuming.

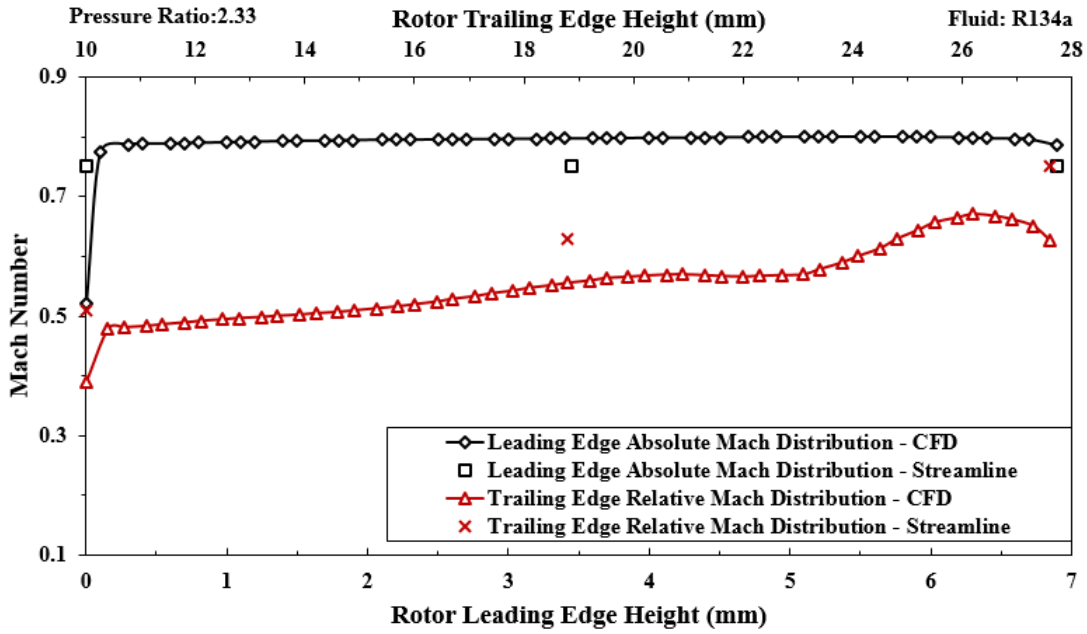

Figure 7.10. R134a - MACH Number Distribution Results at 3.5 bar Inlet Pressure by Streamline and CFD calculation.

7.3. Conclusions

In this study, design and analysis of a single stage radial inflow turbine with a subsonic flow path which works with R245fa were studied. Design point of the turbine was determined by satisfying the BURET Lab. ORC test system limitations. Design procedure starts with preliminary design studies. In this stage, relationship between cycle and turbine requirements was investigated. As a result, dimensions of turbines for different power inputs were determined. Then, preliminary turbine design process for specific cycle conditions was completed. By using the preliminary design result, 3D turbine geometry was generated in the software.

As the second step of the design process, streamline analysis was performed for this geometry. Analysis results have showed that the mass flow rate and turbine efficiency values were not matched up with preliminary design predictions. Therefore, 3D turbine geometry optimisation was performed by investigating the streamline and CFD

analyses results to create an efficient subsonic turbine flow path. As a consequence, small scale turbine was created which gives 3.97 kW power with 87.5 % total to static efficiency at its design point according to streamline analysis results. For the same working condition, CFD analysis results have showed that the power output is 3.83 kW while the efficiency is 89.7 %.

As the final part of the thesis study, turbine performance maps were created for R245fa and R134a by using streamline calculation method. Reliability of the streamline analyses results were checked with CFD analyses results at different boundary conditions. During the comparison, mach numbers , efficiencies, mass flow rates are calculated. It was observed that the CFD results give absolute Mach numbers 0.5 higher than streamline results at the rotor inlet while streamline analyses results give relative Mach numbers 1.0 higher than CFD results. In general, meanline section gives closer results to CFD analyses results. However, differences in Mach numbers have not created an inconsistency in the efficiency, power and mass flow rate values between streamline and CFD analyses results.

REFERENCES

1. Hung, T.-C., T. Shai and S. Wang, "A review of organic Rankine cycles (ORCs) for the recovery of low-grade waste heat", *Energy*, Vol. 22, No. 7, pp. 661–667, 1997.

2. Desai, N. B. and S. Bandyopadhyay, "Process integration of organic Rankine cycle", *Energy*, Vol. 34, No. 10, pp. 1674–1686, 2009.

3. Tchanche, B. F., G. Lambrinos, A. Frangoudakis and G. Papadakis, "Low-grade heat conversion into power using organic Rankine cycles–A review of various applications", *Renewable and Sustainable Energy Reviews*, Vol. 15, No. 8, pp. 3963–3979, 2011.

4. Wang, X. and L. Zhao, "Analysis of zeotropic mixtures used in low-temperature solar Rankine cycles for power generation", *Solar Energy*, Vol. 83, No. 5, pp. 605–613, 2009.

5. Hettiarachchi, H. M., M. Golubovic, W. M. Worek and Y. Ikegami, "Optimum design criteria for an organic Rankine cycle using low-temperature geothermal heat sources", *Energy*, Vol. 32, No. 9, pp. 1698–1706, 2007.

6. Liu, B.-T., K.-H. Chien and C.-C. Wang, "Effect of working fluids on organic Rankine cycle for waste heat recovery", *Energy*, Vol. 29, No. 8, pp. 1207–1217, 2004.

7. Bao, J. and L. Zhao, "A review of working fluid and expander selections for organic Rankine cycle", *Renewable and Sustainable Energy Reviews*, Vol. 24, pp. 325–342, 2013.

8. Yamamoto, T., T. Furuhata, N. Arai and K. Mori, "Design and testing of the organic Rankine cycle", *Energy*, Vol. 26, No. 3, pp. 239–251, 2001.

9. Sauret, E. and A. S. Rowlands, "Candidate radial-inflow turbines and high-density working fluids for geothermal power systems", *Energy*, Vol. 36, No. 7, pp. 4460–4467, 2011.

10. Fiaschi, D., G. Manfrida and F. Maraschiello, "Thermo-fluid dynamics preliminary design of turbo-expanders for ORC cycles", *Applied energy*, Vol. 97, pp. 601–608, 2012.

11. Fiaschi, D., G. Manfrida and F. Maraschiello, "Design and performance prediction of radial ORC turboexpanders", *Applied Energy*, Vol. 138, pp. 517–532, 2015.

12. Fiaschi, D., G. Innocenti, G. Manfrida and F. Maraschiello, "Design of micro radial turboexpanders for ORC power cycles: From 0D to 3D", *Applied Thermal Engineering*, Vol. 99, pp. 402–410, 2016.

13. Ventura, C. A., P. A. Jacobs, A. S. Rowlands, P. Petrie-Repar and E. Sauret, "Preliminary design and performance estimation of radial inflow turbines: An automated approach", *Journal of Fluids Engineering*, Vol. 134, No. 3, p. 031102, 2012.

14. Pei, G., J. Li, Y. Li, D. Wang and J. Ji, "Construction and dynamic test of a small-scale organic rankine cycle", *Energy*, Vol. 36, No. 5, pp. 3215–3223, 2011.

15. Kang, S. H., "Design and experimental study of ORC (organic Rankine cycle) and radial turbine using R245fa working fluid", *Energy*, Vol. 41, No. 1, pp. 514–524, 2012.

16. Kang, S. H., "Design and preliminary tests of ORC (organic Rankine cycle) with two-stage radial turbine", *Energy*, Vol. 96, pp. 142–154, 2016.

17. Sauret, E. and Y. Gu, "Three-dimensional off-design numerical analysis of an organic Rankine cycle radial-inflow turbine", *Applied Energy*, Vol. 135, pp. 202–211, 2014.

18. Nithesh, K., D. Chatterjee, C. Oh and Y.-H. Lee, "Design and performance analysis of radial-inflow turboexpander for OTEC application", *Renewable Energy*, Vol. 85, pp. 834–843, 2016.

19. Pini, M., G. Persico, E. Casati and V. Dossena, "Preliminary design of a centrifugal turbine for organic rankine cycle applications", *Journal of Engineering for Gas turbines and power*, Vol. 135, No. 4, p. 042312, 2013.

20. Aungier, R., *Turbine Aerodynamics: Axial-flow and Radial-inflow Turbine Design and Analysis*, ASME Press, 2006.

21. Cohen, H., G. F. C. Rogers, H. I. H. Saravanamuttoo and H. (r.) Saravanamutto, "Gas turbine theory", 1987.

22. *Waste Heat Recovery Systems Fundamentals Training Course*, Softinway, 2015.

23. Benson, R. S., "A review of methods for assessing loss coefficients in radial gas turbines", *International Journal of Mechanical Sciences*, Vol. 12, No. 10, pp. 905–932, 1970.

24. Whitfield, A. and N. C. Baines, "Design of radial turbomachines", 1990.

25. Futral Samuel M. Jr., W. C. A., *Off design performance prediction with experimental verification for a radial-inflow turbine*, Tech. rep., Ohio, Washington, DC; Lewis Research Cener Cleveland, National Aeronautics and Space Administration, 1965.

26. Rohlik, H. E., *Analytical Determination of Radial Inflow Turbine Design Geometry for Maximum Efficiency*, Tech. rep., NASA TN D-4384, 1968.

27. Rodgers, C. and R. Geiser, "Performance of a high-efficiency radial/axial turbine", *Journal of turbomachinery*, Vol. 109, No. 2, pp. 151–154, 1987.

28. Daily, J. W. and R. E. Nece, "Chamber dimension effects on induced flow and fric-

tional resistance of enclosed rotating disks", *Journal of basic engineering*, Vol. 82, No. 1, pp. 217–230, 1960.

29. Whitfield, A., "The preliminary design of radial inflow turbines", *ASME 1989 International Gas Turbine and Aeroengine Congress and Exposition*, pp. V001T01A049–V001T01A049, American Society of Mechanical Engineers, 1989.

30. Rodgers, C., *Efficiency and performance characteristics of radial turbines*, Tech. rep., SAE Technical Paper, 1966.

31. Qiu, X. and N. Baines, "Performance prediction for high pressure-ratio radial inflow turbines", *ASME Turbo Expo 2007: Power for Land, Sea, and Air*, pp. 945–956, American Society of Mechanical Engineers, 2007.

APPENDIX A: TABLE OF CYCLE PRELIMINARY DESIGN MAPS

Fluid: R245fa	Unit	Case-1		Case-2		Case-3		Case-4		Case-5		Case-6	
		Inlet	Outlet	Inlet	Outlet	Inlet	Outlet	Inlet	Outlet	Inlet	Outlet	Inlet	Outlet
Pressure Ratio	-	1.60		1.60		1.60		1.60		1.60		1.60	
Pressure	bar	2.40	1.50	3.20	2.00	4.00	2.50	4.80	3.00	5.60	3.50	6.40	4.00
Temperature	Celcius	40.00	28.19	48.00	35.71	55.01	42.31	62.00	48.92	67.00	53.52	72.00	58.18
Density	kg/m3	13.47	8.54	17.87	11.26	22.25	13.94	26.54	16.55	31.03	19.25	35.49	21.90
Enthalpy	kJ/kg	434.07	425.75	439.61	431.20	444.50	436.06	449.72	441.19	452.99	444.45	456.44	447.90
Entropy	kj/kg-K	1.76	1.76	1.76	1.76	1.77	1.77	1.77	1.77	1.77	1.77	1.78	1.78
Speed of Sound	m/s	134.80	135.13	134.13	135.18	133.41	135.16	132.97	135.35	131.89	134.95	130.98	134.69

	Unit	Case-1	Case-2	Case-3	Case-4	Case-5	Case-6
Max. Heater Power Input	kW	100.00	100.00	100.00	100.00	100.00	100.00
Ideal Enthalpy Drop	kJ/kg	8.32	8.41	8.44	8.53	8.54	8.54
Mass Flow Rate	kg/s	0.497	0.510	0.521	0.528	0.538	0.546
Power Output	kW	3.52	3.60	3.65	3.69	3.72	3.73
Estimated Turbine Efficiency	%	85.00	84.00	83.00	82.00	81.00	80.00
Cycle Efficiency	%	3.52	3.60	3.65	3.69	3.72	3.73

Saturation Point		Case-1	Case-2	Case-3	Case-4	Case-5	Case-6
Pressure	bar	1.50	2.00	2.50	3.00	3.50	4.00
Temperature	Celcius	25.32	33.35	39.94	45.59	25.32	25.32
Liquid Enthalpy	kJ/kg	232.88	243.59	252.49	260.20	267.05	273.24

Chiller Power Required (kW)			
Case-1	95.86	Case-4	109.91
Case-2	101.17	Case-5	113.78
Case-3	105.82	Case-6	117.37

Figure A.1. R245fa Cycle Analysis - Pressure Ratio:1.6.

Fluid: R245fa	Unit	Case-1		Case-2		Case-3		Case-4		Case-5		Case-6	
		Inlet	Outlet	Inlet	Outlet	Inlet	Outlet	Inlet	Outlet	Inlet	Outlet	Inlet	Outlet
Pressure Ratio	-	2.00		2.00		2.00		2.00		2.00		2.00	
Pressure	bar	3.00	1.50	4.00	2.00	5.00	2.50	6.00	3.00	7.00	3.50	8.00	4.00
Temperature	Celcius	46.00	28.32	55.00	36.59	63.00	43.94	70.00	50.34	76.00	55.74	81.00	60.14
Density	kg/m3	16.78	8.53	22.25	11.21	27.70	13.84	33.17	16.44	38.74	19.04	44.50	21.69
Enthalpy	kJ/kg	438.18	425.87	444.50	432.07	450.24	437.70	455.27	442.65	459.44	446.77	462.66	449.99
Entropy	kj/kg-K	1.76	1.76	1.77	1.77	1.77	1.77	1.78	1.78	1.78	1.78	1.78	1.78
Speed of Sound	m/s	134.26	135.17	133.40	135.48	132.57	135.74	131.65	135.86	130.55	135.79	129.15	135.46

	Unit	Case-1	Case-2	Case-3	Case-4	Case-5	Case-6
Max. Heater Power Input	kW	100.00	100.00	100.00	100.00	100.00	100.00
Ideal Enthalpy Drop	kJ/kg	12.31	12.43	12.54	12.62	12.67	12.67
Mass Flow Rate	kg/s	0.487	0.498	0.506	0.513	0.520	0.528
Power Output	kW	5.10	5.20	5.26	5.30	5.33	5.35
Estimated Turbine Efficiency	%	85.00	84.00	83.00	82.00	81.00	80.00
Cycle Efficiency	%	5.10	5.20	5.26	5.30	5.33	5.35

Saturation Point		Case-1	Case-2	Case-3	Case-4	Case-5	Case-6
Pressure	bar	1.50	2.00	2.50	3.00	3.50	4.00
Temperature	Celcius	25.32	33.35	39.94	45.59	25.32	25.32
Liquid Enthalpy	kJ/kg	232.88	243.59	252.49	260.20	267.05	273.24

Chiller Power Required (kW)			
Case-1	94.00	Case-4	107.54
Case-2	99.14	Case-5	111.18
Case-3	103.58	Case-6	114.62

Figure A.2. R245fa Cycle Analysis - Pressure Ratio:2.

Fluid: R245fa	Unit	Case-1		Case-2		Case-3		Case-4		Case-5		Case-6	
		Inlet	Outlet	Inlet	Outlet	Inlet	Outlet	Inlet	Outlet	Inlet	Outlet	Inlet	Outlet
Pressure Ratio	-	3.00		3.00		3.00		3.00		3.00		3.00	
Pressure	bar	4.50	1.50	6.00	2.00	7.50	2.50	9	3	10.5	3.5	12	4
Temperature	Celcius	60.00	31.18	70.30	40.12	78.00	46.57	86	53.477	92	58.274	98	63.171
Density	kg/m3	24.86	8.43	33.13	11.04	41.75	13.68	50.233	16.205	59.342	18.822	68.501	21.383
Enthalpy	kJ/kg	448.41	428.60	455.55	435.52	460.43	440.35	466.06	445.86	469.57	449.42	473.34	453.21
Entropy	kj/kg-K	1.77	1.77	1.78	1.78	1.78	1.78	1.7852	1.7852	1.7873	1.7873	1.7912	1.7912
Speed of Sound	m/s	133.37	136.07	131.78	136.64	129.56	136.64	127.95	136.98	125.56	136.72	123.48	136.62

	Unit	Case-1	Case-2	Case-3	Case-4	Case-5	Case-6
Max. Heater Power Input	kW	100.00	100.00	100.00	100.00	100.00	100.00
Ideal Enthalpy Drop	kJ/kg	19.81	20.03	20.08	20.20	20.15	20.13
Mass Flow Rate	kg/s	0.464	0.472	0.481	0.486	0.494	0.500
Power Output	kW	7.81	8.03	8.21	8.34	8.46	8.55
Estimated Turbine Efficiency	%	85.00	85.00	85.00	85.00	85.00	85.00
Cycle Efficiency	%	7.81	8.03	8.21	8.34	8.46	8.55

Saturation Point		Case-1	Case-2	Case-3	Case-4	Case-5	Case-6
Pressure	bar	1.50	2.00	2.50	3.00	3.50	4.00
Temperature	Celcius	25.32	33.35	39.94	45.59	25.32	25.32
Liquid Enthalpy	kJ/kg	232.88	243.59	252.49	260.20	267.05	273.24

Chiller Power Required (kW)			
Case-1	90.81	Case-4	103.46
Case-2	95.60	Case-5	106.92
Case-3	99.77	Case-6	110.11

Figure A.3. R245fa Cycle Analysis - Pressure Ratio:3.

Fluid: R245fa	Unit	Case-1		Case-2		Case-3		Case-4		Case-5		Case-6	
		Inlet	Outlet	Inlet	Outlet	Inlet	Outlet	Inlet	Outlet	Inlet	Outlet	Inlet	Outlet
Pressure Ratio	-	4.00		4.00		4.00		4.00		4.00		4.00	
Pressure	bar	6.00	1.50	8.00	2.00	10.00	2.50	12	3	14	3.5	16	4
Temperature	Celcius	70.30	33.00	80.54	41.37	89.75	48.81	97.657	54.981	104.64	60.254	110.91	64.765
Density	kg/m3	33.13	8.36	44.63	10.98	56.39	13.54	68.683	16.097	81.587	18.653	95.226	21.226
Enthalpy	kJ/kg	455.55	430.33	462.10	436.75	468.05	442.59	472.88	447.4	476.89	451.48	480.21	454.89
Entropy	kj/kg-K	1.78	1.78	1.78	1.78	1.79	1.79	1.7899	1.7899	1.7935	1.7935	1.7962	1.7962
Speed of Sound	m/s	131.78	136.64	128.90	137.05	126.16	137.39	123.23	137.5	120.15	137.44	116.94	137.21

	Unit	Case-1	Case-2	Case-3	Case-4	Case-5	Case-6
Max. Heater Power Input	kW	100.00	100.00	100.00	100.00	100.00	100.00
Ideal Enthalpy Drop	kJ/kg	25.22	25.35	25.46	25.48	25.41	25.32
Mass Flow Rate	kg/s	0.449	0.458	0.464	0.470	0.477	0.483
Power Output	kW	9.63	9.86	10.04	10.18	10.29	10.40
Estimated Turbine Efficiency	%	85.00	85.00	85.00	85.00	85.00	85.00
Cycle Efficiency	%	9.63	9.86	10.04	10.18	10.29	10.40

Saturation Point		Case-1	Case-2	Case-3	Case-4	Case-5	Case-6
Pressure	bar	1.50	2.00	2.50	3.00	3.50	4.00
Temperature	Celcius	25.32	33.35	39.94	45.59	25.32	25.32
Liquid Enthalpy	kJ/kg	232.88	243.59	252.49	260.20	267.05	273.24

Chiller Power Required (kW)			
Case-1	88.67	Case-4	100.87
Case-2	93.30	Case-5	104.17
Case-3	97.29	Case-6	87.77

Figure A.4. R245fa Cycle Analysis - Pressure Ratio:4.

Fluid: R134a	Unit	Case-1		Case-2		Case-3		Case-4		Case-5		Case-6	
		Inlet	Outlet	Inlet	Outlet	Inlet	Outlet	Inlet	Outlet	Inlet	Outlet	Inlet	Outlet
Pressure Ratio	-	1.60		1.60		1.60		1.60		1.60		1.60	
Pressure	bar	4.80	3.00	6.40	4.00	7.20	4.50	8	5	8.80	5.50	9.6	6
Temperature	Celcius	16.73	1.00	26.46	10.00	29.85	13.00	33.201	16	36.53	19.00	39.861	22
Density	kg/m3	23.06	14.75	30.59	19.42	34.57	21.85	38.551	24.28	42.54	26.69	46.502	29.08
Enthalpy	kJ/kg	408.97	399.29	414.48	404.72	415.94	406.19	417.46	407.73	419.04	409.33	420.71	411
Entropy	kj/kg-K	1.73	1.73	1.73	1.73	1.72	1.72	1.7206	1.7206	1.72	1.72	1.7189	1.7189
Speed of Sound	m/s	146.98	147.06	145.93	146.95	144.88	146.38	143.91	145.89	143.03	145.46	142.26	145.11

	Unit	Case-1	Case-2	Case-3	Case-4	Case-5	Case-6
Max. Heater Power Input	kW	1000.00	1000.00	1000.00	1000.00	1000.00	1000.00
Ideal Enthalpy Drop	kJ/kg	9.68	9.76	9.75	9.73	9.71	9.71
Mass Flow Rate	kg/s	4.806	4.941	5.026	5.103	5.173	5.235
Power Output	kW	39.54	40.99	41.66	42.21	42.69	43.21
Estimated Turbine Efficiency	%	85.00	85.00	85.00	85.00	85.00	85.00
Cycle Efficiency	%	3.95	4.10	4.17	4.22	4.27	4.32

Saturation Point		Case-1	Case-2	Case-3	Case-4	Case-5	Case-6
Pressure	bar	3.00	4.00	4.50	5.00	5.50	6.00
Temperature	Celcius	0.67	8.93	12.48	15.74	18.75	21.57
Liquid Enthalpy	kJ/kg	200.90	212.11	216.99	221.50	225.72	229.68

Chiller Power Required (kW)			
Case-1	953.48	Case-4	1055.47
Case-2	1007.17	Case-5	1078.16
Case-3	1031.87	Case-6	949.17

Figure A.5. R134a Cycle Analysis - Pressure Ratio:1.6.

Fluid: R134a	Unit	Case-1		Case-2		Case-3		Case-4		Case-5		Case-6	
		Inlet	Outlet	Inlet	Outlet	Inlet	Outlet	Inlet	Outlet	Inlet	Outlet	Inlet	Outlet
Pressure Ratio	-	2.00		2.00		2.00		2.00		2.00		2.00	
Pressure	bar	6.00	3.00	8.00	4.00	9.00	4.50	10	5	11.00	5.50	12	6
Temperature	Celcius	24.62	1.00	34.80	10.00	38.41	13.00	41.981	16	45.52	19.00	49.054	22
Density	kg/m3	28.64	14.75	38.16	19.42	43.23	21.85	48.322	24.28	53.44	26.69	58.549	29.08
Enthalpy	kJ/kg	413.63	399.29	419.15	404.72	420.59	406.19	422.09	407.73	423.64	409.33	425.3	411
Entropy	kj/kg-K	1.73	1.73	1.73	1.73	1.72	1.72	1.7206	1.7206	1.72	1.72	1.7189	1.7189
Speed of Sound	m/s	146.42	147.06	144.80	146.95	143.45	146.38	142.19	145.89	141.04	145.46	140.02	145.11

	Unit	Case-1	Case-2	Case-3	Case-4	Case-5	Case-6
Max. Heater Power Input	kW	100.00	100.00	100.00	100.00	100.00	100.00
Ideal Enthalpy Drop	kJ/kg	14.34	14.43	14.40	14.36	14.31	14.30
Mass Flow Rate	kg/s	0.470	0.483	0.491	0.499	0.505	0.511
Power Output	kW	5.73	5.92	6.01	6.09	6.15	6.21
Estimated Turbine Efficiency	%	85.00	85.00	85.00	85.00	85.00	85.00
Cycle Efficiency	%	5.73	5.92	6.01	6.09	6.15	6.21

Saturation Point		Case-1	Case-2	Case-3	Case-4	Case-5	Case-6
Pressure	bar	3.00	4.00	4.50	5.00	5.50	6.00
Temperature	Celcius	0.67	8.93	12.48	15.74	18.75	21.57
Liquid Enthalpy	kJ/kg	200.90	212.11	216.99	221.50	225.72	229.68

Chiller Power Required (kW)			
Case-1	93.26	Case-4	103.11
Case-2	98.44	Case-5	105.31
Case-3	100.83	Case-6	92.69

Figure A.6. R134a Cycle Analysis - Pressure Ratio:2.

Fluid: R134a	Unit	Case-1		Case-2		Case-3		Case-4		Case-5		Case-6	
		Inlet	Outlet	Inlet	Outlet	Inlet	Outlet	Inlet	Outlet	Inlet	Outlet	Inlet	Outlet
Pressure Ratio	-	3.00		3.00		3.00		3.00		3.00		3.00	
Pressure	bar	9.00	3.00	12.00	4.00	13.50	4.50	15	5	16.50	5.50	18	6
Temperature	Celcius	39.85	1.00	51.04	10.00	55.19	13.00	59.276	16	63.31	19.00	67.318	22
Density	kg/m3	42.82	14.75	57.69	19.42	65.73	21.85	73.894	24.28	82.16	26.69	90.477	29.08
Enthalpy	kJ/kg	422.15	399.29	427.63	404.72	428.99	406.19	430.41	407.73	431.90	409.33	433.51	411
Entropy	kj/kg-K	1.73	1.73	1.73	1.73	1.72	1.72	1.7206	1.7206	1.72	1.72	1.7189	1.7189
Speed of Sound	m/s	144.28	147.06	141.36	146.95	139.34	146.38	137.46	145.89	135.75	145.46	134.23	145.11

	Unit	Case-1	Case-2	Case-3	Case-4	Case-5	Case-6
Max. Heater Power Input	kW	100.00	100.00	100.00	100.00	100.00	100.00
Ideal Enthalpy Drop	kJ/kg	22.86	22.91	22.80	22.68	22.57	22.51
Mass Flow Rate	kg/s	0.452	0.464	0.472	0.479	0.485	0.491
Power Output	kW	8.78	9.04	9.14	9.23	9.30	9.39
Estimated Turbine Efficiency	%	85.00	85.00	85.00	85.00	85.00	85.00
Cycle Efficiency	%	8.78	9.04	9.14	9.23	9.30	9.39

Saturation Point		Case-1	Case-2	Case-3	Case-4	Case-5	Case-6
Pressure	bar	3.00	4.00	4.50	5.00	5.50	6.00
Temperature	Celcius	0.67	8.93	12.48	15.74	18.75	21.57
Liquid Enthalpy	kJ/kg	200.90	212.11	216.99	221.50	225.72	229.68

Chiller Power Required (kW)			
Case-1	89.67	Case-4	99.00
Case-2	94.57	Case-5	101.09
Case-3	96.83	Case-6	88.96

Figure A.7. R134a Cycle Analysis - Pressure Ratio:3.

Fluid: R134a	Unit	Case-1		Case-2		Case-3		Case-4		Case-5		Case-6	
		Inlet	Outlet	Inlet	Outlet	Inlet	Outlet	Inlet	Outlet	Inlet	Outlet	Inlet	Outlet
Pressure Ratio	-	4.00		4.00		4.00		4.00		4.00		4.00	
Pressure	bar	12.00	3.00	16.00	4.00	18.00	4.50	20	5	22.00	5.50	24	6
Temperature	Celcius	51.52	1.00	63.67	10.00	68.31	13.00	72.878	16	77.37	19.00	81.803	22
Density	kg/m3	57.49	14.75	78.25	19.42	89.64	21.85	101.3	24.28	113.19	26.69	125.18	29.08
Enthalpy	kJ/kg	428.18	399.29	433.57	404.72	434.84	406.19	436.18	407.73	437.59	409.33	439.13	411
Entropy	kj/kg-K	1.73	1.73	1.73	1.73	1.72	1.72	1.7206	1.7206	1.72	1.72	1.7189	1.7189
Speed of Sound	m/s	141.68	147.06	137.66	146.95	135.10	146.38	132.77	145.89	130.70	145.46	128.92	145.11

	Unit	Case-1	Case-2	Case-3	Case-4	Case-5	Case-6
Max. Heater Power Input	kW	100.00	100.00	100.00	100.00	100.00	100.00
Ideal Enthalpy Drop	kJ/kg	28.89	28.85	28.65	28.45	28.26	28.13
Mass Flow Rate	kg/s	0.440	0.452	0.459	0.466	0.472	0.477
Power Output	kW	10.80	11.07	11.18	11.26	11.34	11.42
Estimated Turbine Efficiency	%	85.00	85.00	85.00	85.00	85.00	85.00
Cycle Efficiency	%	10.80	11.07	11.18	11.26	11.34	11.42

Saturation Point		Case-1	Case-2	Case-3	Case-4	Case-5	Case-6
Pressure	bar	3.00	4.00	4.50	5.00	5.50	6.00
Temperature	Celcius	0.67	8.93	12.48	15.74	18.75	21.57
Liquid Enthalpy	kJ/kg	200.90	212.11	216.99	221.50	225.72	229.68

Chiller Power Required (kW)			
Case-1	87.29	Case-4	96.34
Case-2	92.03	Case-5	98.38
Case-3	94.23	Case-6	86.57

Figure A.8. R134a Cycle Analysis - Pressure Ratio:4.

APPENDIX B: TABLE OF TURBINE PRELIMINARY DESIGN MAPS

Fluid: R245fa	Unit	Case-1		Case-2		Case-3		Case-4		Case-5		Case-6	
		Inlet	Outlet	Inlet	Outlet	Inlet	Outlet	Inlet	Outlet	Inlet	Outlet	Inlet	Outlet
GEOMETRIC RESULTS													
Specific Speed		0.55		0.55		0.55		0.55		0.55		0.55	
Rotational Speed	rpm	18964.15		21667.65		23929.35		26105.56		27912.29		29554.40	
Total to Static Velocity Ratio:		0.65		0.65		0.65		0.65		0.65		0.65	
Spouting Velocity		129.00		129.69		129.92		130.61		130.69		130.69	
Blade Tip Velocity	m/s	84.36	59.85	84.81	60.17	84.96	60.28	85.41	60.60	85.46	60.64	85.46	60.64
Absolute Flow Velocity	m/s	86.83	24.95	86.27	24.82	85.40	24.60	84.82	24.47	83.83	24.22	82.80	23.95
Absolute Flow Velocity(Tan)	m/s	83.84	0.00	83.30	0.00	82.45	0.00	81.89	1.00	80.94	1.00	79.94	1.00
Absolute Flow Velocity(Axial)	m/s	22.61	24.95	22.47	24.82	22.24	24.60	22.09	24.47	21.83	24.22	21.56	23.95
Relative Flow Velocity	m/s	22.62	64.84	22.52	65.09	22.38	65.11	22.37	65.35	22.30	65.29	22.26	65.20
RotorTip Radius	mm	42.48	30.14	37.38	26.52	33.91	24.06	31.24	22.17	29.24	20.74	27.61	19.59
Rotor Hub Radius	mm	42.48	7.86	37.38	6.91	33.91	6.27	31.24	5.78	29.24	5.41	27.61	5.11
Blade Height (LE and TE)	mm	6.11	22.28	5.41	19.60	4.94	17.78	4.59	16.39	4.32	15.34	4.11	14.48
Rotor Axial Length	mm	33.42		29.41		26.67		24.58		23.00		21.73	
Rotor Blade thickness	mm	1.70	0.85	1.50	0.75	1.36	0.68	1.25	0.62	1.17	0.58	1.10	0.55
Rotor Abs. Flow Angle	deg	15.10	90.00	15.10	90.00	15.10	90.00	15.10	91.00	15.10	91.00	15.10	91.00
Blade Angle	deg	90.00		90.00		90.00		90.00		90.00		90.00	
THERMODYNAMICS RESULTS													
Mass Flow Rate	kg/s	0.50		0.51		0.52		0.53		0.54		0.55	
Temperature	C	40.00	28.19	48.00	35.71	55.01	42.31	62.00	48.92	67.00	53.52	72.00	58.18
Pressure	bar	2.40	1.50	3.20	2.00	4.00	2.50	4.80	3.00	5.60	3.50	6.40	4.00
Absolute Mach Number	-	0.64	0.18	0.64	0.18	0.64	0.18	0.64	0.18	0.64	0.18	0.63	0.18
Density	kg/m3	13.47	8.54	17.87	11.26	22.25	13.94	26.54	16.55	31.03	19.25	35.49	21.90

Figure B.1. R245fa Turbine Analysis - Pressure Ratio:1.6.

Fluid: R245fa	Unit	Case-1		Case-2		Case-3		Case-4		Case-5		Case-6	
		Inlet	Outlet	Inlet	Outlet	Inlet	Outlet	Inlet	Outlet	Inlet	Outlet	Inlet	Outlet
GEOMETRIC RESULTS													
Specific Speed		0.55		0.55		0.55		0.55		0.55		0.55	
Rotational Speed	rpm	25692.33		29347.32		32558.76		35411.83		37965.30		40204.92	
Total to Static Velocity Ratio:		0.65		0.65		0.65		0.65		0.65		0.65	
Spouting Velocity		156.91		157.67		158.37		158.87		159.19		159.19	
Blade Tip Velocity	m/s	102.61	72.80	103.11	73.15	103.56	73.48	103.89	73.71	104.10	73.86	104.10	73.86
Absolute Flow Velocity	m/s	105.62	29.34	104.88	29.15	104.09	28.94	103.17	28.69	102.11	28.42	100.85	28.08
Absolute Flow Velocity(Tan)	m/s	101.97	0.00	101.27	0.00	100.50	0.00	99.61	1.00	98.59	1.00	97.37	1.00
Absolute Flow Velocity(Axial)	m/s	27.51	29.34	27.31	29.15	27.11	28.94	26.87	28.69	26.59	28.42	26.26	28.08
Relative Flow Velocity	m/s	27.51	78.49	27.38	78.75	27.28	78.97	27.21	79.10	27.16	79.14	27.11	79.02
RotorTip Radius	mm	38.14	27.06	33.55	23.80	30.37	21.55	28.02	19.88	26.18	18.58	24.72	17.54
Rotor Hub Radius	mm	38.14	7.06	33.55	6.21	30.37	5.62	28.02	5.18	26.18	4.84	24.72	4.57
Blade Height (LE and TE)	mm	4.40	20.00	3.88	17.60	3.53	15.93	3.27	14.69	3.07	13.73	2.91	12.97
Rotor Axial Length	mm	30.00		26.40		23.90		22.04		20.60		19.45	
Rotor Blade thickness	mm	1.53	0.76	1.34	0.67	1.21	0.61	1.12	0.56	1.05	0.52	0.99	0.49
Rotor Abs. Flow Angle	deg	15.10	90.00	15.10	90.00	15.10	90.00	15.10	91.00	15.10	91.00	15.10	91.00
Blade Angle	deg	90.00		90.00		90.00		90.00		90.00		90.00	
THERMODYNAMICS RESULTS													
Mass Flow Rate	kg/s	0.49		0.50		0.51		0.51		0.52		0.53	
Temperature	C	46.00	28.32	55.00	36.59	63.00	43.94	70.00	50.34	76.00	55.74	81.00	60.14
Pressure	bar	3.00	1.50	4.00	2.00	5.00	2.50	6.00	3.00	7.00	3.50	8.00	4.00
Absolute Mach Number	-	0.79	0.22	0.79	0.22	0.79	0.21	0.78	0.21	0.78	0.21	0.78	0.21
Density	kg/m3	16.78	8.53	22.25	11.21	27.70	13.84	33.17	16.44	38.74	19.04	44.50	21.69

Figure B.2. R245fa Turbine Analysis - Pressure Ratio:2.

Fluid: R245fa	Unit	Case-1		Case-2		Case-3		Case-4		Case-5		Case-6	
		Inlet	Outlet	Inlet	Outlet	Inlet	Outlet	Inlet	Outlet	Inlet	Outlet	Inlet	Outlet
GEOMETRIC RESULTS													
Specific Speed		0.55		0.55		0.55		0.55		0.55		0.55	
Rotational Speed	rpm	37380.00		13527.76		47244.95		51399.41		54841.23		58059.70	
Total to Static Velocity Ratio:		0.65		0.65		0.65		0.65		0.65		0.65	
Spouting Velocity		199.05		200.15		200.40		201.00		200.75		200.65	
Blade Tip Velocity	m/s	130.17	92.35	130.89	92.86	131.05	92.98	131.44	93.26	131.28	93.14	131.21	93.10
Absolute Flow Velocity	m/s	133.99	35.93	134.73	36.09	134.90	36.10	135.30	36.18	135.13	36.10	135.06	36.06
Absolute Flow Velocity(Tan)	m/s	129.36	0.00	130.08	0.00	130.24	0.00	130.63	1.00	130.47	1.00	130.40	1.00
Absolute Flow Velocity(Axial)	m/s	34.89	35.93	35.09	36.09	35.13	36.10	35.24	36.18	35.19	36.10	35.17	36.06
Relative Flow Velocity	m/s	34.90	99.09	35.10	99.63	35.14	99.74	35.24	100.03	35.20	99.89	35.18	99.83
RotorTip Radius	mm	33.25	23.59	92.39	65.55	26.49	18.79	24.42	17.33	22.86	16.22	21.58	15.31
Rotor Hub Radius	mm	33.25	6.15	92.39	17.09	26.49	4.90	24.42	4.52	22.86	4.23	21.58	3.99
Blade Height (LE and TE)	mm	2.56	17.44	6.99	48.46	1.97	13.89	1.79	12.81	1.65	11.99	1.53	11.32
Rotor Axial Length	mm	26.16		72.69		20.84		19.21		17.98		16.98	
Rotor Blade thickness	mm	1.33	0.67	3.70	1.85	1.06	0.53	0.98	0.49	0.91	0.46	0.86	0.43
Rotor Abs. Flow Angle	deg	15.10	90.00	15.10	90.00	15.10	90.00	15.10	91.00	15.10	91.00	15.10	91.00
Blade Angle	deg	90.00		90.00		90.00		90.00		90.00		90.00	
THERMODYNAMICS RESULTS													
Mass Flow Rate	kg/s	0.46		4.72		0.48		0.49		0.49		0.50	
Temperature	C	60.00	31.18	70.30	40.12	78.00	46.57	86.00	53.48	92.00	58.27	98.00	63.17
Pressure	bar	4.50	1.50	6.00	2.00	7.50	2.50	9.00	3.00	10.50	3.50	12.00	4.00
Absolute Mach Number	-	1.00	0.26	1.02	0.26	1.04	0.26	1.06	0.26	1.08	0.26	1.09	0.26
Density	kg/m3	24.86	8.43	33.13	11.04	41.75	13.68	50.23	16.21	59.34	18.82	68.50	21.38

Figure B.3. R245fa Turbine Analysis - Pressure Ratio:3.

Fluid: R245fa	Unit	Case-1		Case-2		Case-3		Case-4		Case-5		Case-6	
		Inlet	Outlet	Inlet	Outlet	Inlet	Outlet	Inlet	Outlet	Inlet	Outlet	Inlet	Outlet
GEOMETRIC RESULTS													
Specific Speed		0.55		0.55		0.55		0.55		0.55		0.55	
Rotational Speed	rpm	45360.53		51686.15		57196.49		61975.41		66131.15		69874.65	
Total to Static Velocity Ratio:		0.65		0.65		0.65		0.65		0.65		0.65	
Spouting Velocity		224.59		225.17		225.65		225.74		225.43		225.03	
Blade Tip Velocity	m/s	146.87	104.20	147.25	104.47	147.57	104.70	147.62	104.74	147.42	104.59	147.16	104.41
Absolute Flow Velocity	m/s	151.18	40.02	151.57	40.09	151.90	40.15	151.95	40.13	151.75	40.05	151.48	39.95
Absolute Flow Velocity(Tan)	m/s	145.96	0.00	146.34	0.00	146.65	0.00	146.71	1.00	146.51	1.00	146.25	1.00
Absolute Flow Velocity(Axial)	m/s	39.37	40.02	39.47	40.09	39.56	40.15	39.57	40.13	39.52	40.05	39.45	39.95
Relative Flow Velocity	m/s	39.38	111.62	39.48	111.90	39.57	112.13	39.58	112.16	39.53	112.00	39.46	111.79
RotorTip Radius	mm	30.92	21.94	27.20	19.30	24.64	17.48	22.75	16.14	21.29	15.10	20.11	14.27
Rotor Hub Radius	mm	30.92	5.72	27.20	5.03	24.64	4.56	22.75	4.21	21.29	3.94	20.11	3.72
Blade Height (LE and TE)	mm	1.77	16.22	1.52	14.27	1.34	12.92	1.21	11.93	1.11	11.17	1.02	10.55
Rotor Axial Length	mm	24.33		21.40		19.38		17.90		16.75		15.82	
Rotor Blade thickness	mm	1.24	0.62	1.09	0.54	0.99	0.49	0.91	0.45	0.85	0.43	0.80	0.40
Rotor Abs. Flow Angle	deg	15.10	90.00	15.10	90.00	15.10	90.00	15.10	91.00	15.10	91.00	15.10	91.00
Blade Angle	deg	90.00		90.00		90.00		90.00		90.00		90.00	
THERMODYNAMICS RESULTS													
Mass Flow Rate	kg/s	0.45		0.46		0.46		0.47		0.48		0.48	
Temperature	C	70.30	33.00	80.54	41.37	89.75	48.81	97.66	54.98	104.64	60.25	110.91	64.77
Pressure	bar	6.00	1.50	8.00	2.00	10.00	2.50	12.00	3.00	14.00	3.50	16.00	4.00
Absolute Mach Number	-	1.15	0.29	1.18	0.29	1.20	0.29	1.23	0.29	1.26	0.29	1.30	0.29
Density	kg/m3	33.13	8.36	44.63	10.98	56.39	13.54	68.68	16.10	81.59	18.65	95.23	21.23

Figure B.4. R245fa Turbine Analysis - Pressure Ratio:4.

Fluid: R134a	Unit	Case-1		Case-2		Case-3		Case-4		Case-5		Case-6	
		Inlet	Outlet	Inlet	Outlet	Inlet	Outlet	Inlet	Outlet	Inlet	Outlet	Inlet	Outlet
GEOMETRIC RESULTS													
Specific Speed		0.55		0.55		0.55		0.55		0.55		0.55	
Rotational Speed	rpm	8977.75		10222.64		10745.46		11223.46		11669.74		12108.67	
Total to Static Velocity Ratio:		0.65		0.65		0.65		0.65		0.65		0.65	
Spouting Velocity		139.14		139.71		139.64		139.50		139.36		139.36	
Blade Tip Velocity	m/s	90.99	64.56	91.37	64.82	91.32	64.79	91.22	64.72	91.13	64.66	91.13	64.66
Absolute Flow Velocity	m/s	93.66	26.96	94.05	27.03	94.00	27.00	93.90	26.96	93.80	26.91	93.80	26.89
Absolute Flow Velocity(Tan)	m/s	90.43	0.00	90.80	0.00	90.75	0.00	90.66	1.00	90.57	1.00	90.57	1.00
Absolute Flow Velocity(Axial)	m/s	24.39	26.96	24.49	27.03	24.48	27.00	24.45	26.96	24.43	26.91	24.43	26.89
Relative Flow Velocity	m/s	24.40	69.96	24.50	70.24	24.49	70.19	24.46	70.11	24.44	70.03	24.44	70.03
RotorTip Radius	mm	96.78	68.67	85.35	60.55	81.15	57.58	77.62	55.07	74.57	52.91	71.87	50.99
Rotor Hub Radius	mm	96.78	17.90	85.35	15.79	81.15	15.01	77.62	14.36	74.57	13.80	71.87	13.30
Blade Height (LE and TE)	mm	14.05	50.76	12.30	44.76	11.65	42.56	11.10	40.71	10.62	39.11	10.20	37.70
Rotor Axial Length	mm	76.14		67.15		63.85		61.07		58.67		56.54	
Rotor Blade thickness	mm	3.87	1.94	3.41	1.71	3.25	1.62	3.10	1.55	2.98	1.49	2.87	1.44
Rotor Abs. Flow Angle	deg	15.10	90.00	15.10	90.00	15.10	90.00	15.10	91.00	15.10	91.00	15.10	91.00
Blade Angle	deg	90.00		90.00		90.00		90.00		90.00		90.00	
THERMODYNAMICS RESULTS													
Mass Flow Rate	kg/s	4.81		4.94		5.03		5.10		5.17		5.23	
Temperature	C	16.73	1.00	26.46	10.00	29.85	13.00	33.20	16.00	36.53	19.00	39.86	22.00
Pressure	bar	4.80	3.00	6.40	4.00	7.20	4.50	8.00	5.00	8.80	5.50	9.60	6.00
Absolute Mach Number	-	0.64	0.18	0.64	0.18	0.65	0.18	0.65	0.18	0.66	0.18	0.66	0.19
Density	kg/m3	23.06	14.75	30.59	19.42	34.57	21.85	38.55	24.28	42.54	26.69	46.50	29.08

Figure B.5. R134a Turbine Analysis - Pressure Ratio:1.6.

Fluid: R134a	Unit	Case-1		Case-2		Case-3		Case-4		Case-5		Case-6	
		Inlet	Outlet	Inlet	Outlet	Inlet	Outlet	Inlet	Outlet	Inlet	Outlet	Inlet	Outlet
GEOMETRIC RESULTS													
Specific Speed		0.55		0.55		0.55		0.55		0.55		0.55	
Rotational Speed	rpm	38546.30		43840.92		46053.25		48081.60		49943.95		51801.21	
Total to Static Velocity Ratio:		0.65		0.65		0.65		0.65		0.65		0.65	
Spouting Velocity		169.35		169.88		169.71		169.47		169.17		169.12	
Blade Tip Velocity	m/s	110.75	78.57	111.09	78.82	110.98	78.74	110.82	78.63	110.63	78.49	110.59	78.46
Absolute Flow Velocity	m/s	114.00	31.72	114.35	31.77	114.23	31.71	114.08	31.64	113.88	31.56	113.84	31.53
Absolute Flow Velocity(Tan)	m/s	110.06	0.00	110.41	0.00	110.29	0.00	110.14	1.00	109.95	1.00	109.91	1.00
Absolute Flow Velocity(Axial)	m/s	29.69	31.72	29.78	31.77	29.75	31.71	29.71	31.64	29.66	31.56	29.65	31.53
Relative Flow Velocity	m/s	29.70	84.73	29.79	84.98	29.76	84.88	29.72	84.76	29.66	84.60	29.65	84.56
RotorTip Radius	mm	27.44	19.47	24.20	17.17	23.01	16.33	22.01	15.62	21.15	15.01	20.39	14.46
Rotor Hub Radius	mm	27.44	5.08	24.20	4.48	23.01	4.26	22.01	4.07	21.15	3.91	20.39	3.77
Blade Height (LE and TE)	mm	3.21	14.39	2.80	12.69	2.64	12.07	2.51	11.54	2.40	11.09	2.30	10.69
Rotor Axial Length	mm	21.59		19.04		18.10		17.32		16.64		16.04	
Rotor Blade thickness	mm	1.10	0.55	0.97	0.48	0.92	0.46	0.88	0.44	0.85	0.42	0.82	0.41
Rotor Abs. Flow Angle	deg	15.10	90.00	15.10	90.00	15.10	90.00	15.10	91.00	15.10	91.00	15.10	91.00
Blade Angle	deg	90.00		90.00		90.00		90.00		90.00		90.00	
THERMODYNAMICS RESULTS													
Mass Flow Rate	kg/s	0.47		0.48		0.49		0.50		0.51		0.51	
Temperature	C	24.62	1.00	34.80	10.00	38.41	13.00	41.98	16.00	45.52	19.00	49.05	22.00
Pressure	bar	6.00	3.00	8.00	4.00	9.00	4.50	10.00	5.00	11.00	5.50	12.00	6.00
Absolute Mach Number	-	0.78	0.22	0.79	0.22	0.80	0.22	0.80	0.22	0.81	0.22	0.81	0.22
Density	kg/m3	28.64	14.75	38.16	19.42	43.23	21.85	48.32	24.28	53.44	26.69	58.55	29.08

Figure B.6. R134a Turbine Analysis - Pressure Ratio:2.

Fluid: R134a	Unit	Case-1		Case-2		Case-3		Case-4		Case-5		Case-6	
		Inlet	Outlet	Inlet	Outlet	Inlet	Outlet	Inlet	Outlet	Inlet	Outlet	Inlet	Outlet
GEOMETRIC RESULTS													
Specific Speed		0.55		0.55		0.55		0.55		0.55		0.55	
Rotational Speed	rpm	55770.59		63265.27		66331.31		69130.60		71743.13		74309.95	
Total to Static Velocity Ratio:		0.65		0.65		0.65		0.65		0.65		0.65	
Spouting Velocity		213.82		214.06		213.54		212.98		212.46		212.18	
Blade Tip Velocity	m/s	139.83	99.21	139.98	99.32	139.64	99.08	139.28	98.82	138.94	98.58	138.75	98.45
Absolute Flow Velocity	m/s	143.93	38.63	144.09	38.62	143.74	38.50	143.36	38.37	143.01	38.26	142.82	38.19
Absolute Flow Velocity(Tan)	m/s	138.96	0.00	139.12	0.00	138.78	0.00	138.42	1.00	138.08	1.00	137.90	1.00
Absolute Flow Velocity(Axial)	m/s	37.48	38.63	37.52	38.62	37.43	38.50	37.34	38.37	37.25	38.26	37.20	38.19
Relative Flow Velocity	m/s	37.49	106.46	37.53	106.56	37.44	106.30	37.35	106.01	37.26	105.74	37.21	105.59
RotorTip Radius	mm	23.94	16.99	21.13	14.99	20.10	14.26	19.24	13.65	18.49	13.12	17.83	12.65
Rotor Hub Radius	mm	23.94	4.43	21.13	3.91	20.10	3.72	19.24	3.56	18.49	3.42	17.83	3.30
Blade Height (LE and TE)	mm	1.87	12.56	1.61	11.08	1.52	10.54	1.44	10.09	1.36	9.70	1.30	9.35
Rotor Axial Length	mm	18.84		16.62		15.82		15.14		14.55		14.03	
Rotor Blade thickness	mm	0.96	0.48	0.85	0.42	0.80	0.40	0.77	0.38	0.74	0.37	0.71	0.36
Rotor Abs. Flow Angle	deg	15.10	90.00	15.10	90.00	15.10	90.00	15.10	91.00	15.10	91.00	15.10	91.00
Blade Angle	deg	90.00		90.00		90.00		90.00		90.00		90.00	
THERMODYNAMICS RESULTS													
Mass Flow Rate	kg/s	0.45		0.46		0.47		0.48		0.49		0.49	
Temperature	C	39.85	1.00	51.04	10.00	55.19	13.00	59.28	16.00	63.31	19.00	67.32	22.00
Pressure	bar	9.00	3.00	12.00	4.00	13.50	4.50	15.00	5.00	16.50	5.50	18.00	6.00
Absolute Mach Number	-	1.00	0.26	1.02	0.26	1.03	0.26	1.04	0.26	1.05	0.26	1.06	0.26
Density	kg/m3	42.82	14.75	57.69	19.42	65.73	21.85	73.89	24.28	82.16	26.69	90.48	29.08

Figure B.7. R134a Turbine Analysis - Pressure Ratio:3.

Fluid: R134a	Unit	Case-1		Case-2		Case-3		Case-4		Case-5		Case-6	
		Inlet	Outlet	Inlet	Outlet	Inlet	Outlet	Inlet	Outlet	Inlet	Outlet	Inlet	Outlet
GEOMETRIC RESULTS													
Specific Speed		0.55		0.55		0.55		0.55		0.55		0.55	
Rotational Speed	rpm	67374.84		76235.94		79803.47		83064.59		86083.95		89032.54	
Total to Static Velocity Ratio:		0.65		0.65		0.65		0.65		0.65		0.65	
Spouting Velocity		240.37		240.21		239.37		238.54		237.74		237.19	
Blade Tip Velocity	m/s	157.19	111.53	157.08	111.45	156.54	111.06	155.99	110.67	155.47	110.30	155.11	110.05
Absolute Flow Velocity	m/s	161.80	42.85	161.69	42.78	161.13	42.61	160.57	42.44	160.03	42.27	159.66	42.16
Absolute Flow Velocity(Tan)	m/s	156.22	0.00	156.11	0.00	155.57	0.00	155.03	1.00	154.51	1.00	154.15	1.00
Absolute Flow Velocity(Axial)	m/s	42.14	42.85	42.11	42.78	41.96	42.61	41.82	42.44	41.68	42.27	41.58	42.16
Relative Flow Velocity	m/s	42.15	119.48	42.12	119.38	41.97	118.95	41.83	118.53	41.69	118.13	41.59	117.85
RotorTip Radius	mm	22.28	15.81	19.68	13.96	18.73	13.29	17.93	12.72	17.25	12.24	16.64	11.80
Rotor Hub Radius	mm	22.28	4.12	19.68	3.64	18.73	3.47	17.93	3.32	17.25	3.19	16.64	3.08
Blade Height (LE and TE)	mm	1.30	11.69	1.11	10.32	1.04	9.82	0.98	9.41	0.92	9.05	0.88	8.73
Rotor Axial Length	mm	17.53		15.48		14.74		14.11		13.57		13.09	
Rotor Blade thickness	mm	0.89	0.45	0.79	0.39	0.75	0.37	0.72	0.36	0.69	0.34	0.67	0.33
Rotor Abs. Flow Angle	deg	15.10	90.00	15.10	90.00	15.10	90.00	15.10	91.00	15.10	91.00	15.10	91.00
Blade Angle	deg	90.00		90.00		90.00		90.00		90.00		90.00	
THERMODYNAMICS RESULTS													
Mass Flow Rate	kg/s	0.44		0.45		0.46		0.47		0.47		0.48	
Temperature	C	51.52	1.00	63.67	10.00	68.31	13.00	72.88	16.00	77.37	19.00	81.80	22.00
Pressure	bar	12.00	3.00	16.00	4.00	18.00	4.50	20.00	5.00	22.00	5.50	24.00	6.00
Absolute Mach Number	-	1.14	0.29	1.17	0.29	1.19	0.29	1.21	0.29	1.22	0.29	1.24	0.29
Density	kg/m3	57.49	14.75	78.25	19.42	89.64	21.85	101.30	24.28	113.19	26.69	125.18	29.08

Figure B.8. R134a Turbine Analysis - Pressure Ratio:4.